Some Issues on Multiuser Detection in DS-CDMA Systems

by

Zhiwei Mao
M.Sc, Beijing University of Posts & Telecommunications, 1999
B.Sc, Beijing University of Posts & Telecommunications, 1996

A Dissertation Submitted in Partial Fulfillment of the Requirements
for the Degree of

DOCTOR OF PHILOSOPHY

in the Department of Electrical and Computer Engineering

We accept this dissertation as conforming
to the required standard

Dr. V. K. Bhargava, Supervisor (Dept. of Elect. & Comp. Eng.)

Dr. W.-S. Lu, Committee Member (Dept. of Elect. & Comp. Eng.)

Dr. T. A. Gulliver, Committee Member (Dept. of Elect. & Comp. Eng.)

Dr. D. Olesky, Outside Member (Dept. of Computer Science)

Dr. C. Leung, External Examiner (University of British Columnbia)

Supervisor: Dr. V. K. Bhargava

ABSTRACT

In this dissertation, direct-sequence code-division multiple access (DS-CDMA) systems with multiuser detectors used at receiver are investigated and two kinds of multiuser detectors are developed for DS-CDMA systems.

In the investigation of DS-CDMA systems using multiuser detectors at receiver, a study on the performance of the system is presented, where heterogeneous traffic with different transmission rates and quality of service (QoS) requirements is supported. The effects of some realistic factors, such as imperfect power control and the existence of multiple cells, on the system performance are studied. In addition, algorithms are proposed to deal with the forward link power allocation problem based on the measurements of random characteristics of the received signals. This power allocation problem is formulated as a constrained optimization problem. To make the problem easy to solve, an additional appropriate constraint is proposed. Two methods are developed to identify the feasible region of this constrained optimization problem.

The first proposed multiuser detector is an adaptive minimum mean-squared-error (MMSE) detector. Particularly, it is desirable for the cases where communication channels have severe near-far problem, and thus the convergence rates of adaptive MMSE detectors for users with different power are quite different. To improve the convergence rates of adaptive MMSE detectors for weak power users, the interference effects of the strong power user signals are subtracted from the received signal successively. The method to estimate the parameters required in the proposed detector is also developed. It is shown that the proposed detector achieves fast convergence rates in various near-far scenarios. Other studies conducted include the transient mean-squared-error (MSE) analysis to explain the different convergence rates of adaptive MMSE detectors for users with different power, and the bit-error-rate (BER) performance analysis for the proposed detector.

The second proposed multiuser detector is a set of semi-blind linear parallel interference cancellation (PIC) detectors for the reverse link of multiple-cell systems, where only information about intra-cell users is available. To decrease the interference from inter-cell users whose information is unavailable to the receiver, the inter-cell user signal subspace is identified first by making use of the available information about intra-cell users. The eigenvectors and eigenvalues of this signal subspace are then used in the traditional linear PIC structure, in place of the unknown inter-cell users' signature codes and signal amplitudes. Based on this idea, three detection schemes are proposed. In addition, an efficient adaptation implementation method is developed, and the performance of the proposed detectors is studied. The proposed detectors are shown to be suitable for practical implementations and have satisfactory performance.

Examiners:

Dr. V. K. Bhargava, Supervisor (Dept. of Elect. & Comp. Eng.)

Dr. W.-S. Lu, Committee Member (Dept. of Elect. & Comp. Eng.)

Dr. T. A. Gulliver, Committee Member (Dept. of Elect. & Comp. Eng.)

Dr. D. Olesky, Outside Member (Dept. of Computer Science)

Dr. C. Leung, External Examiner (University of British Columnbia)

Table of Contents

List of Tables

List of Figures

List of Abbreviations

ACTS	Advanced Communications Technologies and Services
AMPS	Advanced Mobile Phone System
AWGN	Additive White Gaussian Noise
BER	Bit Error Rate
BPSK	Binary Phase-Shift-Keying
BS	Base Station
CDMA	Code Division Multiple Access
CGM	Conjugate Gradient Method
CMOE	Constrained Minimum Output Energy
CP	Convex Programming
DD	Decorrelating Detector
DF	Decision Feedback
DS-CDMA	Direct Sequence Code Division Multiple Access
DS/SS	Direct Sequence Spread Spectrum
ED	Eigenvalue Decomposition
E-TACS	Extended Total Access Cellular System
FDMA	Frequency Division Multiple Access
FH/SS	Frequency Hopping Spread Spectrum
GCD	Greatest Common Divisor
GSIC	Groupwise Successive Interference Cancellation
GSM	Global System for Mobile
IC	Interference Cancellation
i.i.d.	independent and identically distributed

IMT-2000	International Mobile Telecommunication 2000
IS-95	Interim Standard 95
ISI	Inter-Symbol Interference
ITU	International Telecommunications Union
JTACS	Japanese Total Access Cellular System
LCCM	Linearly Constrained Constant Modulus
LMS	Least Mean Square
MAI	Multiple Access Interference
MBS	Mobile Broadband System
MC	Multi-Code
MF	Matched Filter
MLSE	Maximum Likelihood Sequence Estimation
MMSE	Minimum Mean Squared Error
MSE	Mean Squared Error
NMTS	Nordic Mobile Telephone System
NTT	Nippon Telephone and Telegraph company
PASTd	Deflation-based Projection Approximation Subspace Tracking
PIC	Parallel Interference Cancellation
PDC	Pacific Digital Cellular
PDF	Probability Distribution Function
QoS	Quality of Service
RACE	European Community Research into Advanced Communications
r.v.	Random Variable
RF	Radio Frequency
RLS	Recursive Least Square
RTT	Radio Transmission Technology
SDM	Steepest Descent Method
SIC	Successive Interference Cancellation

SINR	Signal-to-Interference-plus-Noise Ratio
SIR	Signal-to-Interference Ratio
SNR	Signal-to-Noise Ratio
SS	Spread Spectrum
TDMA	Time Division Multiple Access
TS	Time Slot
UMTS	Universal Mobile Telecommunication System
USDC	U.S. Digital Cellular system
UTXPA	Unit Transmission Power Allocation
VCR	Variable Chip Rate
VSF	Variable Spreading Factor

Acknowledgement

First of all, I would like to express my deepest gratitude to my thesis advisor Dr. Vijay K. Bhargava. His trust, support and encouragement are invaluable to me. I have benefited a lot from the research laboratory he provided, the best one that I have met.

I would like to thank Dr. Wu-Sheng Lu, Dr. Aaron Gulliver, Dr. Dale Olesky, and Dr. C. Leung for being on my thesis committee, and for their precious time and effort in providing valuable suggestions and comments to improve the quality of this thesis.

I really enjoyed being part of the CITR (Canadian Institute for Telecommunications Research) communication group led by Dr. Bhargava. I thank my colleagues Dr. Ekram Hossain (currently with University of Manitoba), Dr. Hlaing Minn (currently with University of Texas at Dallas), Dr. Dejan Djonin, Poramate Tarasak, Daniela Djonin, Zeljko Blazek, Serkan Dost, Olivier Gervais-Harreman, Jahangir Hossain, and many others with names not listed here for their generous friendship, enlightening discussion, friendly assistance, and productive cooperation.

I'm greatly indebted to my family for their understanding and encouragement through all the years.

Finally but not the least, I wish to extend my special gratefulness to my husband Xianmin Wang. Without his encouragement and support in both academic and everyday life, I would not be able to achieve what I have finished today.

Chapter 1

Introduction

Although Guglielmo Marconi first demonstrated the possibility to communicate with people on the move by electromagnetic waves as early as in 1897, wireless communications have not gained its popularity until the 1980s. The main problems hindering the development of wireless communications are high cost and the technological challenges involved. Only with the development of highly reliable, miniature radio frequency (RF) hardware in the 1970s did the wireless communications really start [1].

In the past two decades, wireless communication systems have undergone rapid evolutions. Since the early and mid- 1980s, the first generation wireless systems based on analog modulation and frequency division multiple access (FDMA) have been successfully deployed around the world. Typical examples of the first generation wireless systems include the Advanced Mobile Phone System (AMPS) in U.S., the Nordic Mobile Telephone System (NMTS) and the Extended Total Access Cellular System (E-TACS) in Europe, and the Japanese Total Access Cellular System (JTACS) and the Nippon Telephone and Telegraph company system (NTT) in Japan. The second generation (2G) wireless systems based on digital modulation and time division multiple access (TDMA) or code division multiple access (CDMA) were introduced in the early 1990s and turned out to be a big success. Some examples of the 2G wireless systems include the pan European Global System for Mobile (GSM), the U.S. Digital Cellular system (USDC), the TDMA Interim Standard 54 (IS-54)/IS-136 and the CDMA IS-95 in North America, and the Pacific Digital Cellular (PDC) in Japan.

In order to provide universal access, global roaming and high-speed multi-function services such as high-speed wireless multimedia communications and mobile Internet access, wireless communication systems called for an evolution further from 2G to the third generation (3G). Since the mid- 1980s, the studies on a worldwide 3G standard, named International Mobile Telecommunication 2000 (IMT-2000), have been carried out by the International Telecommunications Union (ITU), which is the standards body for the United Nations. In Europe, studies on 3G technology, where they are named as Universal Mobile Telecommunication System (UMTS) and Mobile Broadband System (MBS), have also been conducted under the European Community Research into Advanced Communications in Europe (RACE) and Advanced Communications Technologies and Services (ACTS) programs [1, 2]. [3] gives an up-to-date description of the development of 3G wireless communication systems.

The radio transmission technology (RTT) in IMT-2000 terrestrial mobile systems is based on direct-sequence CDMA (DS-CDMA) technology, which is also known as direct sequence spread spectrum (DS/SS). The development of spread spectrum (SS) technique dates back to about the mid- 1950s. Besides DS/SS, another important SS technique is frequency hopping spread spectrum (FH/SS). By spreading the spectrum of the user signal, SS technique uses a transmission bandwidth in much excess of the user signal's bandwidth, and the spreaded user signal appears indistinguishable from the background noise. The initial applications of SS technique was in the development of military guidance and communication systems, which primarily fell into two categories: anti-jamming (to overcome the effects of strong intentional interference) and covertness (to hide the signal from the eavesdropper) [4]. Due to the characteristics of SS, however, it also became important in civilian applications of multiple access communications. [5] gives a good account of the historical development of SS communications. DS-CDMA has the inherent advantages in terms of high spectrum efficiency, soft capacity, multipath resistance, interference rejection, soft handoff, security and etc. [1, 3], which makes it a leading multiple access technique in 3G wireless communication systems.

As shown in Fig. 1.1, in FDMA systems, each user requesting service is allocated a unique frequency band, which can not be used by any other user until the current service is finished. In TDMA systems, the transmission time on a single frequency band is divided into cyclically repeating, non-overlapping time slots (TS). One such TS can support only one user to transmit or receive. All users in a DS-CDMA system, however, use the same frequency band and may transmit at the same time. They can be distinguished from each other from the different spreading or signature waveforms [6], which are multiplied with the narrow-band information signals to get the wide-band transmission signals. The user signals overlap in time and frequency, and the received signal consists of the sum of all user signals and noise.

1.1 Signal Model of DS-CDMA Systems

As shown in Fig. 1.2, the received signal in a DS-CDMA system can be expressed as

$$r(t) = \sum_{k=1}^{K} \sum_{j=-\infty}^{\infty} A_k b_k^j f_k(t - jT) + n(t), \tag{1.1}$$

where K is the number of active users in the system, and b_k^j is the jth information symbol of the kth user. In a binary phase-shift-keying (BPSK) system, $b_k^j \in \{+1, -1\}$. A_k is the signal amplitude and $f_k(t) = s_k(t) * h_k(t)$ with $s_k(t)$ and $h_k(t)$ being the signature waveform and the channel impulse response of user k, respectively. T is the symbol interval, $n(t)$ is an additive white Gaussian noise (AWGN) with zero mean and variance σ^2. The signature waveform of the kth user $s_k(t)$ is given by

$$s_k(t) = \sum_{i=0}^{N-1} a_k^i \psi(t - iT_c), \quad \text{for } 0 \le t \le T, \tag{1.2}$$

where $N = T/T_c$ is the *processing gain*, $a_k^i \in \{+1, -1\}$ is the ith element of the kth user's signature code, T_c is the chip interval, and $\psi(t)$ is the chip waveform which only takes nonzero value in the interval $[0,\ T_c]$. $s_k(t)$ is normalized so that $\|s_k(t)\|^2 = 1$. The above

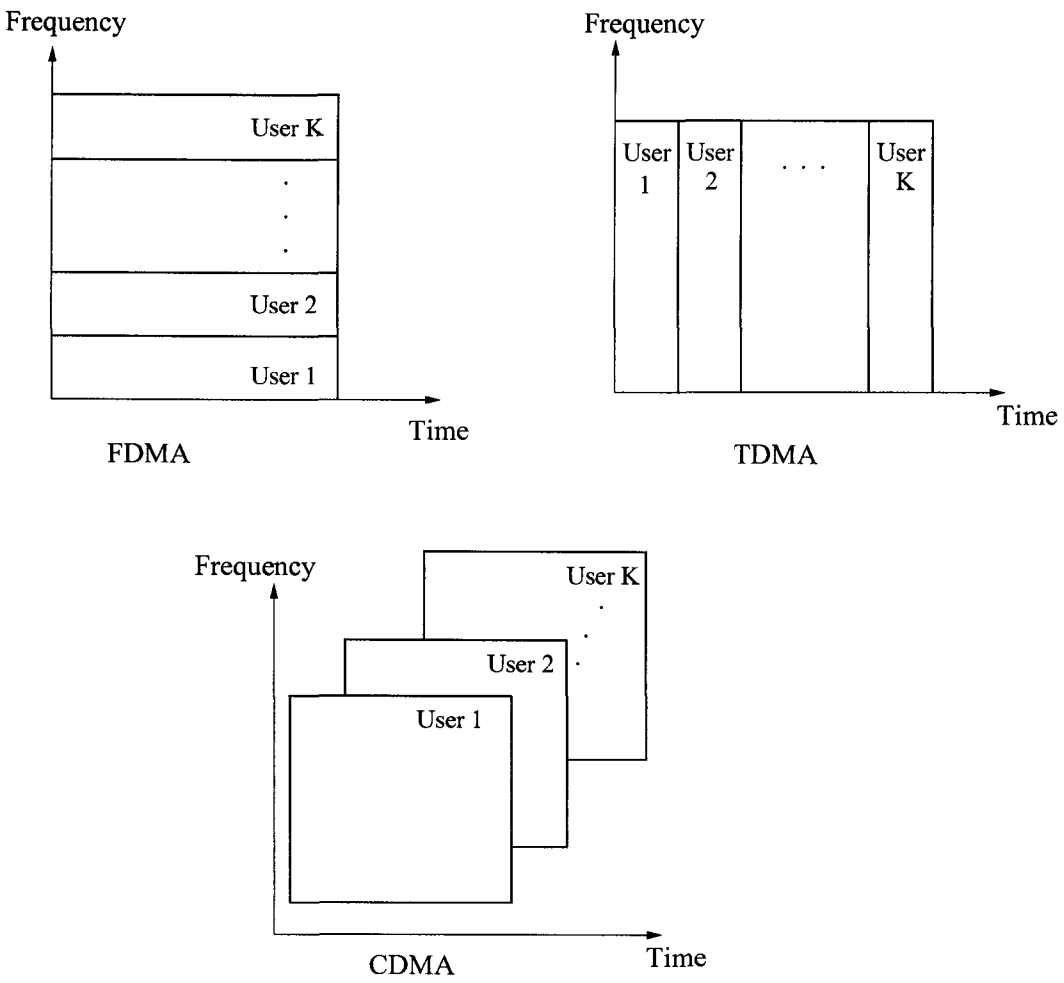

Figure 1.1. *Multiple access schemes.*

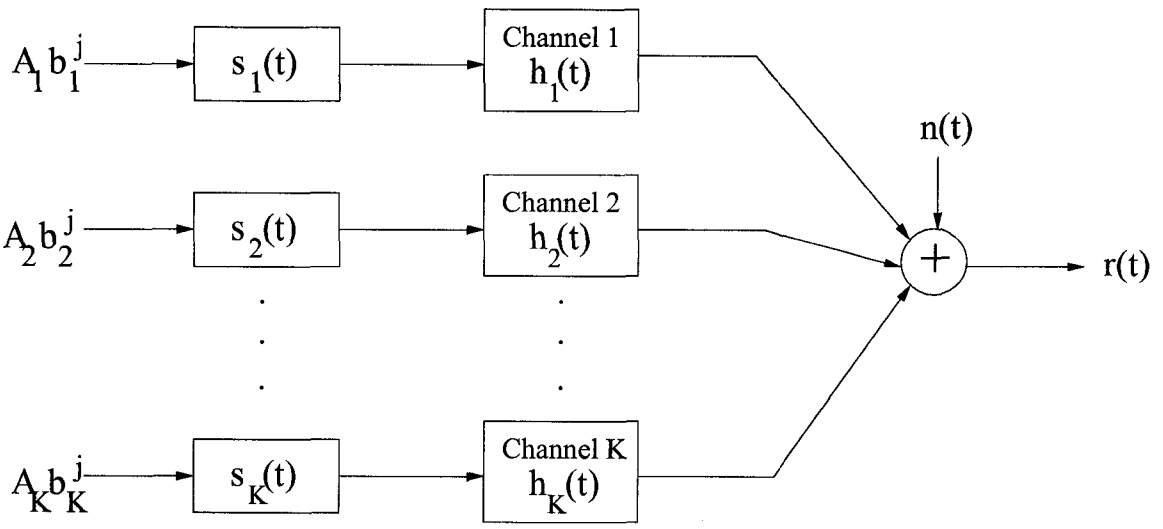

Figure 1.2. *Signal Model of DS-CDMA Systems.*

signature waveform expression is applicable to systems using short-codes, where the users' signature codes repeat in every symbol. In a system using long-codes, however, the code length is much longer than the processing gain and the users' signature codes change in each symbol period. Therefore, the value of a_k^i also depends on j. In this dissertation, we will mainly consider the short-code systems.

The impulse response of the wireless channel for user k can be expressed as

$$h_k(t) = \sum_{l=1}^{L_k} \alpha_{kl}\delta(t - \tau_{kl}), \tag{1.3}$$

where $\delta(t)$ is a unit impulse function, L_k is the number of resolvable paths, τ_{kl} is the excess delay, and α_{kl} is the complex channel coefficient of the lth path of the kth user's signal. In the special cases of synchronous and asynchronous channels, $h_k(t)$ are

$$h_k(t) = \delta(t) \tag{1.4}$$

$$h_k(t) = \delta(t - \tau_k), \tag{1.5}$$

respectively, where τ_k is the transmission delay of the kth user's signal.

1.2 Previous Work

It is obvious that the capacities of FDMA and TDMA systems are bandwidth limited. The capacity of DS-CDMA systems, as opposed to that of FDMA or TDMA systems, is multiple-access-interference (MAI) limited [7].

In conventional DS-CDMA systems, e.g. IS-95, the demodulation of signals is performed by matched filter (MF) detectors, the simplest demodulation strategy in DS-CDMA systems. A particular user's signal is detected by that user's MF which correlates the received signal with that user's signature waveform and ignores the existence of other users [8]. It follows that MF detector is a *single-user detection* strategy in which each user is detected separately, without any consideration of other users. With AWGN, MF detectors are optimal for single-user channel or multiuser channel with orthogonal signature waveforms [9]. However, in practical DS-CDMA systems, the crosscorrelations between the signature waveforms for different users are nonzero due to the asynchronism of channels which almost always exists to some extent. Therefore, a much stronger interference signal can disrupt the detection of a highly attenuated desired signal, which is known as *near-far problem*. The classical way to deal with this problem is *power control*, which requires command from receiver to transmitter to control the transmission power such that the signals from all users are received at about the same power. However, the use of power control increases the system complexity and decreases the efficiency of bandwidth utilization, and the performance of the system is directly affected by the accuracy of power control.

The primary objective of *multiuser detection*, on the other hand, is to demodulate mutually interfering digital streams of information reliably by considering the existence of other users and making use of the information about multiple users. Multiuser detection is one of the attractive technologies having been proposed in 3G systems, as additional features of the systems, to further enhance system performance and capacity. It has been a very active research area over the past decade, and many multiuser detection schemes have been proposed in the literature [10, 11, 12].

The optimum multiuser detector was proposed by Verdú [13], which is a maximum likelihood sequence estimation (MLSE) receiver/detector. It can be implemented using a bank of MFs followed by a Viterbi algorithm. The optimum multiuser detector is robust to near-far problem and yields a bit error rate indistinguishable from the (individually optimum) minimum probability of error for CDMA systems. However, the computational complexity of optimal multiuser detector increases exponentially with the number of users, and it requires the knowledge or estimates of signature waveforms, amplitudes and phases of all the received signals. All these make the optimal detector hardly practical in realistic systems and various suboptimal multiuser detectors have been proposed with significantly reduced system complexity.

An important group of suboptimal multiuser detectors is linear multiuser detectors. These detectors perform a linear transformation to the soft outputs of the bank of conventional MF detectors to obtain a new set of outputs, based on which the final decisions are made. It is hoped that the linear transformation outputs can provide better performance than the outputs directly from the MF bank. In linear decorrelating detector (DD) [14, 15, 16, 17], the linear transformation is the inverse of the signature waveform crosscorrelation matrix. Analogous to the zero-forcing equalizer in single-user channels which eliminates intersymbol-interference (ISI) completely, DD can remove all MAI. Although it does not need to estimate the received signal powers, DD still needs to know the signature waveforms of all the users. And similar to the situation with zero-forcing equalizer, it causes noise enhancement.

The linear transformation in the linear minimum mean-squared-error (MMSE) multiuser detector corresponds to a modified inverse of the signature waveform crosscorrelation matrix taking into account the noise and the received signal powers [18]. Analogous to the MMSE equalizer in single-user channels to combat ISI, the linear MMSE detector minimizes the mean-squared-error (MSE) at the detector output. It also maximizes the output signal-to-interference-plus-noise ratio (SINR), and typically provides better probability of error performance than the DD. The linear MMSE detector can be considered as a com-

promise between the desire to eliminate MAI and the desire not to enhance the background noise. As background noise goes to zero, the performance of the linear MMSE detector approaches that of the linear DD. As background noise gets very large, on the other hand, the performance of the linear MMSE detector approaches that of the conventional MF detector.

The most attractive property of the linear MMSE multiuser detector is that it can be implemented as an adaptive tapped-delay-line filter for each desired user, which requires no knowledge about the interference user signals. Thus the computational complexity of adaptive linear MMSE multiuser detector is comparable to that of the conventional MF detector. Although [19] showed that the linear DD can also be implemented adaptively, it needs quite a lot information about the interference user signals and is only appropriate for centralized applications. This is why the adaptive linear MMSE detector is particularly appealing. The adaptive MMSE detector can be adapted with the help of training sequence [20, 21, 22, 23], where a training sequence is needed at the beginning of each transmission. In order to eliminate the need for training sequence, which contains no user information and turns out to be the overhead of the system, blind adaptive techniques can be adopted. [24] and [25] proposed two blind adaptive multiuser detectors, i.e., the blind adaptive constrained minimum output energy (CMOE) detector and the blind adaptive linearly constrained constant modulus (LCCM) detector. In these blind adaptive detectors, only the knowledge of the desired user's signature sequence, timing and channel response is needed.

Both the linear DD and the linear MMSE detectors can also be implemented in a blind manner using the signal subspace concept, which are referred to as subspace-based blind linear multiuser detectors [26].

Apart from linear multiuser detectors, interference cancellation (IC) detectors are another important group of suboptimal multiuser detectors, which include successive interference cancellation (SIC) detector, parallel interference cancellation (PIC) detector, decision-feedback (DF) multiuser detector and etc. The basic principle behind IC detectors is to estimate the interference signals first and then remove all or part of the MAI seen by the

user of interest before demodulating this user's signal. Decisions on the bits of interference signals are needed in estimating the interference signals. We can use soft-decisions or hard-decisions, and the corresponding IC detectors are referred to as linear or non-linear IC detectors, respectively.

The SIC detector detects user signals and cancels the effect of interference in a serial manner [27, 28, 29, 30, 31]. In each stage of the SIC detector, the signal of one of the users in the system is demodulated, regenerated and canceled from the "renewed" received signal from previous stage. If the decision at one stage is correct, the remaining users encounter less MAI in the next stage. The SIC detector is easy to implement and the involved computational complexity and demodulation delay are linear in the number of users in the system. It has the potential to provide significant performance improvement over the conventional MF detector. However, from the above description, the problem associated with SIC detector is also obvious, i.e., its performance depends largely on the accuracy of data and amplitude estimates, especially at the initial stages, and a particular user's performance in SIC detector can be greatly affected by the order in which users are canceled.

In each stage of the PIC detector, on the other hand, the MAI signals of each user are regenerated based on the data estimates from previous stage and canceled from the received signal simultaneously in parallel. Then a new, hopefully better, set of data estimates can be obtained at the output of this stage [32, 33, 34, 35]. PIC detector generally has lower demodulation delay than the SIC detector.

The linear SIC and linear PIC detectors can also be considered as efficient methods to implement linear multiuser detectors by approximating matrix inversion using Gauss-Seidel and Jacobi iterations, respectively [36, 37].

The DF multiuser detector, which is characterized by a feed-forward filter and a feedback filter, combines linear preprocessing with SIC. There are decorrelating DF [38, 39] and MMSE DF [40, 41]. The DF multiuser detector is analogous to the DF equalizer in single-user channels to combat ISI.

After introducing the research area we will focus in this dissertation, we will present our research contributions in the following section. A brief outline of this dissertation will also be included.

1.3 Dissertation Outline and Contributions

This dissertation consists of five chapters. Chapters 2, 3 and 4 are the main body of this dissertation. Concluding remarks and suggestions for future research are presented in Chapter 5. In order to make each chapter independently readable, appendices referred in the text are attached at the end of the corresponding chapters.

Chapter 2 is concerned with the DS-CDMA systems supporting heterogeneous traffic with different transmission rates and quality of service (QoS) requirements. In the reverse link, user synchronization is difficult, therefore asynchronous transmission is assumed. In the forward link, synchronous transmission is assumed. The performance of such a CDMA system in a realistic scenario, considering the employment of DD for multi-rate systems, the effect of imperfect power control, and possible existence of multiple cells, is analyzed. Another contribution of this chapter is to propose power allocation algorithms for the forward link based on the measurements of random characteristics of the received signals. Since performance of the system is of most interest, and generally the transmission powers of base stations (BS) are limited and different traffic has different QoS requirements, the power allocation problem in the forward link is formulated as a constrained optimization problem. It is shown that by imposing another appropriate constraint, the problem is converted to a convex programming (CP) problem for both single-cell and multiple-cell systems. According to the different methods to identify the feasible region of this CP problem, two power allocation algorithms are proposed and compared.

Chapter 3 is focused on adaptive MMSE multiuser detection. Since tracking rate and computational complexity are the major concerns in adaptive detectors, these two properties of the existing adaptive MMSE detectors are studied in communication channels with

near-far problem. It is shown that it is highly desirable to design a fast converging adaptive detector with low computational load. Based on the groupwise successive interference cancellation (GSIC) technique, we propose a novel adaptive MMSE multiuser detection method. In a CDMA system, the adaptive MMSE detectors for strong power users usually have higher convergence rates than those for weak power users. In the proposed method, the convergence rates of the adaptive MMSE detectors for weak power users are increased by successively canceling the interference of the strong power user signals from the received signal. Consequently, the length of training sequence required for the system is reduced, and fast convergence rates can be achieved even using adaptive algorithms involving low computational complexity. The transient MSE analysis is also presented to explain why adaptive MMSE detectors for users with different powers have different convergence rates. Other contributions include proposing parameter estimation scheme needed in the proposed detector, and analyzing the bit-error-rate (BER) performance. Note that the proposed detection scheme can be readily extended to the case of blind adaptive multiuser detectors.

In Chapter 4, we consider the multiuser detection problem for the reverse link of CDMA systems with multiple cells. Unlike the discussion in Chapter 2 where multiuser detectors designed for single-cell systems are used directly in multiple-cell systems, in this chapter, multiuser detection schemes designed especially for the multiple-cell scenarios are considered. Multiuser detectors in this scenario are "semi-blind" in the sense that the BS only knows the signature codes of intra-cell users but does not know those of inter-cell users, although the received signal at BS comes from both intra-cell and inter-cell users. Three new semi-blind multiuser detectors that combine the ideas of signal subspace decomposition and linear PIC are proposed. In the proposed detectors, the inter-cell user signal subspace is obtained first by making use of the known intra-cell users' signature codes. Then the eigenvectors and eigenvalues of the inter-cell user signal subspace, together with the known intra-cell users' signature codes and the estimated intra-cell user signal amplitudes, are used in PIC structures to help the demodulation of intra-cell user signals. An

efficient adaptation implementation method is then developed. In addition, the performance of the proposed semi-blind linear PIC detectors is also studied through theoretical analysis and simulations. It is shown that the proposed detectors, which are especially suitable for practical implementations, have a satisfactory performance in various near-far scenarios.

Chapter 2

Analysis of DS-CDMA System Supporting Heterogeneous Traffic with Decorrelating Detector

DS-CDMA technology has received extensive attention in wireless communication systems for homogeneous type of traffic in the last decade. Future wideband DS-CDMA systems are likely to integrate various stream and packet types of traffic such as voice, image, video and data which can be identified by different transmission rates and requirements of QoS. This motivates us to consider DS-CDMA systems where heterogeneous traffic is supported.

Many schemes have been proposed to deal with heterogeneous traffic of different data rates in DS-CDMA systems through appropriate choices of modulation format, spreading factor, chip rate and number of spreading codes. In the variable-spreading-factor (VSF) method [42, 43], shorter spreading codes are used for high-rate users and longer spreading codes are used for low-rate users, with chip rates being the same for all users. In the variable-chip-rate (VCR) scheme [44], the chip rates for high-rate users are high while the chip rates for low-rate users are low, but their spreading factors are the same. In the multi-code (MC) scheme [45, 46], each high-rate user transmits information in parallel substreams. Each of the substreams uses a separate spreading code with the same spreading factor, and thus has the same data rate.

To fully utilize the potentials provided by DS-CDMA systems, multiuser detection

needs to be considered at receiver. Several multiuser detection schemes taking into account the nature of signals with different data rates have been proposed, among which are the optimal detector [47], the DD [48, 49] and the MMSE detector [50, 51, 52, 53]. Multiuser detection can be used at BS. Due to the adaptive implementations, it can also be used at mobiles.

In this chapter, we consider DS-CDMA systems supporting heterogeneous traffic where the DD is used at receiver. Signal models are developed and theoretical analyses are presented to study the system performance for both the reverse and the forward links of single-cell and multiple-cell systems in the realistic scenario of imperfect power control. In the forward link, since the transmission power of BSs is limited, efficient power allocation for each mobile at BSs is a problem worthy to be considered. The power control problem has been analyzed for narrow band systems in [54, 55, 56] and generalized to CDMA system in [57]. All these analyses were based on the availability of perfect measurements of deterministic quantities such as signal-to-interference ratio (SIR), received power or interference power. [58] and [59] integrated power control with multiuser detection, the motivation of which is to achieve a performance gain over multiuser detection without power control. Based on the stochastic approximation methods, [60] developed a power control algorithm for a multi-rate decorrelator with a class of BER-based link quality objectives. This algorithm uses actual random measurements to converge stochastically to the optimal transmission power vector. The power control algorithms proposed in this chapter, however, are fundamentally different from those that have been presented in the literature. Based on the measurements of random characteristics, algorithms are developed in this chapter to optimize the performance of the CDMA system supporting heterogeneous traffic and with decorrelator used at the receiver. At the same time, each user's QoS requirement is guaranteed and the maximum BS transmission power and maximum outer-cell interference leakage constraints are satisfied. Therefore, the forward link power control problem, also known as the forward link power allocation problem, is formulated as a constrained optimization problem. When the feasible region defined by the constraints is empty, the

current transmission can not be supported and some users need to be removed from the system. Two algorithms, the optimal algorithm and the unit transmission power allocation (UTXPA) algorithm, are proposed to identify the feasible region and then allocate the BS power. The comparison of these algorithms shows that the UTXPA algorithm offers performance close to that of the optimal algorithm with much reduced computational complexity.

This chapter is organized as follows. Section 2.1 describes the considered system and the DD. The reverse link performance in single-cell and multiple-cell CDMA systems is analyzed in Section 2.2. In Section 2.3, the forward link performance is studied first and then the power allocation algorithms are developed. Numerical results for the reverse link, as well as a comparison of the proposed forward link power allocation algorithms through numerical examples, are presented in Section 2.4. Finally, conclusions are made in Section 2.5. We focus on the stream type of traffic in this chapter.

2.1 Preliminaries

2.1.1 System Description

We consider a BPSK DS-CDMA system with asynchronous flat fading channels, where S classes of heterogeneous traffic is supported. The transmission rate and the number of physical users of the sth ($s = 1, \ldots, S$) class traffic are denoted as R_s and K_s, respectively. By exploiting the multi-rate schemes proposed in [42]-[46], each *physical* user in the heterogeneous CDMA system can be considered as certain number of *effective* users having identical transmission rate [61, 62, 63]. Denoting the greatest common divisor (GCD) of $R_1,\ R_2,\ \ldots,\ R_S$ by R_0, the set $\{R_1,\ R_2,\ \ldots,\ R_S\}$ is equivalent to $\{M_1R_0,\ M_2R_0,\ \ldots,\ M_SR_0\}$, where M_s ($s = 1, \ldots, S$) is an integer satisfying $M_sR_0 = R_s$. Consequently, the heterogeneous CDMA system with $\bar{K} = \sum_{s=1}^{S} K_s$ physical users can be regarded as an equivalent homogeneous system of $\sum_{s=1}^{S} M_sK_s$ effective users having the same transmission rate. Denoting $T_b = 1/R_0$, the received baseband signal

is expressed as

$$r(t) = \sum_{j=-\infty}^{\infty} \sum_{s=1}^{S} \sum_{i=1}^{M_s K_s} A_{si} b_{si}^{j} s_{si}(t - jT_b - \tau_{si}) + n(t), \tag{2.1}$$

where A_{si} is the amplitude, $b_{si}^{j} \in \{1, -1\}$ is the jth information bit, and $\tau_{si} \in [0, T_b)$ is the transmission delay of the ith effective user in the sth class traffic. $n(t)$ is zero-mean white Gaussian noise with variance σ^2. $s_{si}(t)$ is the spreading waveform given by

$$s_{si}(t) = \sum_{n=1}^{N} c_{si}^{n} \psi[t - (n-1)T_c], \qquad \text{for } t \in [0, T_b), \tag{2.2}$$

where T_c is the chip interval, $N = T_b/T_c$ is the processing gain and $\psi(t)$ is the chip-waveform which takes nonzero value only in $[0, T_c)$. Typically, $s_{si}(t)$ is normalized to have unit energy, i.e., $\|s_{si}(t)\|^2 = \int_0^{T_b} s_{si}^2(t)dt = 1$, and $\mathbf{c}_{si} = [c_{si}^1\ c_{si}^2\ \ldots\ c_{si}^N]^T$ is the associated spreading code vector.

For simplicity, the homogeneous system is assumed to be chip-synchronous, and for the simplicity of description, the $\sum_{s=1}^{S} M_s K_s$ effective users are renumbered from 1 to K ($K = \sum_{s=1}^{S} M_s K_s$). Then the baseband signal model in (2.1) becomes

$$r(t) = \sum_{j=-\infty}^{\infty} \sum_{k=1}^{K} A_k b_k^j s_k(t - jT_b - d_k T_c) + n(t), \tag{2.3}$$

where the subscript k is the index of effective users after the renumbering and d_k is an positive integer satisfying $\tau_k = d_k T_c$.

In asynchronous systems, the detection relies on the received signals of not only the current information bit, but also the preceding and the following information bits. This leads that the ideal decorrelator is of infinite memory length. It was demonstrated in [64] that the truncated-window decorrelators of moderate memory length, which is shown to be roughly no greater than 13 [64], are sufficient to approach the performance of the ideal decorrelators. Therefore, in the rest of this paper, a truncated-window decorrelator of length $M = 2W + 1$ is used at the receiver with W being a positive integer.

The demodulation begins by passing the received signal through a chip MF and sampling at the end of each chip. The sampled output of the chip MF for the time interval

$t \in [\,(n-W)T_b,\ (n+W+1)T_b\,]$ is expressed as [1]

$$\boldsymbol{r} = \boldsymbol{\mathcal{S}}\boldsymbol{\mathcal{A}}\boldsymbol{b} + \boldsymbol{\mathcal{S}}_e\boldsymbol{\mathcal{A}}_e\boldsymbol{b}_e + \boldsymbol{m}, \tag{2.4}$$

where

$$\boldsymbol{b} = [\,\mathbf{b}^T(n-W)\ \cdots\ \mathbf{b}^T(n)\ \cdots\ \mathbf{b}^T(n+W)\,]^T$$

$$\mathbf{b}(j) = [\,b_1^j\ b_2^j\ \cdots\ b_K^j\,]^T$$

$$\boldsymbol{\mathcal{S}} = \begin{bmatrix} \mathbf{S}(0) & \mathbf{0} & \cdots & \mathbf{0} & \mathbf{0} \\ \mathbf{S}(-1) & \mathbf{S}(0) & \cdots & \mathbf{0} & \mathbf{0} \\ \vdots & \vdots & \vdots & \vdots & \vdots \\ \mathbf{0} & \mathbf{0} & \cdots & \mathbf{S}(-1) & \mathbf{S}(0) \\ \mathbf{0} & \mathbf{0} & \cdots & \mathbf{0} & \mathbf{S}(-1) \end{bmatrix} \in \mathcal{C}^{(M+1)N\times MK}$$

$$\boldsymbol{\mathcal{S}}_e = [\,[\,\mathbf{S}^T(-1)\ \mathbf{0}\ \cdots\ \mathbf{0}\,]^T\ [\,\mathbf{0}\ \cdots\ \mathbf{0}\ \mathbf{S}^T(0)\,]^T\,] \in \mathcal{C}^{(M+1)N\times 2K}$$

$$\boldsymbol{\mathcal{A}} = \mathrm{diag}\{\mathbf{A},\ \ldots,\ \mathbf{A}\} \in \mathcal{C}^{MK\times MK}$$

$$\boldsymbol{\mathcal{A}}_e = \mathrm{diag}\{\mathbf{A},\ \mathbf{A}\} \in \mathcal{C}^{2K\times 2K}$$

$$\mathbf{A} = \mathrm{diag}\{A_1,\ A_2,\ \ldots,\ A_K\} \in \mathcal{C}^{K\times K}$$

$$\boldsymbol{b}_e = [\,\mathbf{b}^T(n-W-1)\ \mathbf{b}^T(n-W+1)\,]^T \in \mathcal{C}^{2K\times 1}.$$

The kth columns of the matrices $\mathbf{S}(0)$ and $\mathbf{S}(-1)(\in \mathcal{C}^{N\times K})$ are given by $[\ \underbrace{0\ \cdots\ 0}_{d_k}\ c_k^1\ c_k^2\ \cdots\ c_k^{N-d_k}\ ]^T$ and $[\ c_k^{N-d_k+1}\ \cdots\ c_k^N\ \underbrace{0\ \cdots\ 0}_{N-d_k}\ ]^T$, respectively. $\boldsymbol{m}$ is a Gaussian random vector with zero-mean and covariance matrix $\sigma^2\mathbf{I}$. In (2.4), the introduction of the second term is due to the edge effect caused by truncation.

Then the output in (2.4) is passed through a bank of symbol MFs, whose sampled outputs in the interval $t \in [jT_b,\ (j+1)T_b)$ form a vector denoted as $\mathbf{y}(j) = [\,y_1^j\ y_2^j\ \cdots\ y_K^j\,]^T$.

[1] A boldface lower case Roman symbol (e.g. $\mathbf{b}(j)$) denotes a vector of variables over one symbol interval. A boldface lower case italic symbol (e.g. $\boldsymbol{b}$) denotes a vector of variables concatenated over a processing window as in [64].

The concatenation of $\mathbf{y}(j)$ over the processing window, namely $\boldsymbol{y} = [\,\mathbf{y}^T(n-W)\ \cdots\ \mathbf{y}^T(n)\ \cdots\ \mathbf{y}^T(n+W)\,]^T \in \mathcal{C}^{MK\times 1}$ can be expressed as

$$\boldsymbol{y} = \boldsymbol{\mathcal{S}}^T\boldsymbol{r} = \boldsymbol{\mathcal{R}}\boldsymbol{\mathcal{A}}\boldsymbol{b} + \boldsymbol{\mathcal{R}}_e\boldsymbol{\mathcal{A}}_e\boldsymbol{b}_e + \boldsymbol{n}, \tag{2.5}$$

where

$$\boldsymbol{\mathcal{R}} = \boldsymbol{\mathcal{S}}^T\boldsymbol{\mathcal{S}} = \begin{bmatrix} \mathbf{R}[0] & \mathbf{R}^T[1] & \mathbf{0} & \cdots & \mathbf{0} & \mathbf{0} \\ \mathbf{R}[1] & \mathbf{R}[0] & \mathbf{R}^T[1] & \cdots & \mathbf{0} & \mathbf{0} \\ \vdots & \vdots & \vdots & \vdots & \vdots & \vdots \\ \mathbf{0} & \mathbf{0} & \mathbf{0} & \cdots & \mathbf{R}[1] & \mathbf{R}[0] \end{bmatrix} \in \mathcal{C}^{MK\times MK}$$

$$\mathbf{R}[0] = \mathbf{S}^T(0)\mathbf{S}(0) + \mathbf{S}^T(-1)\mathbf{S}(-1) \in \mathcal{C}^{K\times K}$$

$$\mathbf{R}[1] = \mathbf{S}^T(0)\mathbf{S}(-1) \in \mathcal{C}^{K\times K}$$

$$\boldsymbol{\mathcal{R}}_e = \boldsymbol{\mathcal{S}}^T\boldsymbol{\mathcal{S}}_e = \left[\,[\,\mathbf{R}^T[1]\ \mathbf{0}\ \cdots\ \mathbf{0}\,]^T\ [\,\mathbf{0}\ \cdots\ \mathbf{0}\ \mathbf{R}[1]\,]^T\,\right] \in \mathcal{C}^{MK\times 2K}$$

and $\boldsymbol{n} = \boldsymbol{\mathcal{S}}^T\boldsymbol{m}$ is a Gaussian random vector with zero mean and covariance matrix $\mathrm{E}[\boldsymbol{n}\boldsymbol{n}^T] = \sigma^2\boldsymbol{\mathcal{R}}$.

In synchronous systems, we have $\tau_1 = \tau_2 = \cdots = \tau_K$ and the demodulation relies only on the received signal in one symbol interval, which simplifies (2.4) and (2.5) into

$$\mathbf{r} = \mathbf{S}\mathbf{A}\mathbf{b} + \mathbf{m}, \tag{2.6}$$

$$\mathbf{y} = \mathbf{S}^T\mathbf{r} = \mathbf{R}\mathbf{A}\mathbf{b} + \mathbf{n}, \tag{2.7}$$

where $\mathbf{S} = [\,\mathbf{s}_1\ \mathbf{s}_2\ \cdots\ \mathbf{s}_K\,] \in \mathcal{C}^{N\times K}$, $\mathbf{b} = [\,b_1\ b_2\ \cdots\ b_K\,]^T$, $\mathbf{R} = \mathbf{S}^T\mathbf{S}$ is the crosscorrelation matrix, $\mathbf{m}$ and $\mathbf{n}$ are zero-mean Gaussian random vectors whose covariance matrixes are $\sigma^2\mathbf{I}$ and $\sigma^2\mathbf{R}$, respectively.

Note that we do not specify the multi-rate scheme in deriving the signal model. It can be easily shown that the multi-rate schemes in [42]-[46] can be well fitted into the same signal models of (2.4)-(2.7).

2.1.2 Decorrelating Detector

The decision statistic of the nth bit by using truncated-window decorrelator is [64]

$$\hat{\mathbf{h}}(n) = \boldsymbol{\mathcal{D}}^T \boldsymbol{y} = \boldsymbol{\mathcal{D}}^T \boldsymbol{\mathcal{R}} \boldsymbol{\mathcal{A}} \boldsymbol{b} + \boldsymbol{\mathcal{D}}^T \boldsymbol{\mathcal{R}}_e \boldsymbol{\mathcal{A}}_e \boldsymbol{b}_e + \boldsymbol{v}, \tag{2.8}$$

where $\boldsymbol{\mathcal{D}}$ is the linear transformation matrix of the decorrelator which satisfies $\boldsymbol{\mathcal{R}}\boldsymbol{\mathcal{D}} = \boldsymbol{\mathcal{U}}$ with $\boldsymbol{\mathcal{U}} = [\ \mathbf{0}_K \ \cdots \ \mathbf{0}_K \ \mathbf{I}_K \ \mathbf{0}_K \ \cdots \ \mathbf{0}_K\ ]^T \in \{0,1\}^{MK \times K}$, $\boldsymbol{v} = \boldsymbol{\mathcal{D}}^T \boldsymbol{n}$ is a zero-mean Gaussian random vector with covariance matrix $\mathrm{E}[\boldsymbol{v}\boldsymbol{v}^T] = \sigma^2 \boldsymbol{\mathcal{D}}^T \boldsymbol{\mathcal{R}} \boldsymbol{\mathcal{D}}$.

For synchronous systems, the decision statistic in (2.8) becomes

$$\hat{\mathbf{y}} = \mathbf{R}^{-1}\mathbf{y} = \mathbf{A}\mathbf{b} + \hat{\mathbf{n}}, \tag{2.9}$$

where $\hat{\mathbf{n}}$ is a zero-mean Gaussian random vector with covariance matrix $\mathrm{E}[\hat{\mathbf{n}}\hat{\mathbf{n}}^T] = \sigma^2 \mathbf{R}^{-1}$. We assume that the columns of $\boldsymbol{\mathcal{S}}$ (or $\mathbf{S}$) are linearly independent such that $\boldsymbol{\mathcal{D}}$ and $\mathbf{R}$ are nonsingular.

In the following analysis, we take the performance of the ideal decorrelator to represent that of the truncated-window decorrelator used at the receiver for the reason stated above. Consequently, the decision statistic in (2.8) of the kth effective user can be approximated by that of the ideal decorrelator, which consists of two components given by

$$[\hat{\mathbf{h}}(n)]_k \approx A_k b_k^n + n_k, \tag{2.10}$$

where n_k is a zero-mean Gaussian random variable (*r.v.*) with variance σ^2/η_k^d, and η_k^d is the asymptotic efficiency of the ideal decorrelator given as [12]

$$\eta_k^d = \left(\frac{1}{2\pi} \int_{-\pi}^{\pi} \left([\ \mathbf{R}^T[1]e^{j\omega} + \mathbf{R}[0] + \mathbf{R}[1]e^{-j\omega}\ ]^{-1} \right)_{kk} d\omega \right)^{-1}. \tag{2.11}$$

The BER of the kth effective user is given by [12]

$$p_{b,k} = \mathcal{Q}\left[\frac{A_k \sqrt{\eta_k^d}}{\sigma} \right], \tag{2.12}$$

where $\mathcal{Q}(x) = \frac{1}{\sqrt{2\pi}} \int_x^\infty e^{-t^2/2} dt$. For synchronous systems, the BER of the kth effective user has the same formulation as (2.12), with η_k^d given by

$$\eta_k^d = \left((\mathbf{R}^{-1})_{kk} \right)^{-1}. \tag{2.13}$$

For the convenience of description, we define user index sets G_s ($s = 1, \ldots, S$) and U_l ($l = 1, \ldots, \bar{K}$) which consist of the indices of all effective users of the sth class traffic and of the lth physical user, respectively. The performance of interest is the outage probability, which is defined as the probability that the BER is larger than a threshold [63], i.e.,

$$P_{out,k} = \Pr[\, p_{b,k} > \varepsilon_s \,], \quad \text{for } k \in G_s, \tag{2.14}$$

where $P_{out,k}$ is the outage probability of the kth effective user, ε_s is the BER threshold for the sth class traffic. The sth class traffic is said to satisfy the QoS requirement when the outage probability of any physical user in the class is no larger than the upper bound p_s.

2.2 Analysis of Reverse Link

In this section, the performance of the reverse link is analyzed for single-cell and multiple-cell systems. In the reverse link of a mobile system, the signal power is usually attenuated by path loss, shadowing and fast fading [1]. In the following analysis, we only consider the effects of path loss and shadowing. This is based on the fact that the effect of fast fading can be eliminated quite well by using efficient antenna diversity combining systems at the receiver [65]. The effect of shadowing is described using a log-normally distributed *r.v.* and the reverse link channel is assumed to be symbol asynchronous.

2.2.1 Performance Analysis of Single-Cell Systems

A single-cell CDMA system consists of a central BS and several mobiles communicating with the BS. When power control is used, a target level of the received signal power is specified at the BS for each class of traffic. If power control is perfect, the received signal power is the same for all the effective users of the same class traffic. If power control is imperfect, however, the received signal power becomes a *r.v.* satisfying log-normal distribution [66, 67]. As a result, the received signal power of the kth effective user P_k is

expressed as

$$P_k = Q^s \gamma_k, \tag{2.15}$$

where Q^s is the target received signal power for each effective user belonging to the sth class[2] and γ_k is a log-normally distributed *r.v.* denoting the degree of power control imperfection. The probability distribution function (PDF) of γ_k is given by [12]

$$f(\gamma_k) = \frac{10\log_{10} e}{\sqrt{2\pi}\sigma_p \gamma_k} \exp\left\{ -\frac{(10\log_{10}\gamma_k)^2}{2\sigma_p^2} \right\}, \tag{2.16}$$

where σ_p is the logarithmic standard deviation of γ_k. $\sigma_p = 0$ dB when power control is perfect. Note that in (2.15) the received signal power of each effective user is denoted as P_k. As a matter of fact, it is the physical user that receives power control commands from the BS and transmits signals to the BS. Therefore, P_k and P_j can be characterized by one *r.v.* if the jth and kth effective users belong to the same physical user.

Due to the normalization of the effective users' spreading waveforms, $P_k = A_k^2 R_0$ and $Q^s = (A^s)^2 R_0$. From (2.15), we have $A_k = A^s \gamma_k^{\frac{1}{2}}$ with $A^s = \sqrt{Q^s/R_0}$. From (2.12) and (2.14), the BER and the outage probability of the kth effective user are given by

$$p_{b,k} = \mathcal{Q}\left[\frac{A^s \gamma_k^{\frac{1}{2}} \sqrt{\eta_k^d}}{\sigma} \right], \quad \text{for } k \in G_s, \tag{2.17}$$

$$\begin{aligned} P_{out,k} &= \Pr[\, p_{b,k} > \varepsilon_s \,] \\ &= \frac{1}{2} + \frac{1}{2}\mathrm{erf}\left\{ \frac{1}{\sqrt{2}\sigma_p} 20\log_{10}\left[\frac{\sigma\, \mathcal{Q}^{-1}(\varepsilon_s)}{A^s \sqrt{\eta_k^d}} \right] \right\}, \quad \text{for } k \in G_s, \end{aligned} \tag{2.18}$$

where η_k^d is given by (2.11), $\mathrm{erf}(\cdot)$ is the error function defined by $\mathrm{erf}(x) = \frac{2}{\sqrt{\pi}} \int_0^x e^{-t^2} dt$, and $\mathcal{Q}^{-1}(\cdot)$ is the inverse $\mathcal{Q}$-function.

From (2.17), it can be seen that the BER of each of the effective users belonging to the same physical user could be different. Exactly speaking, the BER of a physical user should be the average of the BERs of all the effective users belonging to that physical user. However, when the spreading codes are chosen appropriately, the BERs of different effective

[2]For notational convenience, in the circumstances of possible confusion, subscripts are used to represent the effective or physical user index and superscripts are used to represent the traffic class.

users belonging to the same physical user could be very similar or even the same. This is also the requirements in most practical applications. Therefore, to simplify the analysis, we only consider the BERs and outage probabilities of effective users in the reverse link.

2.2.2 Performance Analysis of Multiple-Cell Systems

A multiple-cell system consists of a number of BSs, each of which communicates with mobiles within its own cell. Therefore, the BS in a multiple-cell system receives signals not only from mobiles within its own cell but also from mobiles in neighboring cells. According to (2.8) and (2.10), the decision statistic of the kth effective user can be expressed as

$$\left[\hat{\mathbf{h}}(n)\right]_k = \left[\boldsymbol{\mathcal{D}}^T\boldsymbol{\mathcal{S}}^T(\boldsymbol{r}+\boldsymbol{r}_I)\right]_k \approx A_k b_k^n + n_k + \left[\boldsymbol{\mathcal{D}}^T\boldsymbol{\mathcal{S}}^T\right]_{k,:}\boldsymbol{r}_I, \tag{2.19}$$

where $\boldsymbol{r}_I \in \mathcal{C}^{(M+1)N\times 1}$ is the sampled output of the chip MF due to the outer-cell interference signals and $\left[\boldsymbol{\mathcal{D}}^T\boldsymbol{\mathcal{S}}^T\right]_{k,:}$ denotes the kth row of $\boldsymbol{\mathcal{D}}^T\boldsymbol{\mathcal{S}}^T$. Denoting K_I as the number of all the outer-cell effective interferers, $\boldsymbol{r}_I$ is given by

$$\boldsymbol{r}_I = \sum_{i=1}^{K_I} A_{I,i}\left(\sum_{j=n-W-1}^{n+W+1} b_{I,i}^j\,\mathbf{s}_{I,i}^j\right), \tag{2.20}$$

where $A_{I,i}$ is the amplitude and $b_{I,i}^j$ is the jth information bit of the ith outer-cell effective interferer. Defining the spreading code vector and delay as $\mathbf{c}_{I,i} = [\, c_{I,i}^1\, c_{I,i}^2 \cdots c_{I,i}^N \,]^T$ and $d_{I,i}T_c$ respectively, the vector $\mathbf{s}_{I,i}^j$ is given by

$$\mathbf{s}_{I,i}^j = \begin{cases} [\, c_{I,i}^{N-d_{I,i}+1} \cdots c_{I,i}^N \underbrace{0\cdots 0}_{(M+1)N-d_{I,i}} \,]^T & j = n-W-1 \\ [\, \underbrace{0\cdots 0}_{MN+d_{I,i}} c_{I,i}^1\, c_{I,i}^2 \cdots c_{I,i}^{N-d_{I,i}} \,]^T & j = n+W+1 \\ [\, \underbrace{0\cdots 0}_{N(j-n+W)+d_{I,i}} c_{I,i}^1 \cdots c_{I,i}^N \underbrace{0\cdots 0}_{(M+n-W-j)N-d_{I,i}} \,]^T & j = n-W,\ldots,n,\ldots,n+W \end{cases} \tag{2.21}$$

It can be shown that the BER of the kth effective user is given by

$$p_{b,k} = \Pr\left\{ n_k > A_k - \left[\boldsymbol{\mathcal{D}}^T \boldsymbol{\mathcal{S}}^T\right]_{k,:} \sum_{i=1}^{K_I} A_{I,i} \left(\sum_{j=n-W-1}^{n+W+1} b_{I,i}^j \, \mathrm{s}_{I,i}^j \right) \right\}$$

$$= \frac{1}{2^{(M+2)K_I}} \sum_{b_{I,i}^j \in \{-1,+1\}} \mathcal{Q}\left[\frac{A_k - \sum_{i=1}^{K_I} A_{I,i} \left(\sum_{j=n-W-1}^{n+W+1} b_{I,i}^j \left[\boldsymbol{\mathcal{D}}^T \boldsymbol{\mathcal{S}}^T\right]_{k,:} \mathrm{s}_{I,i}^j \right)}{\sqrt{\sigma^2/\eta_k^d}} \right] \quad (2.22)$$

where η_k^d is given by (2.11).

The computational complexity required in computing (2.22) grows exponentially in the product of K_I and $(M+2)$. To simplify the computation, we approximate $\sum_{i=1}^{K_I} A_{I,i} \left(\sum_{j=n-W-1}^{n+W+1} b_{I,i}^j \left[\boldsymbol{\mathcal{D}}^T \boldsymbol{\mathcal{S}}^T\right]_{k,:} \mathrm{s}_{I,i}^j \right)$ in (2.22) by a Gaussian *r.v.* of the same variance [12, 68]. Denoting $\rho_{I,i} = \sum_{j=n-W-1}^{n+W+1} \left(\left[\boldsymbol{\mathcal{D}}^T \boldsymbol{\mathcal{S}}^T\right]_{k,:} \mathrm{s}_{I,i}^j \right)^2$, the approximated BER of the kth effective user becomes

$$p_{b,k} = \mathcal{Q}\left[\left(\frac{A_k^2}{\sigma^2/\eta_k^d + \sum_{i=1}^{K_I} A_{I,i}^2 \, \rho_{I,i}} \right)^{\frac{1}{2}} \right]. \quad (2.23)$$

Similar to the case of single-cell systems, the received signal amplitudes of effective interferers belonging to the same physical interferer are identical. Therefore, (2.23) can be rewritten as

$$p_{b,k} = \mathcal{Q}\left[\left(\frac{A_k^2}{\sigma^2/\eta_k^d + \sum_{l=1}^{\bar{K}_I} \bar{A}_{I,l}^2 \, \bar{\rho}_{I,l}} \right)^{\frac{1}{2}} \right], \quad (2.24)$$

where $\bar{K}_I$ is the number of outer-cell physical interferers, $\bar{\rho}_{I,l} = \sum_{i \in U_{I,l}} \rho_{I,i}$ with $U_{I,l}$ being a user index set consisting of the indices of all effective interferers belonging to the lth physical interferer. $\bar{A}_{I,l}$ is the received signal amplitude of each effective interferer belonging to the lth physical interferer, whose interference signal power can be denoted as $\bar{I}_l = \bar{A}_{I,l}^2 R_0$. Then

$$\mathcal{Z} = \sum_{l=1}^{\bar{K}_I} \bar{A}_{I,l}^2 \, \bar{\rho}_{I,l} = \sum_{l=1}^{\bar{K}_I} \bar{I}_l \bar{\rho}_{I,l}/R_0 = \sum_{l=1}^{\bar{K}_I} \mathcal{Y}_l \quad (2.25)$$

It is shown in Appendix 2.A that $\bar{I}_l$ $(l = 1, \ldots, \bar{K}_I)$ can be well approximated by a log-normal *r.v.* with the same variance, and thus so does $\mathcal{Y}_l = \bar{I}_l \bar{\rho}_{I,l}/R_0$, whose mean

and variance in dB are $\mu_{\mathcal{Y}_l}(\text{dB}) = 10\log_{10}(\bar{\rho}_{I,l}/R_0) + \mu_{\bar{I}_l}(\text{dB})$ and $\sigma^2_{\mathcal{Y}_l}(\text{dB}) = \sigma^2_I(\text{dB})$, respectively. $\mu_{\bar{I}_l}(\text{dB})$ and $\sigma^2_I(\text{dB})$ can be obtained through (2.53) in Appendix 2.A.

$\mathcal{Z} = \sum_{l=1}^{\bar{K}_I} \mathcal{Y}_l$ is the sum of independent log-normally distributed *r.v.*s. Although exact closed-form expression for the PDF of such a sum is not yet available in literature, it is widely accepted that such a sum can be well approximated by a log-normal *r.v.* [69]. Fenton [70], Schwartz and Yeh [71] and others [69] have proposed several methods to find the mean and variance of the resulting log-normal *r.v.*. In this chapter, the Fenton-Wilkinson method is used for its relative simplicity [65]. Denoting the mean and variance of $\mathcal{Z}$ in dB as $\mu_{\mathcal{Z}}(\text{dB})$ and $\sigma^2_{\mathcal{Z}}(\text{dB})$, the outage probability of the kth effective user can thus be derived as

$$P_{out,k} = \Pr\left\{ \mathcal{Q}\left[\left(\frac{(A^s)^2\gamma_k}{\sigma^2/\eta_k^d + \mathcal{Z}} \right)^{\frac{1}{2}} \right] > \varepsilon_s \right\}, \quad \text{for } k \in G_s. \tag{2.26}$$

When power control is perfect, (2.26) is given by

$$P_{out,k} = \frac{1}{2}\text{erfc}\left[\frac{10\log_{10}\left(\frac{1-ab}{a}\right) - \mu_{\mathcal{Z}}(\text{dB})}{\sqrt{2}\sigma_{\mathcal{Z}}(\text{dB})} \right], \tag{2.27}$$

where $a = [\mathcal{Q}^{-1}(\varepsilon_s)]^2/(A^s)^2$ and $b = \sigma^2/\eta_k^d$. When power control is imperfect, however, (2.26) becomes

$$P_{out,k} = \int_0^\infty \left\{ \int_0^{ab} f(\gamma_k)d\gamma_k \right\} f(\mathcal{Z})d\mathcal{Z} + \int_0^\infty \left\{ \int_{ab}^{a(\mathcal{Z}+b)} f(\gamma_k)d\gamma_k \right\} f(\mathcal{Z})d\mathcal{Z}. \tag{2.28}$$

After some manipulations, (2.28) can be expressed as

$$P_{out,k} = \frac{1}{2} + \frac{1}{2\sqrt{\pi}} \int_{-\infty}^{\infty} \exp(-y^2)\cdot \text{erf}\left[\frac{1}{\sqrt{2}\sigma_p} 10\log_{10}\left(ab + a10^{[\sqrt{2}\sigma_{\mathcal{Z}}(\text{dB})y + \mu_{\mathcal{Z}}(\text{dB})]/10} \right) \right] dy. \tag{2.29}$$

2.3 Analysis of Forward Link

In the forward link of DS-CDMA systems, each BS transmits signals to all mobiles within its own cell. The mobiles receive signals from its home BS and the neighboring BSs as

well. In this section, the outage probability of the forward link will be analyzed for both single-cell and multiple-cell systems, which provides an efficient tool to describe the power allocation problem at the BSs. In the following discussion, the forward links of the whole system are assumed to be globally synchronous.

2.3.1 Performance Analysis of Single-Cell Systems

In the forward link of a single-cell system, the desired and interference signals received at a mobile undergo identical effects of channel attenuation, which may include both path loss and log-normal shadowing [67]. Due to the normalization of the spreading waveforms, we have

$$A_k^2 = P_k/R_0 = T_k r_k^{-\beta}\Gamma/R_0, \tag{2.30}$$

where P_k is the received signal power, T_k is the power transmitted by the BS to the kth effective user, r_k is the distance between the mobile and the BS antenna, β is the path loss exponent, and Γ is a log-normally distributed *r.v.* with logarithmic zero mean and standard deviation σ_L which represents the effect of shadowing. According to (2.12)-(2.14), when the decorrelator is used at the receiver, the outage probability of the kth effective user is shown to be

$$P_{out,k} = \frac{1}{2} + \frac{1}{2}\text{erf}\left\{ \frac{1}{\sqrt{2}\sigma_L} 10\log_{10}\left[\frac{\sigma^2 R_0 (\mathcal{Q}^{-1}(\varepsilon_s))^2 (\mathbf{R}^{-1})_{k,k}}{T_k r_k^{-\beta}} \right] \right\}, \quad \text{for } k \in G_s. \tag{2.31}$$

2.3.2 Performance Analysis of Multiple-Cell Systems

In a multiple-cell system, the situation becomes complicated: The signals received at a mobile includes the signal from its home BS and the interference from neighboring BSs. Based on (2.7) and (2.9), the decision statistic of the kth effective user is

$$\hat{\mathbf{y}}_k = A_k b_k + \hat{n}_k + \left[\mathbf{R}^{-1}\mathbf{S}^T\mathbf{r}_I\right]_k. \tag{2.32}$$

The variance of $\hat{n}_k$ is $\sigma^2(\mathbf{R}^{-1})_{k,k}$, and the third term is due to the interference from BSs other than the home BS. $\mathbf{r}_I$ can be expressed as

$$\mathbf{r}_I = \sum_{i \notin C_0} A_i^k b_i \mathbf{c}_i, \qquad k \in C_0, \tag{2.33}$$

where $k \in C_0$ denotes that the kth effective user is located in the home cell which is numbered zero, $i \notin C_0$ denotes that the ith effective user is located in the cell other than the home cell and is an interferer to the user of interest, and A_i^k is the amplitude of the interference signal received at the kth effective user due to the existence of the ith effective user. Denoting $K_{I,0}$ as the number of all effective interferers to the home cell, the BER of the kth effective user is given as

$$p_{b,k} = \frac{1}{2^{K_{I,0}}} \sum_{b_i \in \{-1,+1\}} Q\left[\frac{A_k - \sum_{i \notin C_0} A_i^k b_i \left[\mathbf{R}^{-1}\mathbf{S}^T\mathbf{c}_i\right]_k}{\sigma\sqrt{(\mathbf{R}^{-1})_{k.k}}} \right], \qquad k \in C_0. \tag{2.34}$$

Similar to the analysis in the reverse link, after Gaussian approximation, $p_{b,k}$ in (2.34) is given as

$$p_{b,k} = Q\left[\left(\frac{T_k / R_0 r_k^{-\beta} \Gamma}{\sigma^2(\mathbf{R}^{-1})_{k,k} + \sum_{i \notin C_0} (A_i^k)^2 \rho_{i,k}} \right)^{\frac{1}{2}} \right], \tag{2.35}$$

where $\rho_{i,k} = \left(\left[\mathbf{R}^{-1}\mathbf{S}^T\mathbf{c}_i\right]_k\right)^2$ is the interference leakage factor of the ith effective user to the kth effective user.

To find the interference part $\sum_{i \notin C_0} (A_i^k)^2 \rho_{i,k}$ in the denominator of (2.35) and for simplicity, we assume that the mobile of interest is affected only by the 11 nearest neighboring BSs (see Fig. 2.1) [67]. Consequently,

$$\sum_{i \notin C_0} (A_i^k)^2 \rho_{i,k} = \sum_{j=1}^{11} \left(\sum_{i \in C_j} T_i \rho_{i,k} \right) \frac{1}{R_0} (r_{C_j})^{-\beta} \Gamma_{C_j} = \frac{1}{R_0} \sum_{j=1}^{11} Y_j = \frac{1}{R_0} Z, \tag{2.36}$$

where $i \in C_j$ $(j = 1, \ldots, 11)$ denotes that the ith effective user is located in the jth interference cell, T_i is the transmitted signal power from the jth BS to the ith effective user, Γ_{C_j} $(j = 1, \ldots, 11)$ are independent and identically distributed (i.i.d.) log-normal *r.v.*s with the same logarithmic standard deviation σ_L, and r_{C_j} denotes the distance from the jth

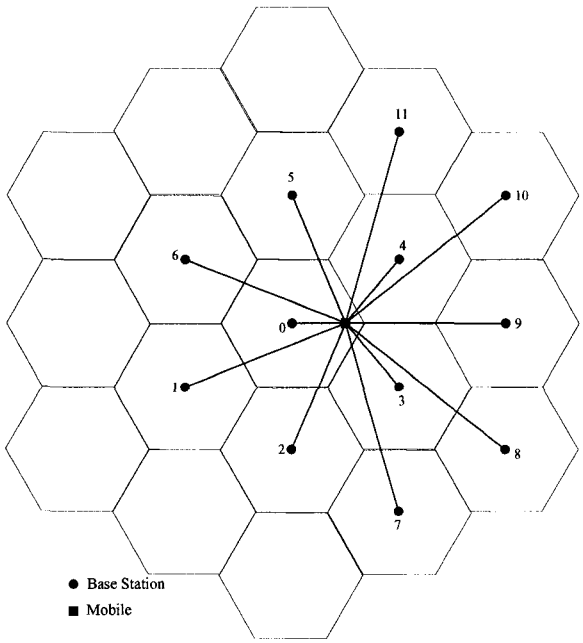

Figure 2.1. *Forward link model in multiple-cell DS-CDMA system.*

BS antenna to the mobile of interest in the home cell. $Y_j = \left(\sum_{i\in C_j} T_i\rho_{i,k}\right)(r_{C_j})^{-\beta}\Gamma_{C_j}$ ($j = 1, \ldots, 11$) are i.i.d. log-normal *r.v.*s, whose mean and variance in dB are $\mu_{Y_j}(\text{dB}) = 10\log_{10}\left[\left(\sum_{i\in C_j} T_i\rho_{i,k}\right)(r_{C_j})^{-\beta}\right]$ and $\sigma^2_{Y_j}(\text{dB}) = \sigma_L^2$, respectively. As described in Section 2.2.2, $Z = \sum_{j=1}^{11} Y_j$ can be approximated as a log-normal *r.v.* whose mean and variance in dB, denoted as $\mu_Z(\text{dB})$ and $\sigma_Z^2(\text{dB})$, can be obtained by using the Fenton-Wilkinson method.

Here we assume that all the users in the system are much stronger than the background thermal noise, i.e., we are considering the asymptotic regime of noise power approaching zero, which is generally true. Therefore, (2.35) can be simplified as

$$p_{b,k} = \mathcal{Q}\left[\left(T_k r_k^{-\beta}\Gamma/Z\right)^{\frac{1}{2}}\right] = \mathcal{Q}\left[\left(T_k r_k^{-\beta}X\right)^{\frac{1}{2}}\right], \tag{2.37}$$

where $X = \Gamma/Z$. It can be shown from Appendix 2.B that X is also a log-normal *r.v.* whose mean and variance in dB are $\mu_X(\text{dB}) = -\mu_Z(\text{dB})$ and $\sigma_X^2(\text{dB}) = \sigma_L^2 + \sigma_Z^2(\text{dB})$.

Then the outage probability of the kth effective user is given as

$$P_{out,k} = \frac{1}{2} + \frac{1}{2}\text{erf}\left\{ \frac{1}{\sqrt{2}\sigma_X(dB)} 10\log_{10}\left[\frac{(\mathcal{Q}^{-1}(\varepsilon_s))^2}{T_k r_k^{-\beta}} \right] - \frac{\mu_X(dB)}{\sqrt{2}\sigma_X(dB)} \right\} \text{ for } k \in G_s. \tag{2.38}$$

2.3.3 Power Allocation

It is observed from (2.31) and (2.38) that higher the transmission power of the BS to a mobile, lower the outage probability of that mobile. In general, however, the total transmission power of a BS is limited. In order to allocate the transmission power of BSs efficiently, power allocation algorithms are required. The power allocation problem can be formulated as a constrained optimization problem, whose objective function is defined as the weighted sum of outage probabilities of all physical users, i.e.,

$$\text{minimize:} \quad \bar{\mathbf{w}}_{out}^T \bar{\mathbf{P}}_{out} \tag{2.39a}$$

$$\text{subject to:} \quad \bar{P}_{out,l} \leq p_s \quad \text{for } l = 1, \ldots, \bar{K};\ U_l \subset G_s \tag{2.39b}$$

$$\sum_{U_l \subset C_j} \bar{T}_l \leq B \quad \text{for } j = 0, \ldots, J \tag{2.39c}$$

where $\bar{\mathbf{P}}_{out} = [\ \bar{P}_{out,1}\ \bar{P}_{out,2}\ \cdots\ \bar{P}_{out,\bar{K}}\ ]^T$ is the outage probability vector and $\bar{\mathbf{w}}_{out} = [\ \bar{w}_{out,1}\ \bar{w}_{out,2}\ \cdots\ \bar{w}_{out,\bar{K}}\ ]^T$ is the outage probability weighting vector of the physical users, $\bar{T}_l$ is the power transmitted by the corresponding BS to the lth physical user and B is the upper bound of the BS transmission power. $U_l \subset C_j$ denotes that the lth physical user is located in the jth cell, and $J+1$ is the total number of cells in the system considered. The variable vector in this problem is $\bar{\mathbf{T}} = [\ \bar{T}_1\ \bar{T}_2\ \cdots\ \bar{T}_{\bar{K}}\ ]^T$, which is the BS transmission power vector of the physical users. In the above formulation, the user distances, the effects of channel attenuation and background noise are assumed known to the power allocation algorithm and unchanged before the algorithm converges.

Based on what has been explained in Section 2.2 and to simplify the analysis, it is assumed that in the forward link, the spreading codes are chosen such that the BERs and outage probabilities of different effective users belonging to the same physical user are the

same if their received signal power is the same. Since all signals transmitted by the same BS undergo identical effect of channel attenuation, the same power is allocated to all effective users belonging to the same physical user. In the following discussion, it is assumed that $p_s < 0.5$ $(s = 1, \ldots, S)$, which is a reasonable requirement in practical systems.

In the case of single-cell systems, the first and second differentials of the objective function in (2.39a) are given by

$$\frac{\partial}{\partial T_k}\bar{\mathbf{w}}_{out}^T\bar{\mathbf{P}}_{out} = -\frac{\bar{w}_{out,l}D_3}{T_k}\exp\left(-D_1^2\log_{10}^2\frac{D_2}{T_k}\right) \text{ with } k \in U_l,\ U_l \subset G_s \quad (2.40)$$

$$\frac{\partial^2}{\partial^2 T_k}\bar{\mathbf{w}}_{out}^T\bar{\mathbf{P}}_{out} = \frac{\bar{w}_{out,l}D_3}{T_k^2}\exp\left(-D_1^2\log_{10}^2\frac{D_2}{T_k}\right)\left(1-\frac{2D_1^2}{\ln 10}\log_{10}\frac{D_2}{T_k}\right) \quad (2.41)$$

$$\frac{\partial^2}{\partial T_k \partial T_j}\bar{\mathbf{w}}_{out}^T\bar{\mathbf{P}}_{out} = 0 \quad \text{for } j \neq k \quad (2.42)$$

where

$$D_1 = \frac{10}{\sqrt{2}\sigma_L} > 0$$
$$D_2 = \sigma^2 R_0 (\mathcal{Q}^{-1}(\varepsilon_s))^2 (\mathbf{R}^{-1})_{k,k}\, r_k^{\beta} > 0$$
$$D_3 = \frac{D_1}{\sqrt{\pi}\ln 10} > 0$$

From (2.31), it can be seen that if $p_s < 0.5$ $(s = 1, \ldots, S)$ then $\log_{10}\frac{D_2}{T_k} < 0$ and $\frac{\partial^2}{\partial^2 T_k}\bar{\mathbf{w}}_{out}^T\bar{\mathbf{P}}_{out} > 0$. Thus the objective function is convex. The constraint in (2.39b) describes a lower bound $T_{min,k}$ for the BS transmission power to each effective user. According to (2.31),

$$T_{min,k} = \frac{\sigma^2 R_0 r_k^{\beta}[\mathcal{Q}^{-1}(\varepsilon_s)]^2\,(\mathbf{R}^{-1})_{k,k}}{10^{\sqrt{2}\sigma_L \text{erf}^{-1}(2p_s-1)/10}} \quad (2.43)$$

for a single-cell CDMA system. Denoting $\bar{T}_{min,l}$ as the lower bound for the BS transmission power to the lth physical user, it is easily shown that $\bar{T}_{min,l} = \sum_{k\in U_l} T_{min,k}$ and $\bar{T}_l = \sum_{k\in U_l} T_k$. It can also be seen that the constraints in (2.39b) and (2.39c) are linear, i.e., the feasible region determined by these constraints is convex. Therefore, the constrained optimization problem in (2.39) is a CP problem [72].

In the case of multiple-cell systems, however, the convexity of the problem is unknown. Considering (2.35)-(2.38), we add the interference leakage constraints to the problem as

follows

$$\sum_{k\in C_j} T_k\rho_{k,i} \leq B' \qquad \text{for } i \in \bar{C}_j;\ j = 0,\ldots,J \tag{2.44}$$

where $\bar{C}_j$ denotes the neighboring cells affected by the BS in the jth cell. It is also assumed that the BS transmission power is determined based on the maximal outer-cell interference leakage. Although this assumption may decrease the system performance, it makes the problem in (2.39) also a CP problem in the case of multiple-cell systems, which can be derived in a similar way as stated above. Therefore, the global minimizer can be found easily in the cases of both single-cell and multiple-cell systems.

Similar to the case of single-cell systems, according to (2.38),

$$T_{min,k} = \frac{r_k^{\beta}[\mathcal{Q}^{-1}(\varepsilon_s)]^2}{10^{\sqrt{2}\sigma_X(dB)\text{erf}^{-1}(2p_s-1)/10+\mu_X(dB)/10}} \tag{2.45}$$

for a multiple-cell CDMA system. We define $\bar{\mathbf{T}}_{min} = [\ \bar{T}_{min,1}\ \bar{T}_{min,2}\ \cdots\ \bar{T}_{min,\bar{K}}\ ]^T$ as the lower bound BS transmission power vector of the physical users. To this end, the minimization problem in (2.39) can be reformulated as

$$\text{minimize:} \quad \sum_{l=1}^{\bar{K}} \bar{w}_{out,l} f(\bar{T}_l) \tag{2.46a}$$

$$\text{subject to:} \quad \bar{T}_l \geq \bar{T}_{min,l} \qquad \text{for } l = 1,\ldots,\bar{K}, \tag{2.46b}$$

$$\sum_{U_l\subset C_j} \bar{T}_l \leq B \qquad \text{for } j = 0,\ldots,J \tag{2.46c}$$

$$\sum_{k\in C_j} T_k\rho_{k,i} \leq B' \qquad \text{for } i \in \bar{C}_j;\ j = 0,\ldots,J \tag{2.46d}$$

where $f(\bar{T}_l) = P_{out,k}(T_k = \bar{T}_l/M_s)$ with $k \in U_l$ and $U_l \subset G_s$. For a single-cell system, $f(\bar{T}_l)$ and $T_{min,k}$ are given by (2.31) and (2.43); while for a multiple-cell system, $f(\bar{T}_l)$ and $T_{min,k}$ are given by (2.38) and (2.45).

If the transmission power of the BSs is not enough to support all the current transmission or the interference leakage constraints cannot be met, i.e., the feasible region defined by the constraints in (2.46b)-(2.46d) is empty, then we need to find a non-empty feasible region of the problem in (2.46) by removing some physical users from different classes of

traffic. A power allocation algorithm will remove the physical users in different classes from the initial system such that the throughput of the final system is maximized with respect to the constraints in (2.46b)-(2.46d). The removed users may be transferred to another cell or disconnected. To avoid frequent hand-off and disconnection, it is highly desirable to remove as few physical users as possible. Therefore, the reduced system is identified according to the following criteria in a decreasing priority:

1. The throughput being maximized;
2. Including the largest number of physical users;
3. Having the lowest objective function value of (2.46a).

In order to make the following description convenient, we define the physical user set $\mathbf{U}_0$ which includes all $\bar{K}_0$ physical users, corresponding to K_0 effective users of the initial system. $\mathbf{U}^*$ is defined as the physical user set of the final system after the feasible region has been found, with $\bar{K}^*$ physical users in it. The throughput of the final system is defined as $H = \sum_{U_l \in \mathbf{U}^*} \bar{w}_{h,l} R_s$ ($U_l \subset G_s$), with $\bar{w}_{h,l}$ being the throughput weighting factor of the lth physical user whose equivalent throughput is $\bar{R}_l = \bar{w}_{h,l} R_s$ ($U_l \subset G_s$).

Based on an exhaustive search approach, the optimal power allocation algorithm is summarized as follows.

Optimal Algorithm

1. Compute $\bar{\mathbf{T}}_{min} = [\, \bar{T}_{min,1}\ \bar{T}_{min,2}\ \cdots\ \bar{T}_{min,\bar{K}_0}\,]^T$ for the initial system based on (2.43) or (2.45). If $\sum_{U_l \subset C_j} \bar{T}_{min,l} \leq B$ and $\sum_{k \in C_j} T_{min,k} \rho_{k,i} \leq B'$ ($i \in \bar{C}_j$) are met for $j = 0, \ldots, J$, set $\mathbf{U}^* = \mathbf{U}$ and go to step 4; otherwise, use the exhaustive search approach to find all possible subsets of $\mathbf{U}_0$, namely $\mathbf{U}_1$, $\mathbf{U}_2$, $\cdots$, $\mathbf{U}_n$, where n is the number of all possible subsets of $\mathbf{U}_0$.
2. For $i = 1, 2, \cdots, n$: Compute the lower bound BS transmission power vector of physical users for the system associated with $\mathbf{U}_i$ based on (2.43) or (2.45), which is denoted as $\bar{\mathbf{T}}_{min,i} = [\, \bar{T}_{min,i,i_1}\ \bar{T}_{min,i,i_2}\ \cdots\ \bar{T}_{min,i,i_{\bar{K}_i}}\,]^T$ with $\bar{K}_i$ being the number of physical users in this system, which corresponds to K_i effective user. If

$\sum_{U_l \subset C_j} \bar{T}_{min,i,l} \leq B$ and $\sum_{k \in C_j} T_{min,i,k} \rho_{k,i} \leq B'$ $(i \in \bar{C}_j)$ are met for $j = 0, \ldots, J$, set the throughput of this system as H_i; otherwise, set H_i as zero.

3. Find the maximizer(s) of $\{H_i\}$. If H_i has only one maximizer, set its associated user set as $\mathbf{U}^*$; otherwise, the user set $\mathbf{U}^*$ can be identified according to the criteria 2 and 3 mentioned above in a decreasing priority.

4. Solve the optimization problem in (2.46) using efficient interior-point algorithm [73] and compute $\bar{\mathbf{T}}^*$ and $\bar{\mathbf{P}}^*_{out}$ for the system associated with $\mathbf{U}^*$.

Note that in the optimal algorithm, $\bar{\mathbf{T}}_{min}$ for every possible sub-system needs to be calculated. Since the number of possible sub-systems increases exponentially in the number of physical users, so does the amount of computation involved in the optimal algorithm. To alleviate this problem, a more practical algorithm, the unit transmission power allocation (UTXPA) algorithm is proposed to achieve a suboptimal solution with considerably reduced computational complexity. The idea behind the proposed UTXPA algorithm is to try to support the same unit equivalent throughput with the lowest requirement of lower bound BS transmission power, taking into account the effect of interference leakage to users in other cells as well. The UTXPA algorithm is summerized as follows.

Unit Transmission Power Allocation (UTXPA) Algorithm

1. Compute $\bar{\mathbf{T}}_{min} = [\ \bar{T}_{min,1}\ \bar{T}_{min,2}\ \cdots\ \bar{T}_{min,\bar{K}_0}\ ]^T$ for the initial system based on (2.43) or (2.45). If $\sum_{U_l \subset C_j} \bar{T}_{min,l} \leq B$ and $\sum_{k \in C_j} T_{min,k} \rho_{k,i} \leq B'$ $(i \in \bar{C}_j)$ are met for $j = 0, \ldots, J$, set $\mathbf{U}^* = \mathbf{U}$ and go to step 3; otherwise, compute $\bar{\alpha}_l = \sum_{i \in \bar{C}_j} \sum_{k \in U_l} T_{min,k} \rho_{k,i} / \bar{R}_l$ $(U_l \subset C_j)$ for $l = 1, \ldots, \bar{K}_0$ and sort them in ascending order as $\{\bar{\alpha}_{i_1}, \bar{\alpha}_{i_2}, \ldots, \bar{\alpha}_{i_{\bar{K}_0}}\}$.

2. Set $\mathbf{U}^*$ as a null set. For $j = 1, 2, \cdots, \bar{K}_0 - 1$: Add the physical user associated with $\bar{\alpha}_{i_j}$ into $\mathbf{U}^*$ and update the value of $\bar{K}^*$ and compute $\bar{\mathbf{T}}^*_{min} = [\ \bar{T}^*_{min,i_1}\ \bar{T}^*_{min,i_2}\ \cdots\ \bar{T}^*_{min,i_{\bar{K}^*}}\ ]^T$ for the system associated with $\mathbf{U}^*$ based on (2.43) or (2.45); if $\sum_{U_l \subset C_j} \bar{T}^*_{min,l} \leq B$ and $\sum_{k \in C_j} T^*_{min,k} \rho_{k,i} \leq B'$ $(i \in \bar{C}_j)$ are met for $j = 0, \ldots, J$, continue the process; otherwise remove the user added last from $\mathbf{U}^*$ and go to step 3.

3. Same as step 4 of the optimal algorithm.

For the UTXPA algorithm, the lower bound BS transmission power vector of physical users needs to be calculated at most $\bar{K}_0$ times. Therefore, the computational complexity required by the UTXPA algorithm is considerably less relative to that required by the optimal algorithm.

From the above description of the proposed power allocation algorithms, it can be easily seen that the throughput weighting factor $\bar{w}_{h,l}$ will affect the probability that a user is removed from the system, and the outage probability weighting factor $\bar{w}_{out,l}$ will affect the outage probabilities of users in the system. The effects of $\bar{w}_{h,l}$ and $\bar{w}_{out,l}$ on the system performance will be explained in details through numerical examples in the next section.

2.4 Numerical Results

Numerical examples were conducted to illustrate the effect of imperfect power control on the reverse link performance and to compare the performance of the power allocation algorithms in the forward link. A DS-CDMA system supporting two classes of traffic was considered, where the data rate of class two was twice as that of class one and the MC multi-rate scheme [45, 46] was adopted. In all the results reported in this section, the BER thresholds for both classes of traffic were assumed to be $\varepsilon_1 = 10^{-2}$ and $\varepsilon_2 = 10^{-4}$, and σ_L and β were assumed to be 4.0 dB and 4. The spreading codes of users were chosen randomly from length 127 Gold codes.

In the examples for the reverse link, the target levels of E_b/N_0 for both classes of traffic were set to 12 dB and 15 dB, respectively. All the results were averaged over 150 different delay combinations, and all these delays were independently sampled from a uniform distribution. Without the loss of generality, the outage probability of the first effective user in each class of traffic was examined.

The outage probabilities in terms of number of users in each class for reverse link in the single-cell system are plotted in Fig. 2.2 where the logarithmic standard deviation of power

control imperfection σ_p was 1 dB. For comparison purpose, the outage probabilities with $\sigma_p = 2$ dB are presented in Fig. 2.3. From these figures, it is observed that when the degree of imperfection of power control increases, the outage probability increases rapidly, which is similar to the result presented in [67] where a traditional MF receiver is used. This can be explained from a careful study of (2.18). In the examples given, the outage probabilities are all less than 0.5, which is also a reasonable requirement in practical systems. It can be easily seen from (2.18) that the logarithm term should give a minus value under this requirement. Therefore, a higher σ_p leads to a higher outage probability. On the other hand, if the system parameters have the values which make the logarithm term positive, the outage probabilities are more than 0.5. Under this circumstance, the outage probability will decrease as the degree of imperfection of power control increases.

In the examples for the reverse link of the multiple-cell system, 120^0 directional antennas were employed at the BSs. In Fig. 2.4, the outage probabilities are plotted when power control is perfect. The outage probabilities are plotted in Fig. 2.5 when $\sigma_p = 1$ dB and in Fig. 2.6 when $\sigma_p = 2$ dB. It is shown that multiple-cell CDMA systems are also sensitive to power control imperfections and that the outage probabilities are much higher than those in the single-cell system. An explanation for the behavior of outage probabilities can be easily obtained from the comparison of (2.17), (2.18) and (2.26). In multiple-cell systems, due to the interference received from neighboring cells, the BER of an effective user is higher than that in single-cell systems given all the other system parameters being the same, which leads directly to a higher outage probability.

In Fig. 2.7, we compare the reverse link capacity in different system configurations through the maximal number of physical users in different traffic classes that the system can support. In all these systems, $p_1 = 5\%$ and $\sigma_p = 1$ dB. It is seen that the employment of decorrelator at the receiver can increase the capacity of the reverse link significantly in single-cell systems. However, in multiple-cell systems, due to the interference from neighboring cells, the capacity is reduced considerably relative to the case of single-cell systems. Similar to the situation using traditional MF detector, the techniques to reduce the

outer-cell interference, such as sectoring, can increase the reverse link capacity. The results also show that if more powerful error control codes are employed such that the upper bound for outage probability can be relaxed, the reverse link capacity can also be increased.

In the examples for the forward link, the values $p_1 = p_2 = 0.01$ and $B = 2$ W were used, and omni-directional antennas were used at the BSs. For simplicity, we confined the users to be located inside the circle inscribed in the hexagonal cell, whose radius was assumed to be 2.0 Km. The height of the BS antenna was 30 m, and the minimum distance between users and the home cell center was 200 m. The locations of users were independently sampled from a uniform distribution over the confined area, which remained unchanged throughout the process, and the home BS of users was chosen to be the closest one. The throughput weighting factors and outage probability weighting factors were assumed to be the same for all effective users in the same traffic class, denoted as w_h^1, w_{out}^1 and w_h^2, w_{out}^2 for class one and class two respectively. w_h^1 and w_{out}^1 were assumed to be one in all the examples given in this section. In the case of the single-cell system, the initial user numbers in the home cell were 5 for both classes of traffic, and the background noise was assumed to be 10^{-13} W in the bandwidth of 1.25×10^6 Hz. In the case of the multiple-cell system, the initial user numbers in the home cell were 5 for class one and 15 for class two.

The performance of the power allocation algorithms is evaluated in terms of system throughput (H), removal probability (P_{rem}) and mean outage probability (O_{ut}). P_{rem} measures the expected proportion of physical users which are removed by a power allocation algorithm [56] and O_{ut} measures the mean value of the outage probability after the process of power allocation. The data rate of a physical user in the first class, which is 10×10^3 bits/sec., was taken as a unit to describe the system throughput and all results were averaged over 50 realizations of different user locations.

Let us first consider the effects of the throughput weighting factor and the outage probability weighting factor on the system performance through numerical examples for the single-cell system. Fig. 2.8 shows how the removal probabilities are affected by the throughput weighting factor. It can be seen that although w_h^1 remains the same, both P_{rem}^1

and P_{rem}^2 are affected by the changes of w_h^2 if it changes within a certain range, i.e., as w_h^2 becomes larger P_{rem}^2 will decrease and P_{rem}^1 will increase. However, when w_h^2 becomes small or large enough, both P_{rem}^1 and P_{rem}^2 will not be affected by w_h^2 any more. Fig. 2.9 shows how the mean outage probabilities are affected by the outage probability weighting factor. Similar to the performance of the removal probability, both O_{ut}^1 and O_{ut}^2 are affected by the changes of w_{out}^2 even though w_{out}^1 remains the same, i.e., as w_{out}^2 becomes larger O_{ut}^2 will decrease and O_{ut}^1 will increase. When w_{out}^2 becomes small (large) enough, the effect of the changes in w_{out}^2 on O_{ut}^1 (O_{ut}^2) will become almost undetectable. From both figures, it can be seen that the performance of the UTXPA algorithm is consistently close to that of the optimal algorithm with much reduced computational complexity.

In the examples for the multiple-cell system, w_h^2 and w_{out}^2 were also assumed as one. The results are presented in Table 2.1. For comparison purposes, we also list the system performance when the spreading codes were chosen from length 63 Gold codes, which will increase the outer-cell interference leakage. Similar to the single-cell case, the UTXPA algorithm has almost as good performance as the optimal one. It can also be seen from Table 2.1 that the forward link performance in a multiple-cell system depends largely on the interference received from neighboring BSs. In order to increase the forward link performance, the methods to suppress the interference from neighboring BSs, like sectoring or decreasing the cross-correlations between users within the home cell and in neighbouring cells, can be used.

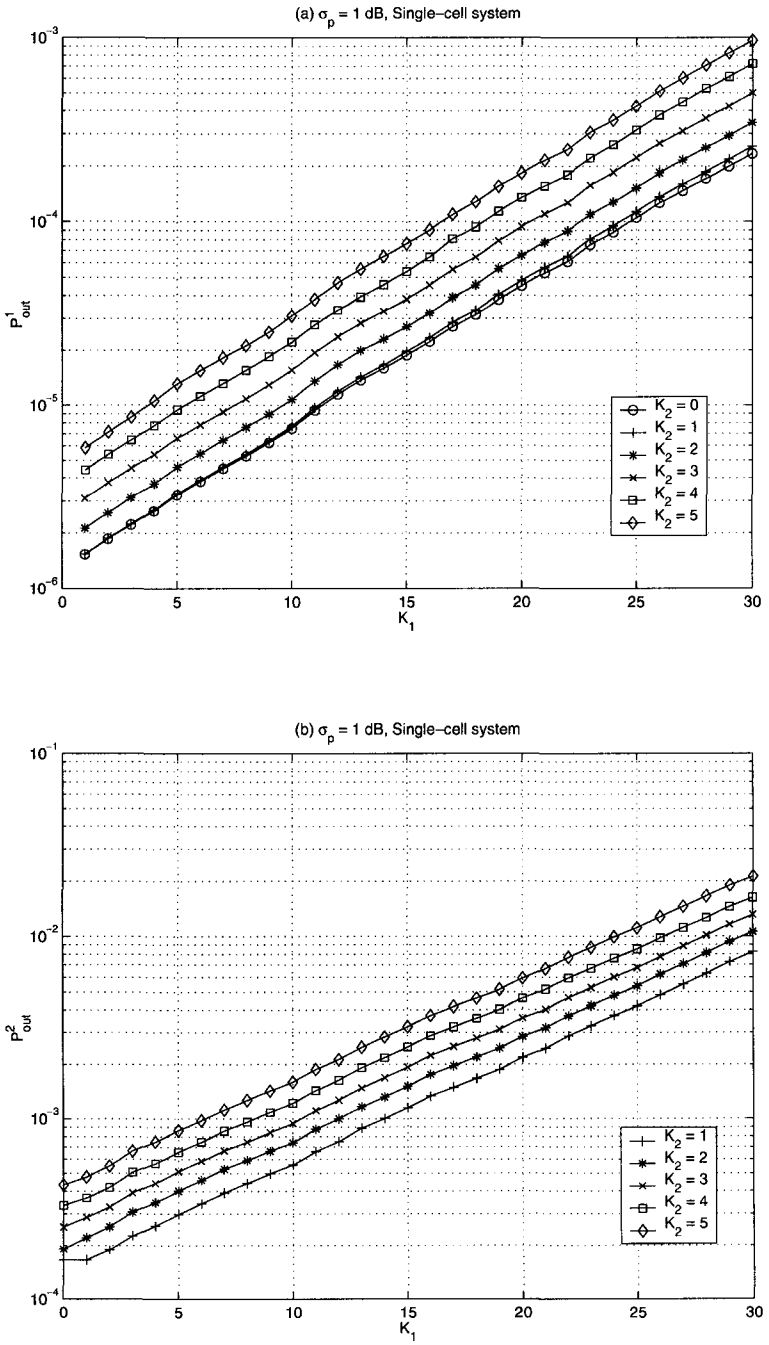

Figure 2.2. *Outage probabilities for reverse link in single-cell system ($\sigma_p = 1$ dB).*

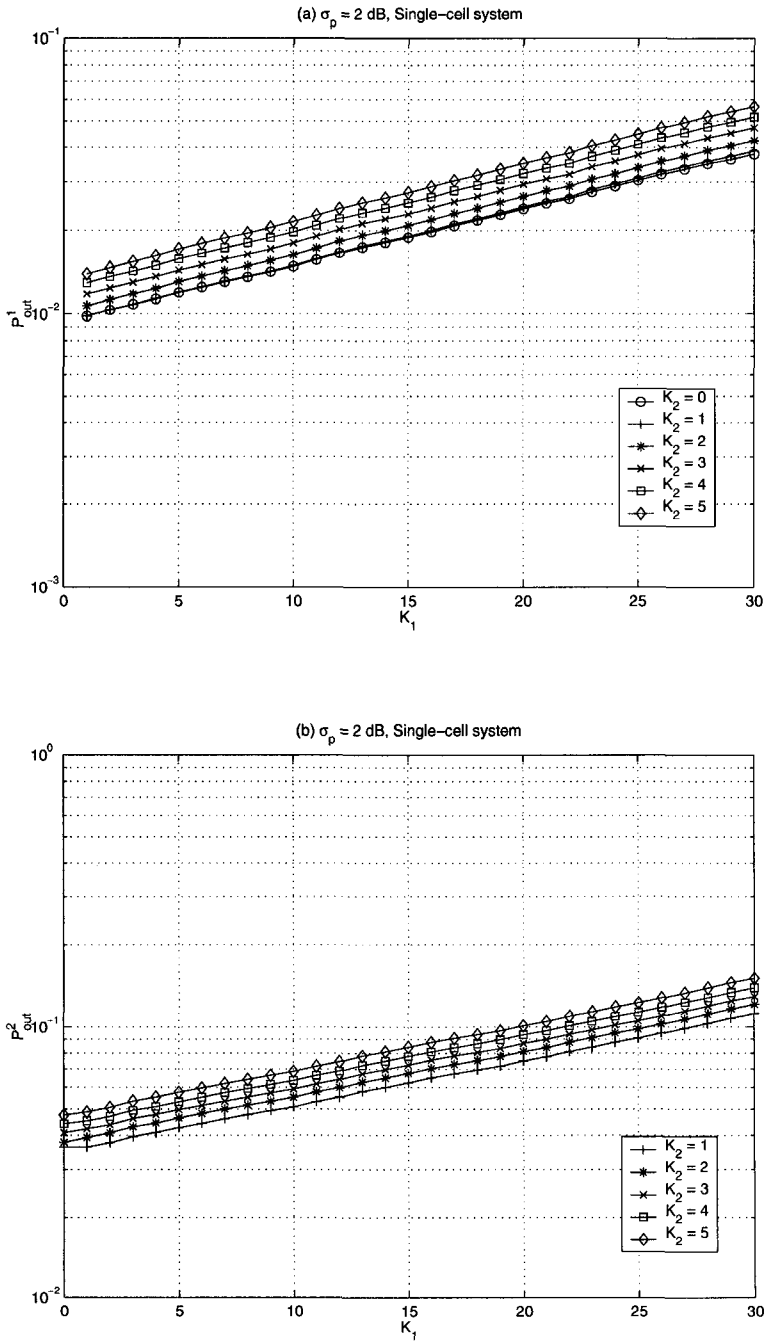

Figure 2.3. *Outage probabilities for reverse link in single-cell system ($\sigma_p = 2$ dB).*

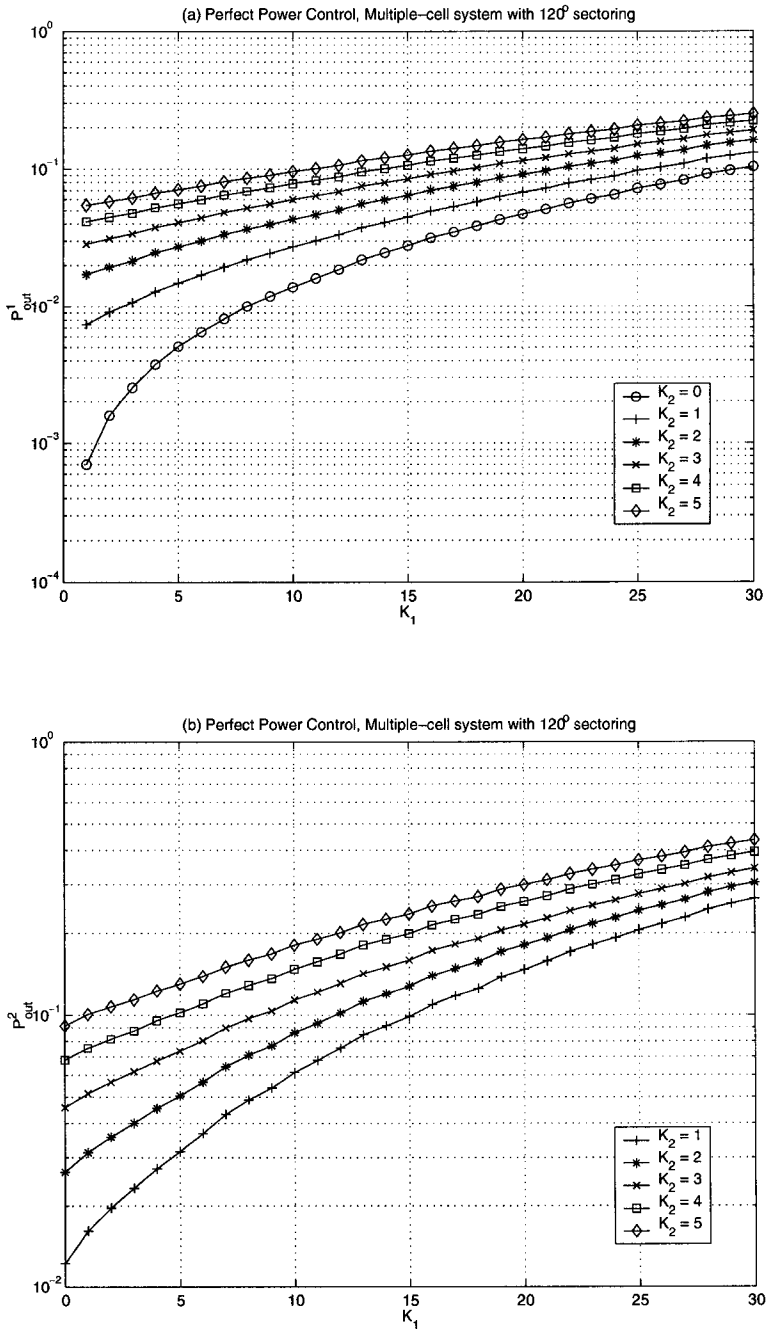

Figure 2.4. *Outage probabilities for reverse link in multiple-cell system (perfect power control).*

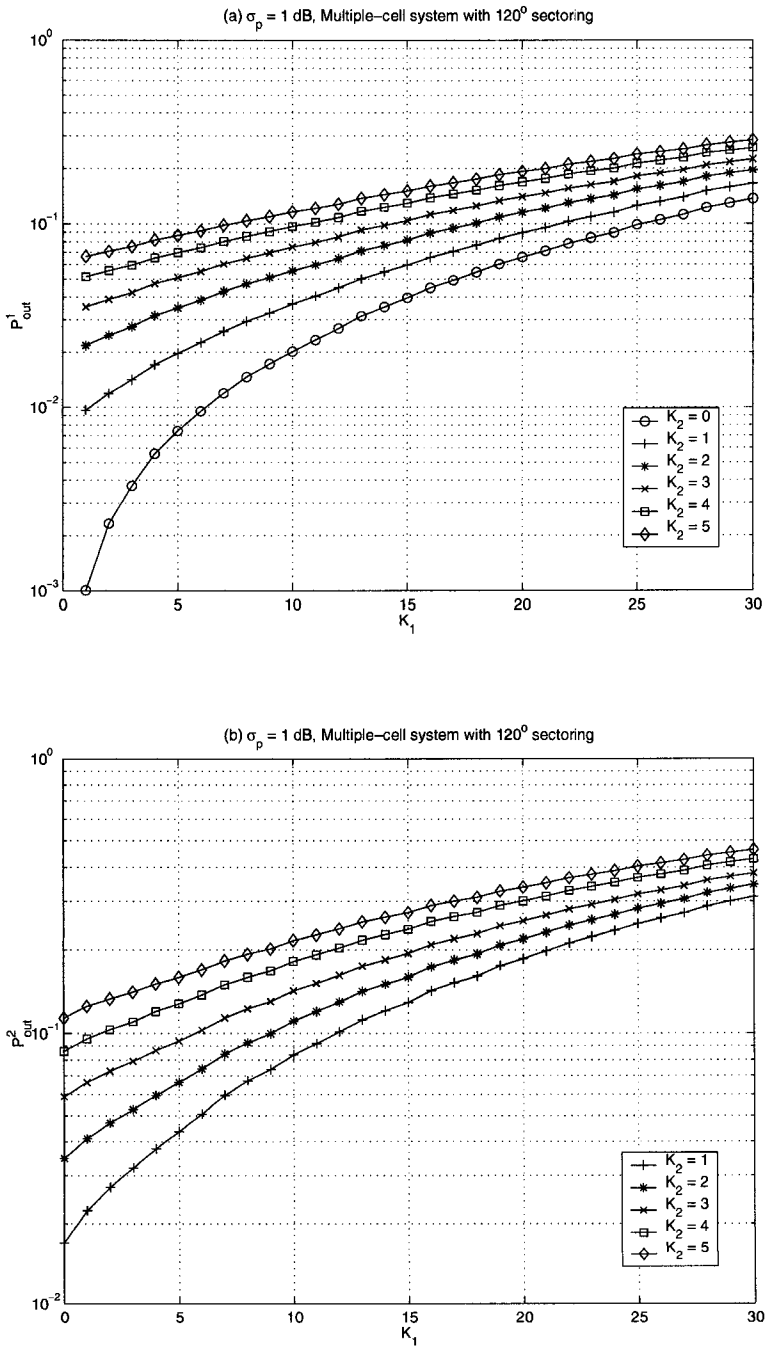

Figure 2.5. *Outage probabilities for reverse link in multiple-cell system ($\sigma_p = 1$ dB).*

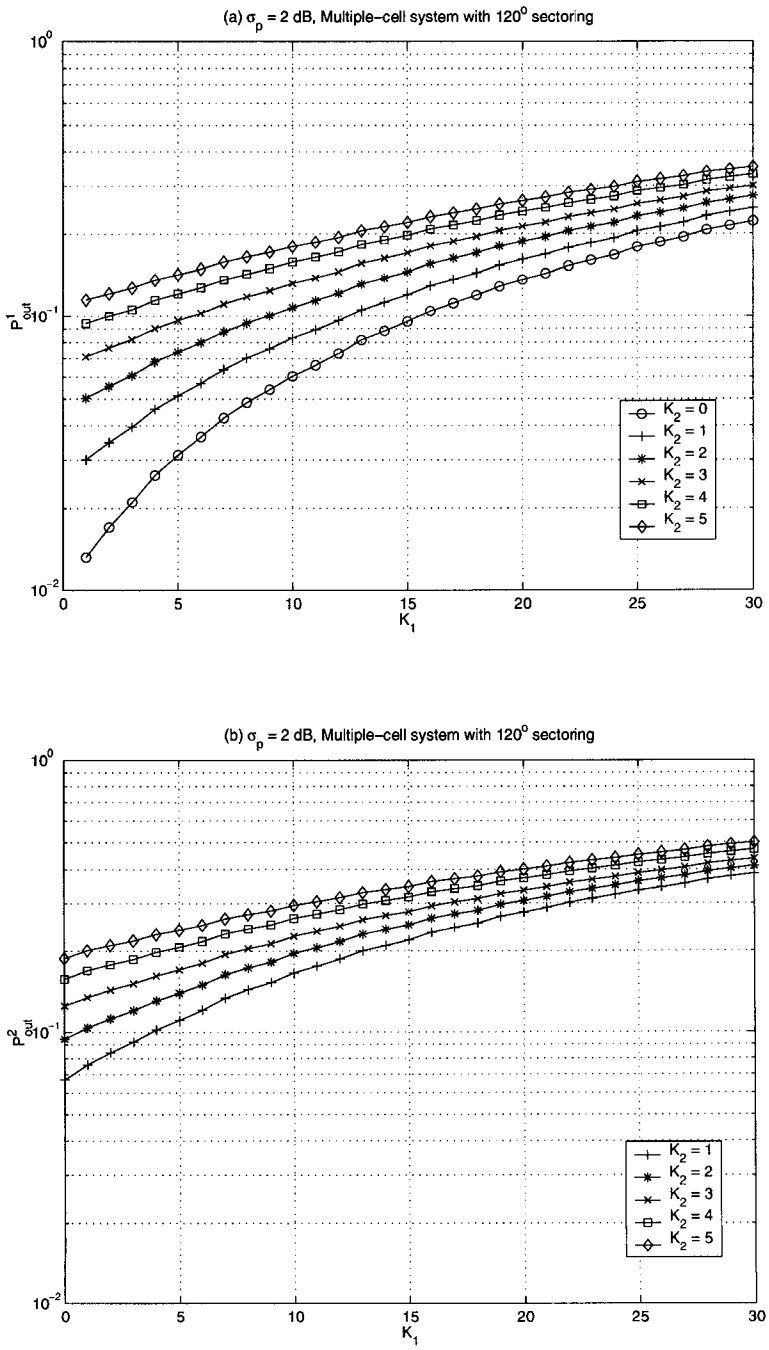

Figure 2.6. *Outage probabilities for reverse link in multiple-cell system ($\sigma_p = 2$ dB).*

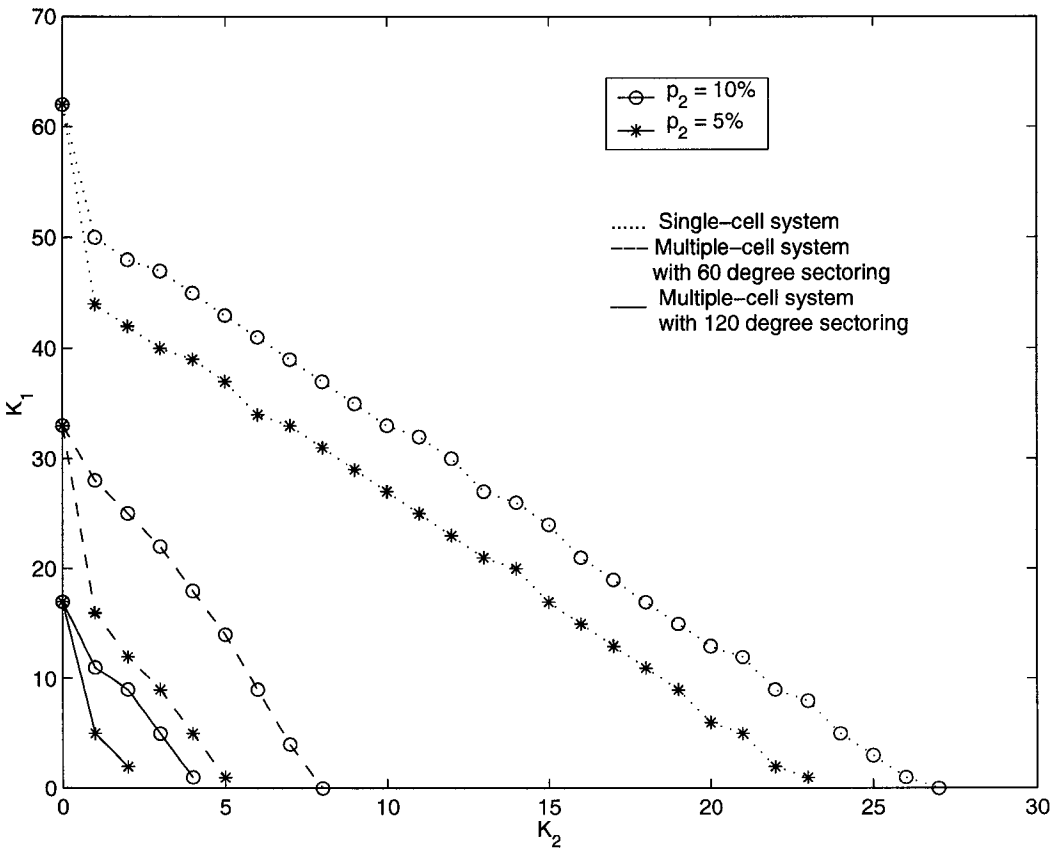

Figure 2.7. *Reverse link capacity comparison ($p_1 = 5\%$, $\sigma_p = 1$ dB).*

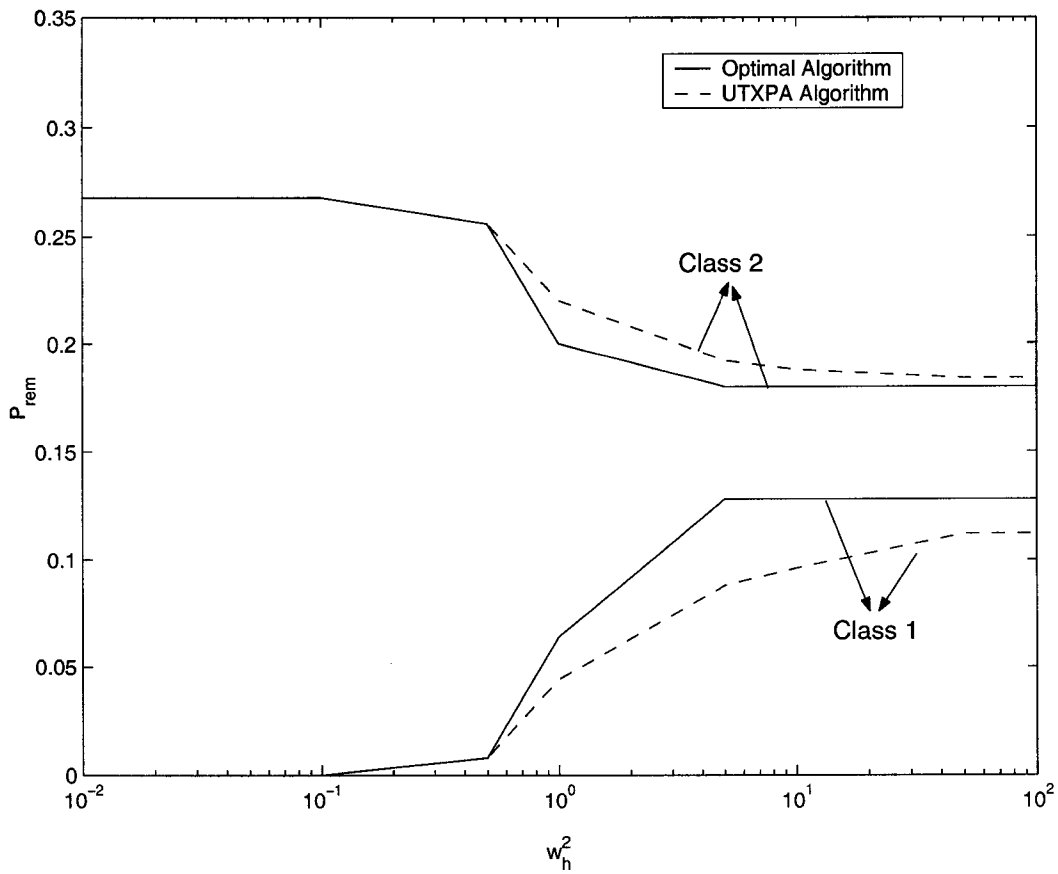

Figure 2.8. *Removal probability comparison among forward link power allocation algorithms in single-cell system.*

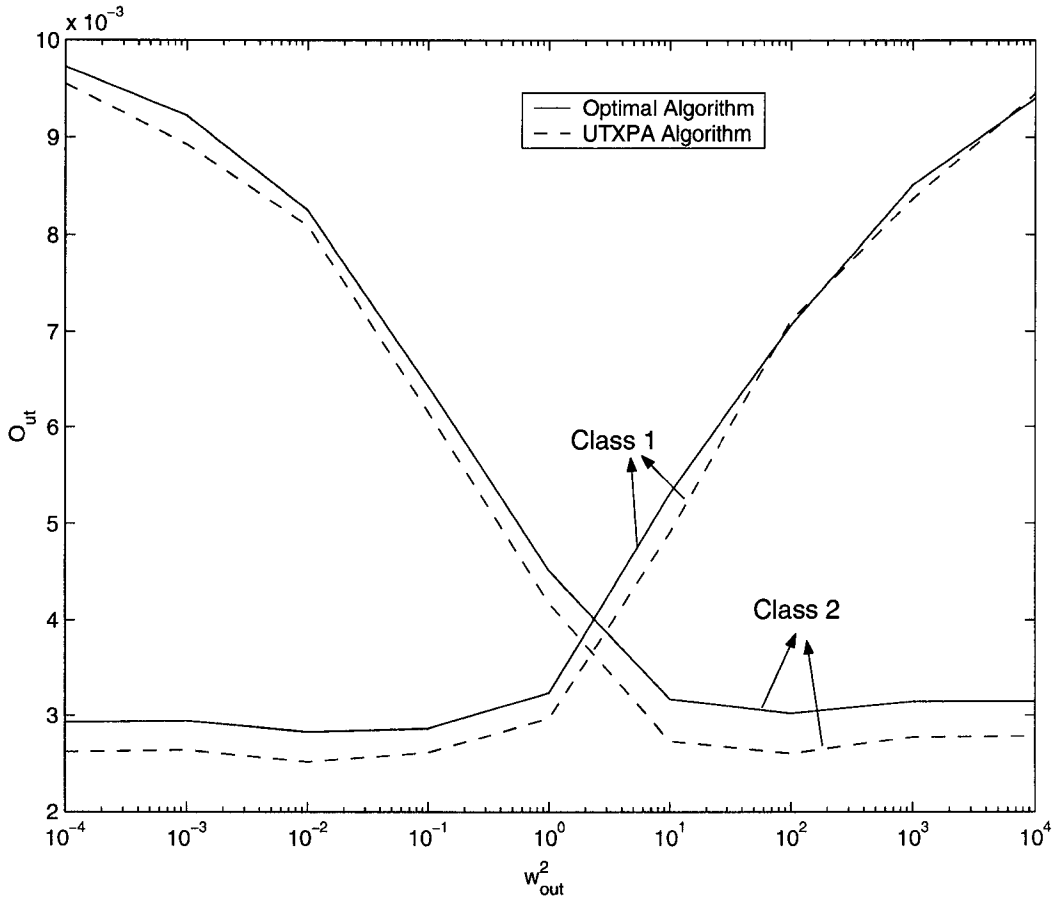

Figure 2.9. *Outage probability comparison among forward link power allocation algorithms in single-cell system.*

Table 2.1. *Power Allocation Algorithms Comparison for Multiple-Cell System.*

N		H	P^1_{rem}	P^2_{rem}	P^1_{out}	P^2_{out}
63	optimal	30.74	0.0520	0.1333	2.63×10^{-3}	4.23×10^{-3}
	UTXPA	30.54	0.0120	0.1467	2.40×10^{-3}	3.72×10^{-3}
127	optimal	35	0	0	4.47×10^{-5}	3.20×10^{-5}
	UTXPA	35	0	0	4.47×10^{-5}	3.20×10^{-5}

2.5 Conclusions

In this chapter, single-cell and multiple-cell DS-CDMA systems supporting heterogeneous traffic have been investigated when DD is used at the receiver. For the reverse link, the effect of imperfect power control on the system performance has been studied through theoretical analysis and numerical examples. The reverse link performance has been found to be sensitive to power control errors. For the forward link, the system performance has been analyzed and two algorithms have been proposed to deal with the power allocation problem at BSs. Numerical examples for the forward link have shown that the performance of the proposed UTXPA algorithm is close to that of the proposed optimal algorithm with considerably reduced computational complexity.

Appendix 2.A

Analysis of Outer-cell Interference in the Reverse Link of DS-CDMA Systems Supporting Homogeneous Traffic

The assumptions for the analysis of the reverse link outer-cell interference are as follows:

1. Mobiles are controlled by the corresponding nearest BSs, which are located at the centers of the equal-size hexagonal cells;
2. Mobiles have equal probability to move to any place within a cell;
3. The reference BS, which is numbered 0, is affected only by the first tier neighboring cells, whose BSs are numbered from 1 to 6 (refer to Fig. 2.10);
4. The characteristics of channels are the same anywhere in the system.

Due to the symmetric nature of the hexagonal cell, we only consider one interference mobile in the first neighboring cell, denoted as 'A' in Fig. 2.10. The analysis of mobile A can be generalized to other interferers and other neighboring cells. It is known that the

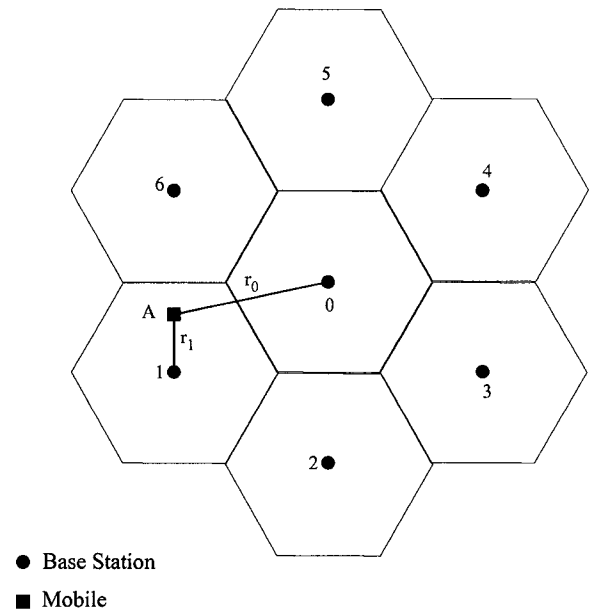

Figure 2.10. *Reverse link model in multiple-cell DS-CDMA system.*

transmission power of mobile A is given by [74] [75]

$$T_1 = r_1^{\beta} 10^{(x_p - x_1)/10} Q_1, \tag{2.47}$$

where r_1 is the distance between mobile A and BS-1, β is the path loss factor, Q_1 is the target power level for mobile A at BS-1, x_p and x_1 are zero-mean Gaussian *r.v.*s representing the effect of power control imperfection and shadowing of the channel between mobile A and BS-1. The standard deviations of x_p and x_1 are denoted as σ_p and σ_1, respectively. At BS-0, the interference power generated by mobile A is given as

$$I_1 = \frac{T_1}{r_0^{\beta}} 10^{x_0/10} = \left(\frac{r_1}{r_0}\right)^{\beta} 10^{(x_0 + x_p - x_1)/10} Q_1, \tag{2.48}$$

where r_0 is the distance between mobile A and BS-0. Similar to x_1, x_0 is also a zero-mean Gaussian *r.v.* with standard deviation σ_0, representing the effect of shadowing of the channel between mobile A and BS-0. According to the fourth assumption, we have $\sigma_0 = \sigma_1 = \sigma_L$. Then the conditional PDF of I_1 is given by

$$f(I_1 | r_1, \theta_1) = \frac{10\log_{10} e}{\sqrt{2\pi(2\sigma_L^2 + \sigma_p^2) I_1}} \exp\left\{ -\frac{(10\log_{10} I_1 - \mu_{I_1}(\text{dB}))^2}{2(2\sigma_L^2 + \sigma_p^2)} \right\}, \tag{2.49}$$

where $\mu_{I_1}(\text{dB}) = 10\log_{10}\left[(r_1/r_0)^{\beta} Q_1\right]$.

According to the second assumption, the unconditional PDF of I_1 can be obtained by averaging $f(I_1|r_1,\theta_1)$ over the whole cell [74] [75]. To simplify the problem, we use the circle inscribed in the hexagonal cell, whose radius is denoted as R, to represent the area of the cell. The unconditional PDF of I_1 is given by

$$f(I_1) = \int_{-\pi}^{\pi}\int_{0}^{R} f(I_1|r_1,\theta_1)\frac{1}{\pi R^2}\, r_1\, dr_1\, d\theta_1. \tag{2.50}$$

The first and second moments of I_1 can thus be computed as [76]

$$\begin{aligned}\text{E}(I_1) =& \int_{-\pi}^{\pi}\int_{0}^{R} \text{E}(I_1|r_1,\theta)\frac{1}{\pi R^2}\, r_1\, dr_1\, d\theta_1 \\ =& \frac{Q_1}{\pi R^2}\exp\left\{\frac{\ln^2 10}{200}(2\sigma_L^2+\sigma_p^2)\right\}\int_{-\pi}^{\pi}\int_{0}^{R}\left(\frac{r_1}{r_0}\right)^{\beta} r_1\, dr_1\, d\theta_1 \qquad (2.51)\\ \text{E}(I_1^2) =& \int_{-\pi}^{\pi}\int_{0}^{R} \text{E}(I_1^2|r_1,\theta_1)\frac{1}{\pi R^2}\, r_1\, dr_1\, d\theta_1 \\ =& \frac{Q_1^2}{\pi R^2}\exp\left\{\frac{\ln^2 10}{50}(2\sigma_L^2+\sigma_p^2)\right\}\int_{-\pi}^{\pi}\int_{0}^{R}\left(\frac{r_1}{r_0}\right)^{2\beta} r_1\, dr_1\, d\theta_1. \qquad (2.52)\end{aligned}$$

The simulated PDF of I_1 is presented in Fig. 2.11. In addition, the PDF of a log-normally distributed *r.v.* $\hat{I}_1$, whose first and second moments are given by (2.51) and (2.52), is also presented. It is observed that the PDF of I_1 is well approximated by that of $\hat{I}_1$, whose mean and variance in dB can be obtained as

$$\mu_{I_1}(\text{dB}) = 10/\ln 10\left[\,2\ln\text{E}(I_1) - \frac{1}{2}\ln\text{E}(I_1^2)\,\right] \tag{2.53a}$$

$$\sigma_{I_1}^2(\text{dB}) = 100/\ln^2 10\left[\,\ln\text{E}(I_1^2) - 2\ln\text{E}(I_1)\,\right]. \tag{2.53b}$$

It is observed that $\sigma_{I_1}^2(\text{dB})$ is independent of Q_1 and can be expressed as $\sigma_I^2(\text{dB})$.

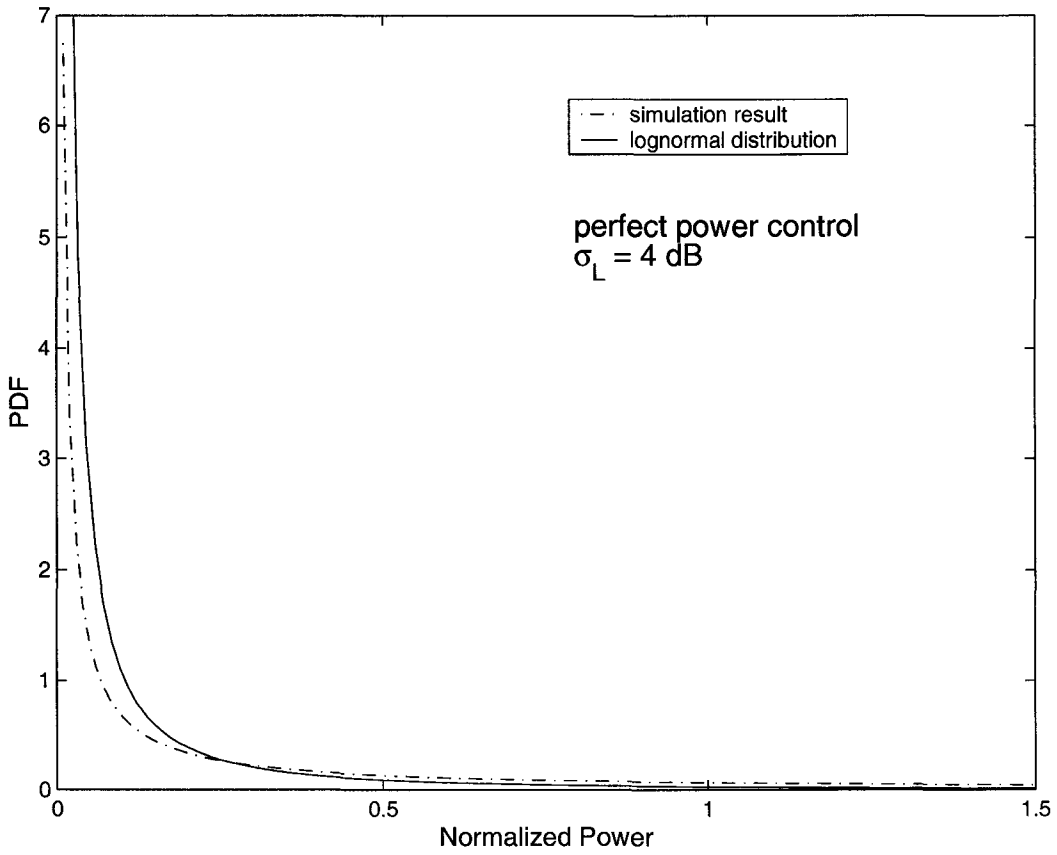

Figure 2.11. *Comparison of log-normal distribution and area-averaged interference PDF.*

Appendix 2.B

Assume that X and Y are log-normal *r.v.*s with logarithmic mean and variance being $\mu_X(\text{dB})$, $\sigma_X^2(\text{dB})$ and $\mu_Y(\text{dB})$, $\sigma_Y^2(\text{dB})$, respectively, i.e., $10\log_{10}X$ and $10\log_{10}Y$ are normal *r.v.*s. If $Z = X/Y$, then it is easy to show that

$$10\log_{10}Z = 10\log_{10}X - 10\log_{10}Y \tag{2.54}$$

is also a normal *r.v.* with mean $\mu_Z(\text{dB}) = \mu_X(\text{dB}) - \mu_Y(\text{dB})$ and variance $\sigma_Z^2(\text{dB}) = \sigma_X^2(\text{dB}) + \sigma_Y^2(\text{dB})$. Therefore, Z is a log-normal *r.v.* with logarithmic mean and variance $\mu_Z(\text{dB})$ and $\sigma_Z^2(\text{dB})$.

Chapter 3

Fast Converging Adaptive MMSE Multiuser Detector

Adaptive MMSE multiuser detector is a promising candidate of the demodulator in DS-CDMA systems and has attracted considerable research interest [20, 21, 22, 23, 24, 25, 77, 78]. It can be implemented as an adaptive tapped-delay-line filter for each desired user that is adapted with the help of training sequence or blindly. The computational complexity involved in the demodulation is comparable to that of the conventional MF receiver, yet a significant performance improvement can be achieved.

In the adaptive MMSE multiuser detectors, tracking speed and computational load are two major concerns. In order to improve the tracking speed in a time varying channel or to reduce the required length of training sequence, fast converging adaptive MMSE detectors with low computational complexity are required. Some algorithms involving low computational complexity, such as the least-mean-square (LMS) algorithm, have been applied to the adaptive MMSE multiuser detector [20]. In communication channels with severe near-far problem, however, the adaptive MMSE detectors for weak power users usually converge much slower than those for strong power users.

To deal with this problem, a fast converging adaptive MMSE multiuser detector is proposed in this chapter where the convergence rate of the adaptive detector is increased by the GSIC technique [30, 31, 79]. After the adaptive MMSE detectors for strong power users converge, the strong power signals are reconstructed based on the steady state parameters

of the corresponding adaptive detectors and then the received signal is updated by subtracting the reconstructed signals successively. Compared with the original received signal, the updated received signal becomes less MAI corrupted. In the proposed detector, the updated received signal is taken as the input of the weak power user detectors and the convergence rates of these detectors are considerably increased. As can be shown, there is no separate channel estimation required in the proposed method. The order of cancellation depends on the convergence rates of the detectors and the estimated signals required for SIC are obtained from the tap-weights and outputs of the converged adaptive detectors. The transient MSE analysis is presented to explain the different convergence rates of adaptive detectors for users with different power and the BER performance analysis of the proposed detector is also presented in this chapter. Simulation results show that the proposed method is robust in various near-far scenarios.

This chapter is organized as follows. In Section 3.1, we describe the considered system. Section 3.2 presents the proposed fast converging adaptive MMSE multiuser detector and discusses the estimation of the parameters which are needed in the proposed detector. In Section 3.3, the transient MSE analysis and the BER performance analysis of the proposed detector are given. Some numerical examples are presented in Section 3.4 and conclusions are made in Section 3.5.

3.1 System Description

Consider an asynchronous BPSK DS-CDMA system with K users. Each of the users is assigned a distinct signature waveform, namely,

$$c_k(t) = \sum_{i=0}^{N-1} c_k^i \psi(t - iT_c), \quad \text{for } 0 \leq t \leq T;\ k = 1,\ \ldots,\ K$$

where T is the symbol interval, T_c is the chip interval, $N = T/T_c$ is the processing gain, and $\psi(t)$ is the chip waveform which only takes nonzero value in the interval $[0,\ T_c]$. $c_k(t)$ is usually normalized so that $\|c_k(t)\|^2 = 1$. $\mathbf{c}_k = [\ c_k^1\ c_k^2\ \cdots\ c_k^N\ ]^T$ (for $k = 1,\ \ldots,\ K$)

is the kth user's signature code. Let the receiver collect M samples per chip, then the discrete-time baseband transmitted signal of the kth user at sample rate can be expressed as

$$x_k(n) = \sum_{i=-\infty}^{\infty} a_k b_k(i) s_k(n - iMN), \tag{3.1}$$

where n is the sampling index, a_k is the complex-valued amplitude of the kth user signal, $b_k(i) \in \{+1, -1\}$ is the information symbol, and $\mathbf{s}_k = [\, s_k(1)\ s_k(2)\ \cdots\ s_k(MN)\,]^T = [\, c_k(1)\ c_k(2)\ \cdots\ c_k(MN)\,]^T / \| [\, c_k(1)\ c_k(2)\ \cdots\ c_k(MN)\,] \|$ with $\|\mathbf{s}_k\|^2 = 1$ and $c_k(n) = c_k(t)|_{t=nT_c/M}$. Let $x_k(n)$ be transmitted through a multipath fading channel whose impulse response can be described as [1]

$$g_k(t) = \sum_{l=1}^{L_k} f_k \alpha_{kl} \delta(t - \tau_{kl}), \tag{3.2}$$

where $\delta(t)$ is a unit impulse function, L_k is the number of resolvable paths of the kth user received signal, τ_{kl} and $f_k\alpha_{kl}$ are the excess delay and the complex channel coefficient of the lth path for the received signal of the kth user with $\sum_{l=1}^{L_k} |\alpha_{kl}|^2 = 1$. Then, the received discrete-time signal due to the kth user is

$$r_k(n) = \sum_{j=-\infty}^{\infty} x_k(j) g_k(n - d_k M - j), \tag{3.3}$$

where $g_k(n) = g_k(t)|_{t=nT_c/M}$ with T_c being the chip period, and d_k is the delay of the kth user in chip periods. From (3.1) and (3.3), we obtain that

$$r_k(n) = \sum_{i=-\infty}^{\infty} A_k b_k(i) h_k(n - d_k M - iMN) \tag{3.4}$$

$$h_k(n) = \sum_{m=-\infty}^{\infty} s_k(m) g_k(n - m)/f_k, \tag{3.5}$$

where $A_k = a_k f_k$, $h_k(n)$ represents the distorted spreading sequence of the kth user due to the multipath fading channel. The received signal consists of the sum of all user signals and noise which is given as

$$r(n) = \sum_{k=1}^{K} r_k(n) + N(n), \tag{3.6}$$

where $N(n)$ is complex AWGN with independent real and imaginary components, whose mean is zero and $\mathrm{E}\{N(m)N^*(n)\} = 2\sigma^2\delta(n-m)$.

In the following discussion, it is assumed that the multipath channel has maximum order $q = \max_k L_k$ with coefficients vector $\mathbf{g}_k = [\, g_k(1)\; g_k(2)\; \cdots\; g_k(q)\,]^T/f_k$ and that the receiver is synchronized to the desired user's first path. To make the description clearer, the case of $M = 1$ will be considered in this chapter. Based on the signal model stated above, it is straightforward to extend it for the case $M > 1$ [80].

Without the loss of generality, it is assumed that the desired user is the kth user. At the receiver for the kth user, defining $\mathbf{r}_k(i) = [\, r(iN + d_k + 1)\; r(iN + d_k + 2)\; \cdots\; r(iN + d_k + N + q - 1)\,]^T$ as the received vector, from (3.4)-(3.6), we have

$$\begin{aligned}\mathbf{r}_k(i) = {} & A_k\mathbf{h}_{0,k}b_k(i) + A_k\mathbf{h}_{-1,k}b_k(i-1) + A_k\mathbf{h}_{1,k}b_k(i+1) \\ & + \sum_{\substack{j=1 \\ j\neq k}}^{K}\left[A_j\mathbf{h}_{-1,j}^{(k)}b_j^{(k)}(i-1) + A_j\mathbf{h}_{0,j}^{(k)}b_j^{(k)}(i) + A_j\mathbf{h}_{1,j}^{(k)}b_j^{(k)}(i+1)\right] + \mathbf{n}, \quad (3.7)\end{aligned}$$

where the first term represents the desired signal, the second and the third terms are ISI, the fourth term is the combination of MAI and $\mathbf{n}$ is a vector of zero-mean complex Gaussian noise with $\mathrm{E}\{\mathbf{n}\mathbf{n}^H\} = 2\sigma^2\mathbf{I}$. Denoting $\mathbf{h}_k = [\, h_k(1)\; h_k(2)\; \cdots\; h_k(N+q-1)\,]^T$ as the distorted spreading sequence of the kth user and $d_{jk} = d_j - d_k$, if $d_{jk} \geq 0$ (for $j = 1, \ldots, K$),

$$\mathbf{h}_{0,j}^{(k)} = [\, \underbrace{0\;\cdots\;0}_{d_{jk}}\; h_j(1)\; \cdots\; h_j(N+q-1-d_{jk})\,]^T \quad (3.8a)$$

$$\mathbf{h}_{-1,j}^{(k)} = [\, h_j(N-d_{jk}+1)\; \cdots\; h_j(N+q-1)\; \underbrace{0\;\cdots\;0}_{N-d_{jk}}\,]^T \quad (3.8b)$$

$$\mathbf{h}_{1,j}^{(k)} = \begin{cases} [\,0\;\cdots\;0\,]^T & \text{for } d_{jk} > q-1 \\ [\, \underbrace{0\;\cdots\;0}_{N+d_{jk}}\; h_j(1)\; \cdots\; h_j(q-d_{jk}-1)\,]^T & \text{otherwise} \end{cases} \quad (3.8c)$$

and if $d_{jk} < 0$ (for $j = 1, \ldots, K$),

$$\mathbf{h}_{0,j}^{(k)} = [\, h_j(1 - d_{jk}) \cdots h_j(N + q - 1) \underbrace{0 \cdots 0}_{-d_{jk}} \,]^T \tag{3.9a}$$

$$\mathbf{h}_{-1,j}^{(k)} = \begin{cases} [\, 0 \cdots 0 \,]^T & \text{for } |d_{jk}| > q - 1 \\ [\, h_j(N - d_{jk} + 1) \cdots h_j(N + q - 1)\, 0 \cdots 0 \,]^T & \text{otherwise} \end{cases} \tag{3.9b}$$

$$\mathbf{h}_{1,j}^{(k)} = [\, 0 \cdots 0\, h_j(1) \cdots h_j(q - d_{jk} - 1) \,]^T \tag{3.9c}$$

In (3.7), in order to simplify the notation, $\mathbf{h}_{0,k}^{(k)}$, $\mathbf{h}_{-1,k}^{(k)}$ and $\mathbf{h}_{1,k}^{(k)}$ are denoted as $\mathbf{h}_{0,k}$, $\mathbf{h}_{-1,k}$ and $\mathbf{h}_{1,k}$, respectively.

With $M = 1$, it can be shown from (3.5) that

$$\mathbf{h}_k = \mathbf{S}_k \mathbf{g}_k = \begin{bmatrix} c_k(1) & & \mathbf{0} \\ \vdots & \ddots & \\ & & c_k(1) \\ c_k(N) & & \\ & \ddots & \vdots \\ \mathbf{0} & & c_k(N) \end{bmatrix} \mathbf{g}_k \tag{3.10}$$

And we have $\mathbf{h}_{0,k} = \mathbf{h}_k$.

Based on (3.7), the received vector at the receiver for the kth user can also be expressed as

$$\begin{aligned} \mathbf{r}_k(i) = {} & \mathbf{p}_{0,k} b_k(i) + \mathbf{p}_{-1,k} b_k(i-1) + \mathbf{p}_{1,k} b_k(i+1) \\ & + \sum_{\substack{j=1 \\ j \neq k}}^{K} \left[\mathbf{p}_{-1,j}^{(k)} b_j^{(k)}(i-1) + \mathbf{p}_{0,j}^{(k)} b_j^{(k)}(i) + \mathbf{p}_{1,j}^{(k)} b_j^{(k)}(i+1) \right] + \mathbf{n}, \end{aligned} \tag{3.11}$$

where $\mathbf{p}_{0,k} = A_k \mathbf{h}_k$, $\mathbf{p}_{-1,k} = A_k \mathbf{h}_{-1,k}$, $\mathbf{p}_{1,k} = A_k \mathbf{h}_{1,k}$, $\mathbf{p}_{-1,j}^{(k)} = A_j \mathbf{h}_{-1,j}^{(k)}$, $\mathbf{p}_{0,j}^{(k)} = A_j \mathbf{h}_{0,j}^{(k)}$ and $\mathbf{p}_{1,j}^{(k)} = A_j \mathbf{h}_{1,j}^{(k)}$ ($j = 1, \ldots, K$, $j \neq k$). $b_k(i-1)$ and $b_k(i+1)$ are the intersymbol interference symbols and $b_j^{(k)}(i-1)$, $b_j^{(k)}(i)$ and $b_j^{(k)}(i+1)$ are the interference symbols from the jth user observed at the receiver for the kth user [22]. Notice that the values of $\mathbf{p}_{-1,j}^{(k)}$, $\mathbf{p}_{0,j}^{(k)}$, $\mathbf{p}_{1,j}^{(k)}$ and $b_j^{(k)}(i-1)$, $b_j^{(k)}(i)$, $b_j^{(k)}(i+1)$ depend directly on the value of $d_{jk} = d_j - d_k$, i.e., observed at the receivers for different users, the same interferer may

distribute different interference vectors and interference symbols. In (3.7) and (3.11), the effect of ISI in multipath channel can be neglected if $q \ll N$.

In this chapter, a slow channel fading is assumed, i.e., the channel parameters remain unchanged throughout the observation period.

3.2 Fast Converging Adaptive MMSE Multiuser Detector Based on Groupwise Successive Interference Cancellation

In this section, we first briefly review the adaptive MMSE multiuser detector, then the proposed fast converging adaptive MMSE multiuser detector is presented and the parameter estimation problem in the proposed detector is also discussed.

3.2.1 Adaptive MMSE Multiuser Detector

The adaptive MMSE multiuser detector for the kth user filters the received vector $\mathbf{r}_k(i)$ with an $(N+q-1)$-tap delay line filter $\mathbf{w}_k$, whose output is used to make the final decision, i.e., $\hat{b}_k(i) = \text{sgn}(\Re[\mathbf{w}_k^H \mathbf{r}_k(i)])$. The tap-weights of the adaptive MMSE filter $\mathbf{w}_k$ are adapted according to a certain adaptive algorithm. In this chapter, the standard LMS algorithm is used [81, 82]. If the step size is chosen small enough, the converged adaptive MMSE multiuser detector can be well approximated by the corresponding linear MMSE detector, whose tap-weights are chosen to minimize the MSE

$$J_k(i) = \text{E}\{|b_k(i) - \mathbf{w}_k^H \mathbf{r}_k(i)|^2\}. \tag{3.12}$$

3.2.2 GSIC-Based Fast Converging Adaptive MMSE Multiuser Detector

In typical CDMA systems with near-far problems, the adaptive MMSE multiuser detectors for users with different power usually have different convergence rates, i.e., the adaptive detectors for strong power users are likely to converge faster than those for weak power users, as will be illustrated by numerical examples in Section 3.4. To increase the convergence rate of the adaptive detectors for weak power users, the recursive-least-square (RLS) algorithm can be used [21, 83]. However, the RLS algorithm use $2.5\tilde{N}^2 + 4.5\tilde{N}$ multiply operations per iteration, while the LMS algorithm only need $2\tilde{N} + 1$ multiply operations per iteration with $\tilde{N}$ being the number of taps in the filter, i.e., the computational complexity of the RLS algorithm is significantly increased relative to the LMS algorithm. The high computational complexity of the RLS algorithm makes its practical implementations difficult.

In the proposed method, we first estimate the parameters of strong power user signals and reconstruct the signals of these users. The received signal is then updated by subtracting the reconstructed strong power user signals. Consequently, the updated received signal becomes less MAI corrupted. Taking the updated received signal as the input of weak power user detectors leads to a significant increase in the convergence rates of these detectors, thus alleviating the near-far problem.

In Fig. 3.1, the proposed multiuser detector scheme is shown. The delay in the figure is one symbol duration. If several strong power interferers are present in the CDMA system, a groupwise successive cancellation method can be adopted to cancel their interference in groups sequentially [31]. The order of groupwise successive cancellation depends on the relative power of user signals, i.e., user signals with the same or similar power are estimated and canceled from the received signal at the same time.

However, the user power is not known beforehand, instead, the cancellation order is determined according to the convergence rates of detectors for different users. Once the

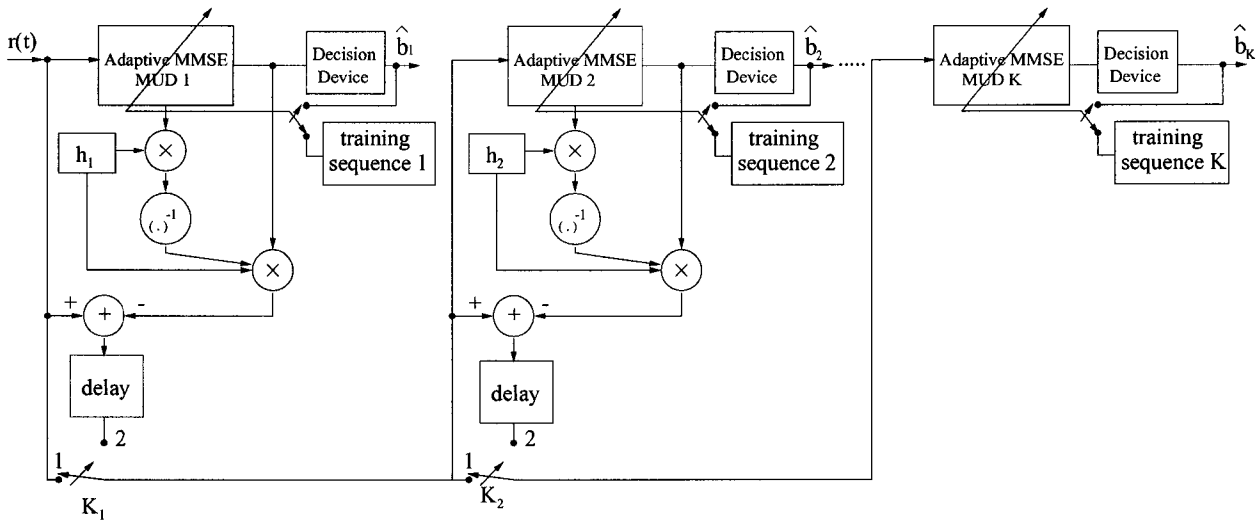

Figure 3.1. *The fast converging adaptive MMSE multiuser detector*

adaptive detector for the kth user reaches steady state, the switch $\mathrm{K}_k (1 \leq k \leq K-1)$ in Fig. 3.1 is adjusted from position 1 to position 2. By doing so, the kth user signal is reconstructed and subtracted from the received signal.

For the simplicity of discussion, the users are numbered and grouped according to their received power in Fig. 3.1, with user 1 and user K being the strongest and the weakest power user, respectively. It is assumed that the signals of user $1, \ldots,$ user K_1 have the same or similar power which is the highest among all the user signals in the system. In the proposed detector, the signals of user $1, \ldots,$ user K_1 are the first group of signals to be estimated and canceled. Similarly, the signals of user $K_1 + \cdots + K_{l-1} + 1, \ldots,$ user $K_1 + \cdots + K_{l-1} + K_l$ are the lth group of signals to be estimated and canceled, i.e., there are K_l users in this group ($l \geq 2$). For the convenience of the following description, we define the user index set G_l which consists of the indices of all users in the lth group. If not stated otherwise, perfect knowledge of spreading sequences and timing of user signals are assumed in the following discussion.

3.2.3 Parameter Estimation in the Proposed Method

It is noted that after the adaptive detectors reach steady state, the interference presented in the detector outputs are well suppressed. Therefore, compared with estimating the user signals from the detector's input, the estimation using its output in steady state tends to present a higher degree of accuracy. After the adaptive detector for the kth user reaches steady state, the interference presented in the output of the detector becomes negligible, i.e., $\mathbf{w}_k^{*H}\mathbf{r}_k(i) \approx b_k(i)$. Also note that $A_k \approx (\mathbf{w}_k^{*H}\mathbf{h}_k)^{-1}$. Therefore, as shown in Fig. 3.1, the signal of the kth user can be estimated as

$$(\mathbf{w}_k^{*H}\mathbf{h}_k)^{-1}(\mathbf{w}_k^{*H}\mathbf{r}_k(i))\mathbf{h}_k. \tag{3.13}$$

From (3.13), it is shown that the knowledge of distorted spreading sequences of the stronger users $\mathbf{h}_k$ is needed in the proposed detector. In the above discussion, this is assumed perfectly known.

It is noted that the MMSE detector $\mathbf{w}_k^*$ satisfies $\mathbf{w}_k^* = \mathbf{R}_k^{-1}\mathbf{h}_k$ with $\mathbf{R}_k$ being the correlation matrix of the received signal at the receiver for the kth user [84]. Therefore, the distorted spreading sequence $\mathbf{h}_k$ can be estimated as

$$\hat{\mathbf{h}}_k = \hat{\mathbf{R}}_k\hat{\mathbf{w}}_k^* \tag{3.14}$$

where $\hat{\mathbf{w}}_k^*$ is the converged adaptive detector tap weights, $\hat{\mathbf{R}}_k$ is the estimated correlation matrix of the received signal at the receiver for the kth user, which is given as $\hat{\mathbf{R}}_k = \frac{1}{L}\sum_{i=1}^{L}\mathbf{r}_k(i)\mathbf{r}_k(i)^H$ with L being the training sequence length.

The process of estimating the distorted spreading sequences is necessary for the systems with multipath channels. In the system with single-path channels, however, $\mathbf{h}_k$ simplifies to $\mathbf{c}_k$. If $\mathbf{c}_k$ is known at the receiver, then the above estimation process of (3.14) is not needed. Although the adaptive MMSE multiuser detector was proposed to cancel MAI in the absence of knowledge of other users' spreading waveforms, in some applications such as reverse link in wireless communications, the knowledge of all users' spreading sequences is easily available at the base station receivers.

3.3 Performance Analysis

In this section, the transient MSE analysis is first presented to explain the phenomenon of different convergence rates of the adaptive detectors for users with different power. Then the BER performance analysis of the proposed multiuser detector is presented.

3.3.1 Transient Mean-Squared Error Analysis

Traditionally, the eigenvalue spread of the tap input correlation matrix is taken as a measure of the convergence rate of the LMS algorithm [81, 82, 85]. However, since the eigenvalue spreads of the tap input correlation matrixes of the detectors for different users are almost the same in asynchronous system and are exactly the same in synchronous system, this measurement cannot explain the phenomenon of different convergence rates of the adaptive detectors for users with different power. To explain this phenomenon, a closer look at the transient MSE analysis will be given.

The time evolution of the MSE is given by [81, 86]

$$J_k(i) = \sum_{n=1}^{N+q-1} \gamma_n t_n^i + J_{min} + J_{ex}(\infty) \tag{3.15}$$

where i is the number of iterations, t_n is the nth eigenvalue of the matrix $\mathbf{B}$ which is an $(N+q-1)$-by-$(N+q-1)$ matrix with elements

$$b_{jk} = \begin{cases} (1-\mu\lambda_j)^2 & j = k \\ \mu^2\lambda_j\lambda_k & j \neq k \end{cases} \tag{3.16}$$

and the associated eigenvector corresponding to t_n is $\mathbf{v}_n$. μ is the step size of the LMS algorithm. The vector $\boldsymbol{\lambda} = [\ \lambda_1\ \lambda_2\ \cdots\ \lambda_{N+q-1}\ ]^T$ is the vector of eigenvalues of the correlation matrix $\mathbf{R}_k = \mathrm{E}\{\mathbf{r}_k(i)\mathbf{r}_k(i)^H\}$, whose matrix of eigenvectors is denoted as $\mathbf{Q}$. γ_n in (3.15) is defined by

$$\gamma_n = \boldsymbol{\lambda}^T\mathbf{v}_n\mathbf{v}_n^T[\mathbf{x}(0) - \mathbf{x}(\infty)] \tag{3.17}$$

where $\mathbf{x}(i)$ is the vector of diagonal elements of the matrix $\mathbf{X}(i)$, which is given by

$$\mathbf{X}(i) = \mathbf{Q}^H\mathbf{K}(i)\mathbf{Q} \tag{3.18}$$

and $\mathbf{K}(i)$ is the auto-covariance matrix of the tap weights at iteration i. The elements of the vector $\mathbf{x}(\infty)$ are found to be

$$x_n(\infty) = \frac{\mu J_{min}}{2 - \mu\lambda_n} \qquad \text{for } n = 1,\ 2,\ \cdots,\ N+q-1 \tag{3.19}$$

where J_{min} is the minimum MSE pertaining to the optimum linear MMSE solution. And $J_{ex}(\infty)$ in (3.15) is given by

$$J_{ex}(\infty) = \boldsymbol{\lambda}^T \mathbf{x}(\infty) \tag{3.20}$$

It is obvious from (3.15) that the transient component of $J_k(i)$ is $\sum_{n=1}^{N+q-1} \gamma_n t_n^i$, with γ_n being the constant coefficient. The LMS algorithm is convergent if the step size μ is small enough so that all the values of t_n are less than 1. The convergence rate depends not only on the values of t_n, but also on the constant coefficients γ_n. The convergence rate is precisely determined by the values of t_n of the dominant terms of $J_k(i)$. As will be illustrated by numerical examples in Section 3.4, although the values of t_n for users with different power in the same system are similar in asynchronous system and are exactly the same in synchronous system, their associated values of γ_n are different, i.e., adaptive detectors for users with different power have different dominant transient terms. This leads to the different convergence rates of these detectors.

3.3.2 BER Analysis

3.3.2.1 the First Stage

The MMSE solution of $\mathbf{w}_k$ satisfies $\nabla_{\mathbf{w}_k} J_k(i) = 0$, which can be shown to be [22, 81]

$$\mathbf{w}_k^* = \left(1 + \mathbf{p}_{0,k}^H \mathbf{A}_k^{-1} \mathbf{p}_{0,k}\right)^{-1} \mathbf{A}_k^{-1} \mathbf{p}_{0,k} \tag{3.21}$$

where

$$\mathbf{A}_k = \mathbf{p}_{-1,k}\mathbf{p}_{-1,k}^H + \mathbf{p}_{1,k}\mathbf{p}_{1,k}^H + \sum_{\substack{j=1 \\ j\neq k}}^{K} \left[\mathbf{p}_{0,j}^{(k)}(\mathbf{p}_{0,j}^{(k)})^H + \mathbf{p}_{-1,j}^{(k)}(\mathbf{p}_{-1,j}^{(k)})^H + \mathbf{p}_{1,j}^{(k)}(\mathbf{p}_{1,j}^{(k)})^H\right] + 2\sigma^2\mathbf{I}. \tag{3.22}$$

Then the output of the MMSE filter is

$$\begin{aligned} z_k(i) &= \mathbf{w}_k^{*H}\mathbf{r}_k(i) \\ &= (1+\mathbf{p}_{0,k}^H\mathbf{A}_k^{-1}\mathbf{p}_{0,k})^{-1}\{\mathbf{p}_{0,k}^H\mathbf{A}_k^{-1}\mathbf{p}_{0,k}b_k(i)+\mathbf{p}_{0,k}^H\mathbf{A}_k^{-1}[\mathbf{p}_{-1,k}b_k(i-1)+\mathbf{p}_{1,k}b_k(i+1)] \\ &\quad +\mathbf{p}_{0,k}^H\mathbf{A}_k^{-1}\sum_{\substack{j=1\\ j\neq k}}^{K}[\mathbf{p}_{-1,j}^{(k)}b_j^{(k)}(i-1)+\mathbf{p}_{0,j}^{(k)}b_j^{(k)}(i)+\mathbf{p}_{1,j}^{(k)}b_j^{(k)}(i+1)]+\mathbf{p}_{0,k}^H\mathbf{A}_k^{-1}\mathbf{n}\} \quad (3.23) \end{aligned}$$

It is easy to show that $\mathbf{A}_k^{-1}$ is Hermitian and $\mathbf{p}_{0,k}^H\mathbf{A}_k^{-1}\mathbf{p}_{0,k}$ is real. The residual noise plus ISI and MAI at the detector output can be approximated as a Gaussian *r.v.*, which turns out to be quite good for the MMSE detector and is commonly used in the analysis of MMSE multiuser detector [68, 87]. Therefore, (3.23) simplifies to

$$z_k(i) = (1+\mathbf{p}_{0,k}^H\mathbf{A}_k^{-1}\mathbf{p}_{0,k})^{-1}\{\mathbf{p}_{0,k}^H\mathbf{A}_k^{-1}\mathbf{p}_{0,k}b_k(i)+\tilde{n}_k(i)\} \quad (3.24)$$

where $\tilde{n}_k(i)$ is a zero-mean complex Gaussian *r.v.* with independent real and imaginary components. It can be easily shown from (3.23) and (3.24) that the variance of $\tilde{n}_k(i)$ is given by

$$\begin{aligned} \mathrm{var}[\tilde{n}_k(i)] =& \left|\mathbf{p}_{0,k}^H\mathbf{A}_k^{-1}\mathbf{p}_{-1,k}\right|^2+\left|\mathbf{p}_{0,k}^H\mathbf{A}_k^{-1}\mathbf{p}_{1,k}\right|^2+\sum_{\substack{j=1\\ j\neq k}}^{K}\left(\left|\mathbf{p}_{0,k}^H\mathbf{A}_k^{-1}\mathbf{p}_{-1,j}^{(k)}\right|^2\right. \\ &\left.+\left|\mathbf{p}_{0,k}^H\mathbf{A}_k^{-1}\mathbf{p}_{0,j}^{(k)}\right|^2+\left|\mathbf{p}_{0,k}^H\mathbf{A}_k^{-1}\mathbf{p}_{1,j}^{(k)}\right|^2\right)+2\sigma^2\mathbf{p}_{0,k}^H\mathbf{A}_k^{-2}\mathbf{p}_{0,k}=\tilde{\sigma}_k^2 \quad (3.25) \end{aligned}$$

Therefore, the BER for the user signals in the first group is given by [9]

$$P_{e,k} = Q\left[\frac{\sqrt{2}\mathbf{p}_{0,k}^H\mathbf{A}_k^{-1}\mathbf{p}_{0,k}}{\tilde{\sigma}_k}\right] \qquad \text{for } k\in G_1 \quad (3.26)$$

where $Q(x)=\frac{1}{\sqrt{2\pi}}\int_x^\infty e^{-t^2/2}dt$.

From (3.11), (3.13) and (3.21)-(3.24), the estimated kth user's signal can be expressed as

$$(\mathbf{w}_k^{*H}\mathbf{h}_k)^{-1}(\mathbf{w}_k^{*H}\mathbf{r}_k(i))\mathbf{h}_k = A_k b_k(i)\mathbf{h}_k + n_k(i)\mathbf{h}_k \quad (3.27)$$

where $n_k(i)=A_k(\mathbf{p}_{0,k}^H\mathbf{A}_k^{-1}\mathbf{p}_{0,k})^{-1}\tilde{n}_k(i)$. After canceling the effect of the kth user signal using the estimated one, the remainder of the kth user signal in the updated received signal

is $\mathbf{e}_k = -n_k(i)\mathbf{h}_k$. $n_k(i)$ in (3.27) is also a Gaussian *r.v.* whose variance is

$$\text{var}[n_k(i)] = \left| \frac{A_k}{\mathbf{p}_{0,k}^H \mathbf{A}_k^{-1} \mathbf{p}_{0,k}} \right|^2 \tilde{\sigma}_k^2 = \sigma_k^2 \tag{3.28}$$

3.3.2.2 the Successive Stages

The received vector at the receiver for any user in the lth group is given as

$$\begin{aligned}
\mathbf{r}_{kl}(i) = {} & \mathbf{p}_{0,k} b_k(i) + \mathbf{p}_{-1,k} b_k(i-1) + \mathbf{p}_{1,k} b_k(i+1) \\
& - \sum_{s=1}^{l-1} \sum_{j \in G_s} \left[n_{js}(i-1)\mathbf{h}_{-1,j}^{(k)} + n_{js}(i)\mathbf{h}_{0,j}^{(k)} + n_{js}(i+1)\mathbf{h}_{1,j}^{(k)} \right] \\
& + \sum_{\substack{j=K_1+\cdots+K_{l-1}+1 \\ j \neq k}}^{K} \left[\mathbf{p}_{0,j}^{(k)} b_j^{(k)}(i) + \mathbf{p}_{-1,j}^{(k)} b_j^{(k)}(i-1) + \mathbf{p}_{1,j}^{(k)} b_j^{(k)}(i+1) \right] \\
& + \mathbf{n}, \qquad \text{for } k \in G_l
\end{aligned} \tag{3.29}$$

where the additional subscript l of the received vector is used to indicate that this process is in the lth stage, $n_{js}(i-1)$, $n_{js}(i)$ and $n_{js}(i+1)$ are the remainder effects of the signal from the jth user, which is in the sth group. The variance of $n_{js}(i-1)$, $n_{js}(i)$ and $n_{js}(i+1)$ is denoted as σ_j^2. If $s = 1$, the value of σ_j^2 can be obtained from (3.25) and (3.28). If $s \geq 2$, the value of σ_j^2 will be given in the following analysis.

Similar to the above derivation, the MMSE filter tap weights for any user in the lth group can be derived as

$$\mathbf{w}_k^* = \left(1 + \mathbf{p}_{0,k}^H \mathbf{A}_{kl}^{-1} \mathbf{p}_{0,k}\right)^{-1} \mathbf{A}_{kl}^{-1} \mathbf{p}_{0,k} \qquad \text{for } k \in G_l \tag{3.30}$$

where

$$\begin{aligned}
\mathbf{A}_{kl} = {} & \mathbf{p}_{-1,k}\mathbf{p}_{-1,k}^H + \mathbf{p}_{1,k}\mathbf{p}_{1,k}^H + \sum_{s=1}^{l-1} \sum_{j \in G_s} \sigma_j^2 \left[\mathbf{h}_{-1,j}^{(k)} (\mathbf{h}_{-1,j}^{(k)})^H + \mathbf{h}_{0,j}^{(k)} (\mathbf{h}_{0,j}^{(k)})^H + \mathbf{h}_{1,j}^{(k)} (\mathbf{h}_{1,j}^{(k)})^H \right] \\
& + \sum_{\substack{j=K_1+\cdots+K_{l-1}+1 \\ j \neq k}}^{K} \left[\mathbf{p}_{-1,j}^{(k)} (\mathbf{p}_{-1,j}^{(k)})^H + \mathbf{p}_{0,j}^{(k)} (\mathbf{p}_{0,j}^{(k)})^H + \mathbf{p}_{1,j}^{(k)} (\mathbf{p}_{1,j}^{(k)})^H \right] + 2\sigma^2 \mathbf{I}
\end{aligned} \tag{3.31}$$

The output of the MMSE filter is

$$z_k(i) = (1 + \mathbf{p}_{0,k}^H \mathbf{A}_{kl}^{-1} \mathbf{p}_{0,k})^{-1} \{\mathbf{p}_{0,k}^H \mathbf{A}_{kl}^{-1} \mathbf{p}_{0,k} b_k(i) + \tilde{n}_{kl}(i)\} \qquad \text{for } k \in G_l \tag{3.32}$$

where $\tilde{n}_{kl}(i)$ is the residual noise plus ISI and MAI, whose variance can be shown from (3.29) and (3.30) to be

$$\begin{aligned}
\text{var}[\tilde{n}_{kl}(i)] =& \left|\mathbf{p}_{0,k}^H \mathbf{A}_k^{-1} \mathbf{p}_{-1,k}\right|^2 + \left|\mathbf{p}_{0,k}^H \mathbf{A}_k^{-1} \mathbf{p}_{1,k}\right|^2 \\
&+ \sum_{s=1}^{l-1} \sum_{j \in G_s} \sigma_j^2 \left(\left|\mathbf{p}_{0,k}^H \mathbf{A}_{kl}^{-1} \mathbf{h}_{-1,j}^{(k)}\right|^2 + \left|\mathbf{p}_{0,k}^H \mathbf{A}_{kl}^{-1} \mathbf{h}_{0,j}^{(k)}\right|^2 + \left|\mathbf{p}_{0,k}^H \mathbf{A}_{kl}^{-1} \mathbf{h}_{1,j}^{(k)}\right|^2 \right) \\
&+ \sum_{\substack{j=K_1+\cdots+K_{l-1}+1 \\ j \neq k}}^{K} \left(\left|\mathbf{p}_{0,k}^H \mathbf{A}_{kl}^{-1} \mathbf{p}_{0,j}^{(k)}\right|^2 + \left|\mathbf{p}_{0,k}^H \mathbf{A}_{kl}^{-1} \mathbf{p}_{-1,j}^{(k)}\right|^2 + \left|\mathbf{p}_{0,k}^H \mathbf{A}_{kl}^{-1} \mathbf{p}_{1,j}^{(k)}\right|^2 \right) \\
&+ 2\sigma^2 \mathbf{p}_{0,k}^H \mathbf{A}_{kl}^{-2} \mathbf{p}_{0,k} = \tilde{\sigma}_k^2
\end{aligned} \tag{3.33}$$

Approximating $\tilde{n}_{kl}(i)$ as a Gaussian *r.v.*, the BER for the user signals in the lth group is given by

$$P_{e,k} = Q\left[\frac{\sqrt{2}\mathbf{p}_{0,k}^H \mathbf{A}_{kl}^{-1} \mathbf{p}_{0,k}}{\tilde{\sigma}_k}\right] \qquad \text{for } k \in G_l \tag{3.34}$$

As discussed above, the kth user signal is estimated as $(\mathbf{w}_k^{*H} \mathbf{h}_k)^{-1} (\mathbf{w}_k^{*H} \mathbf{r}_{kl}(i)) \mathbf{h}_k$, and after cancellation, the remainder affect of this signal in the updated received signal is $\mathbf{e}_k = -n_{kl}(i)\mathbf{h}_k$, where $n_{kl}(i) = A_k (\mathbf{p}_k^H \mathbf{A}_{kl}^{-1} \mathbf{p}_k)^{-1} \tilde{n}_{kl}(i)$ with the variance given as $\text{var}[n_{kl}(i)] = \left|\frac{A_k}{\mathbf{p}_{0,k}^H \mathbf{A}_{kl}^{-1} \mathbf{p}_{0,k}}\right|^2 \tilde{\sigma}_k^2 = \sigma_k^2$.

3.4 Numerical Results

Computer simulations were carried out to evaluate the performance of the proposed fast converging adaptive MMSE multiuser detector and to investigate the accuracy of our analysis. The performance measurements of interest here are the MSE at the output of the detectors and the BER. In the following simulations, a DS-CDMA system with six users was considered. The spreading sequences were length 15 Gold codes. Unless mentioned otherwise, the standard LMS algorithm was used as the tap-weights adaptation rule [81, 82], and

the MSE was obtained through averaging over 100 independent runs of the experiment. In each simulation example, the tap weights were initially set to all zeros and the step size was chosen as indicated. In the systems with single-path channels, spreading sequences of all the users were assumed known at the receiver.

In the first example, a synchronous system was considered. The users of interest are user 1 and user 2, which were received with user 1 having E_b/N_0 30 dB more than that of user 2. The other four interferers were received with E_b/N_0 2 dB, 4 dB, 6 dB and 8 dB less than that of user 2, respectively. The plots of MSE versus time of the detectors for the users of interest using the RLS algorithm, with user 2 received with E_b/N_0 of 10 dB, are given in Fig. 3.2. The plots of MSE versus time when using the standard LMS algorithm with and without the proposed successive cancellation are shown in Fig. 3.3. In the case of "with SIC" in Fig. 3.3, after the first 100 iterations, which is chosen randomly after the detector for the first user has converged, the first user signal was reconstructed and subtracted from the received signal. Then the tap weights of the detector for the second user were adapted from all zeros again. From these figures, it is shown that when the standard LMS algorithm is used and no SIC is applied, the detector for the strong power user tends to converge much faster than the detector for the weak power user. This phenomenon is explained explicitly by the comparison of the transient terms of $J_k(i)$ in (3.15) of the users of interest, which is given in Table 3.1. Although the problem of slow convergence of adaptive detectors for weak power users is not obvious when the RLS algorithm is used, the extremely high computational complexity of the RLS algorithm makes it hardly practical. When the proposed successive cancellation is applied, however, the weak power user detector using the standard LMS algorithm shows a much faster tracking speed.

Fig. 3.4 compares the BER of the proposed detector for user 2 obtained by Monte Carlo simulations with those based on the analysis in Section 3.3. The BERs of the adaptive MMSE and MF receivers are plotted in Fig. 3.4 as references [12]. For comparison purposes, we also plot the BER of the MF detector with SIC presented in [30, 31], where the order and the estimated signals used in the cancellation are determined from the MF

outputs. In Fig. 3.4 and all the following BER performance figures, the BER performance of the adaptive MMSE receiver was obtained by using the RLS algorithm as the detector adaptation rule. From the results obtained, it is found that this MF detector with SIC works well in this system configuration. It is also found that the analysis in Section 3.3 gives a good estimation to the true BER.

However, since in MF receiver, the interference leakage is determined by the projection of the interference signal onto the desired one, the leakage will become non-negligible to the desired signal in the presence of much stronger interference signals. A second example was carried out to illustrate this problem. In the second example, four users were received with equal E_b/N_0, which was 30 dB more than those of the other two users, both of which were received with equal E_b/N_0. The users of interest are user 1 and user 2, which were one of the strong and weak users, respectively. Other simulation parameters were kept the same as those in the first example. The MSE versus time curves of the detectors for the users of interest, obtained from both simulation and computation and with user 2 received with E_b/N_0 of 10 dB are plotted in Fig. 3.5. And the BER performances are plotted in Fig. 3.6. The results show that in this near-far scenario, the MF detector with SIC can not work properly, but the proposed adaptive MMSE detector with SIC maintains a good performance. This shows the advantage of the proposed detector over the MF detector with SIC.

When the near-far problem in the system is slight, the situation becomes different. In the third example, user 2 was received with E_b/N_0 of 10 dB and the other five users were received with equal E_b/N_0 of 15 dB, one of which was user 1. All the users were synchronous. The plots of MSE versus time of the detectors for the users of interest are shown in Fig. 3.7. Although there is still some difference in the convergence rates: The detector for user 1 requires about 30 iterations before convergence can be reached, and the detector for user 2 requires about 50 iterations, the difference is so slight that it is almost indistinguishable. In this situation, user 1 and user 2 can be considered as one group and no SIC is needed.

In the remaining examples, five users were received with equal E_b/N_0, which was 10 dB more than that of the other user. The users of interest are user 1 and user 2, which were one of the strong users and the weak user, respectively. The fourth example examined the asynchronous system with time delays chosen randomly and then kept fixed. The MSE versus time curves of the detectors for the users of interest, with user 2 received with E_b/N_0 of 10 dB are plotted in Fig. 3.8. The comparison of transient terms of $J_k(i)$ of the users of interest, which explains the different convergence rates when the standard LMS algorithm is used, is also given in Table 3.1. And the BER performances of the detector for user 2 are plotted in Fig. 3.9. The results show that the proposed detector works well in this asynchronous system.

Comparing Figs. 3.4 and 3.6 with Fig. 3.9, it can be seen that by using the proposed detector instead of using the adaptive detector without SIC, a great BER performance improvement is gained in the asynchronous example; while in the two synchronous examples, this gain is almost negligible. This can be explained by the impact of MAI. In the synchronous case, the MAI comes only from current symbol. In the asynchronous case, however, the MAI comes from both current and previous (or following) symbols. The impact of MAI is greater in asynchronous systems than that in synchronous systems. The proposed detector can reduce the MAI greatly. Therefore, greater performance gain can be achieved in asynchronous system.

The fifth example considered the system with flat-fading channels. The phases were chosen randomly and then kept fixed. Similarly, the proposed detector works well, and the BER performances of the detector for user 2 are plotted in Fig. 3.10.

In the sixth example, we considered a system with multipath channels. The channel was assumed to have maximum order 2 and the impulse response coefficient vectors of the channels for all users were generated randomly. The BER performances of the detector for user 2 are given in Fig. 3.11. The BER curve labeled with "estimated" was obtained using the estimated distorted spreading sequences using the method in Section 3.2.3, and all the other curves were obtained using perfect knowledge of the distorted spreading sequences.

It is shown that in this system configuration, although the MF with SIC can not work properly, the proposed detector still maintains good performance, as the situation in the second example. Although the analysis result does not agree with the simulation result as well as in the system with single-path channels, they are still quite close. The degradation incurred by the estimation of the distorted spreading sequences is almost negligible.

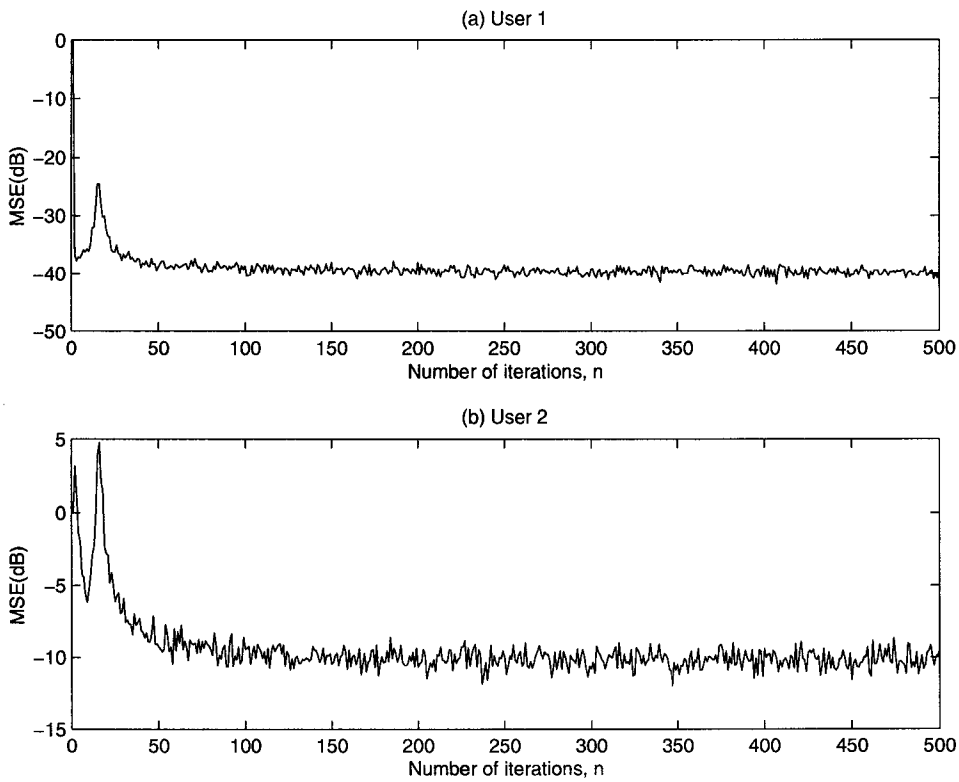

Figure 3.2. *MSE for a synchronous system (the first example), using the RLS algorithm.*

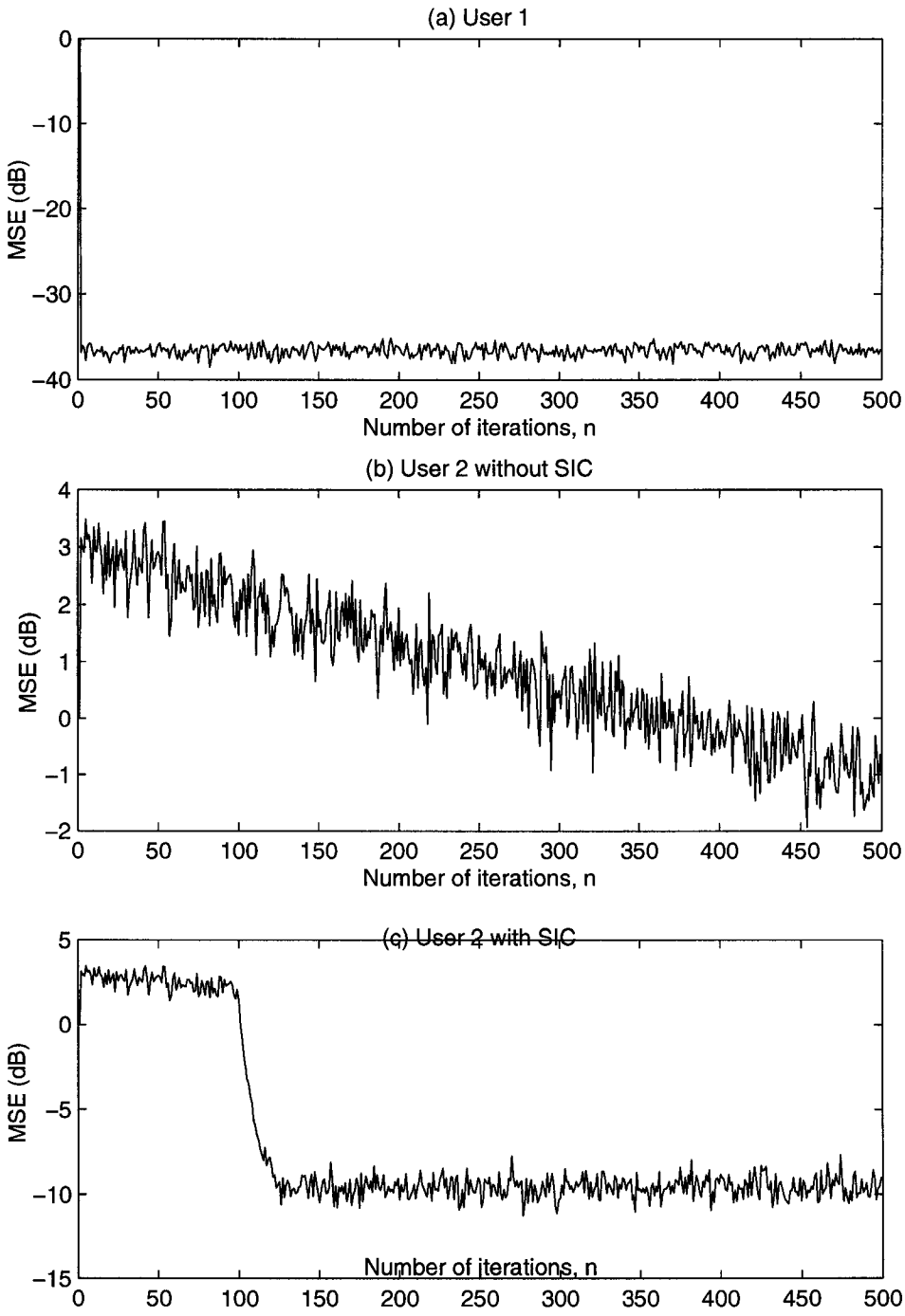

Figure 3.3. *MSE for a synchronous system (the first example), step size = 1/(input power) when without SIC and step size = 0.25/(input power) when with SIC.*

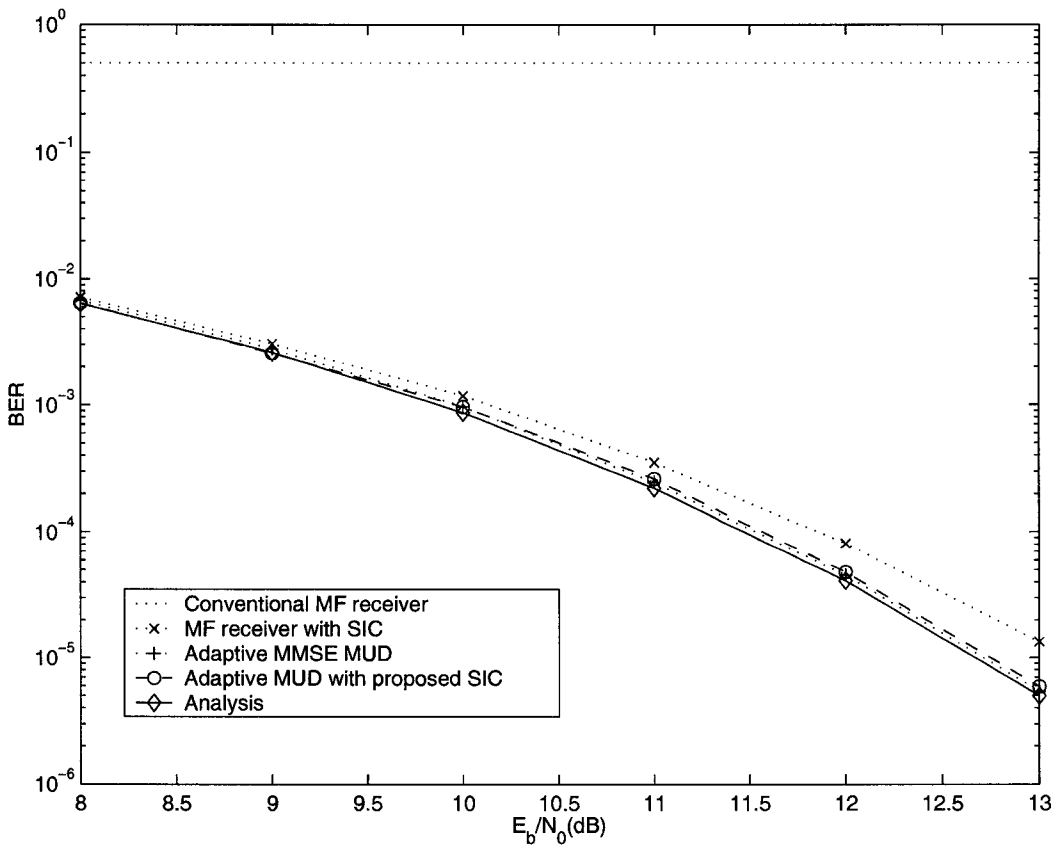

Figure 3.4. *BER of the detector for user 2 in a synchronous system (the first example).*

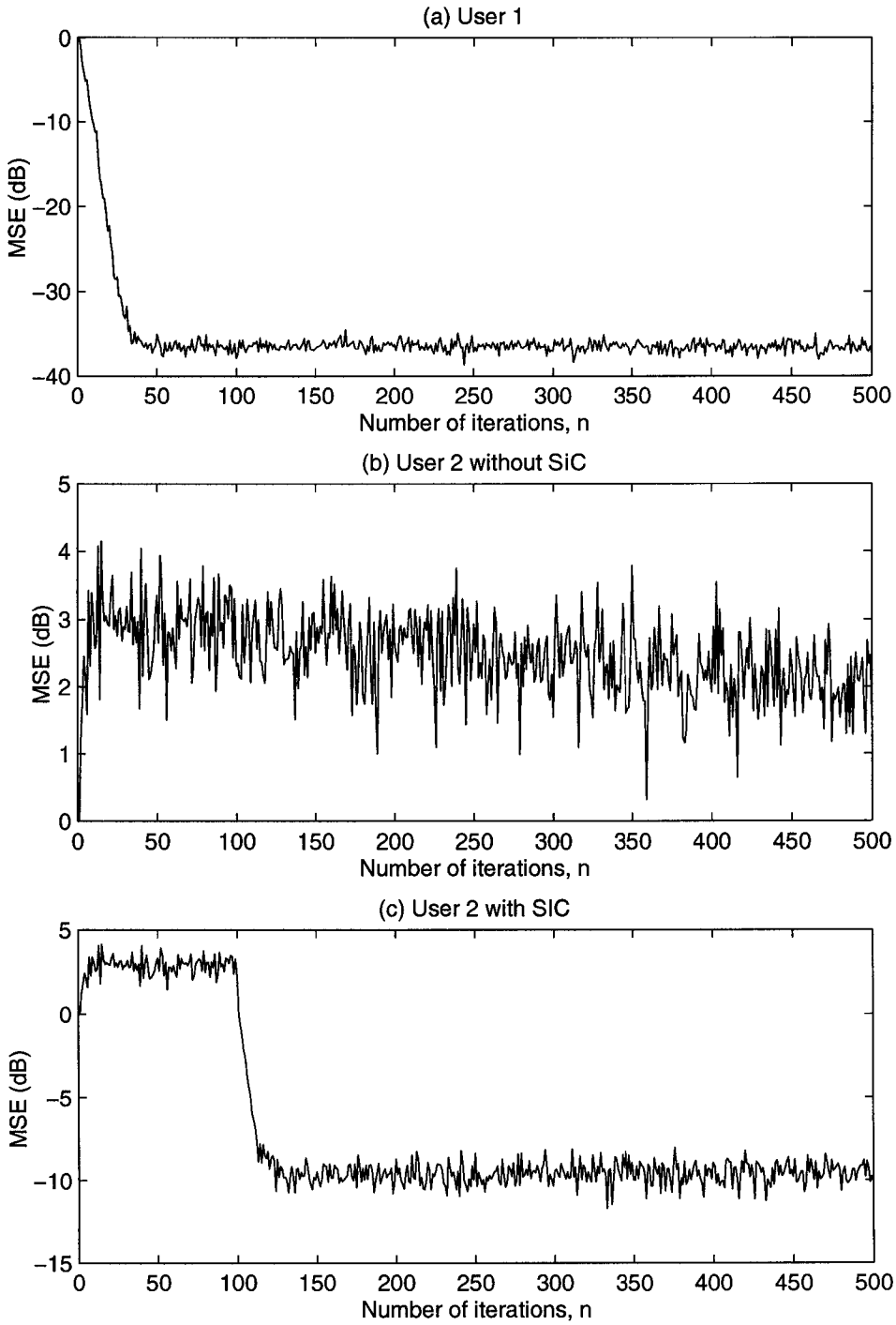

Figure 3.5. *MSE for a synchronous system (the second example), step size = 1/(input power) when without SIC and step size = 0.25/(input power) when with SIC.*

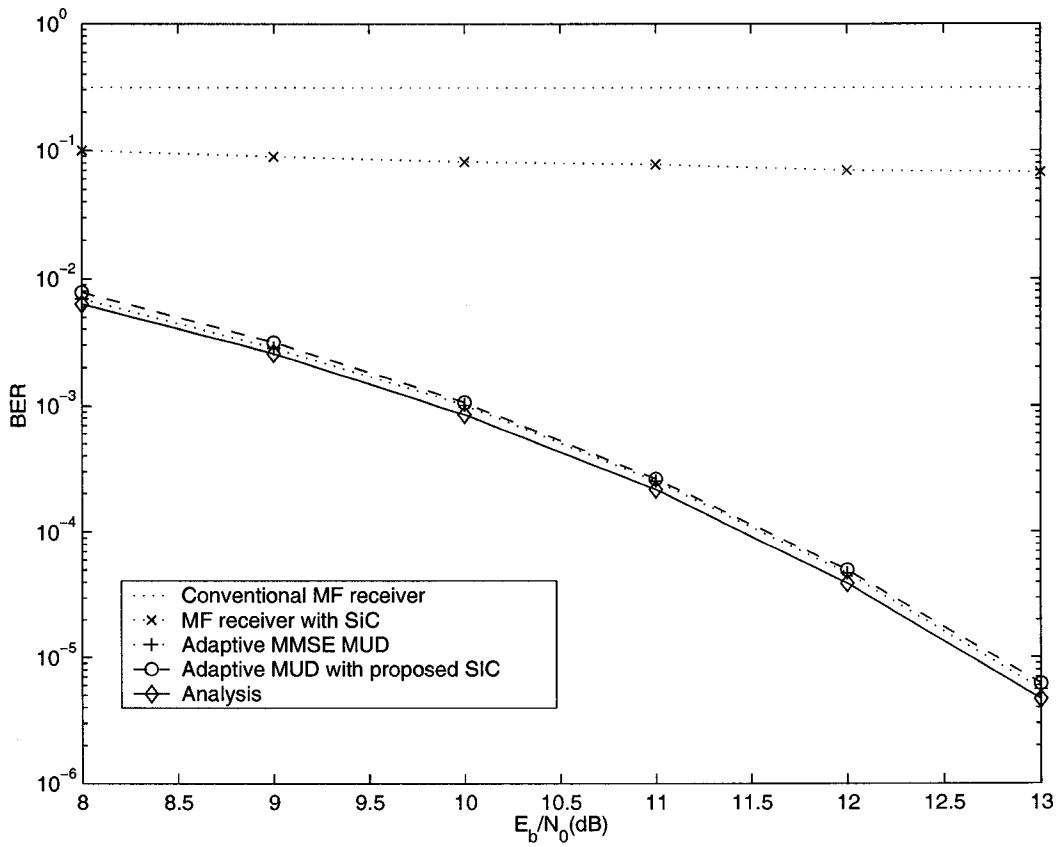

Figure 3.6. *BER of the detector for user 2 in a synchronous system (the second example).*

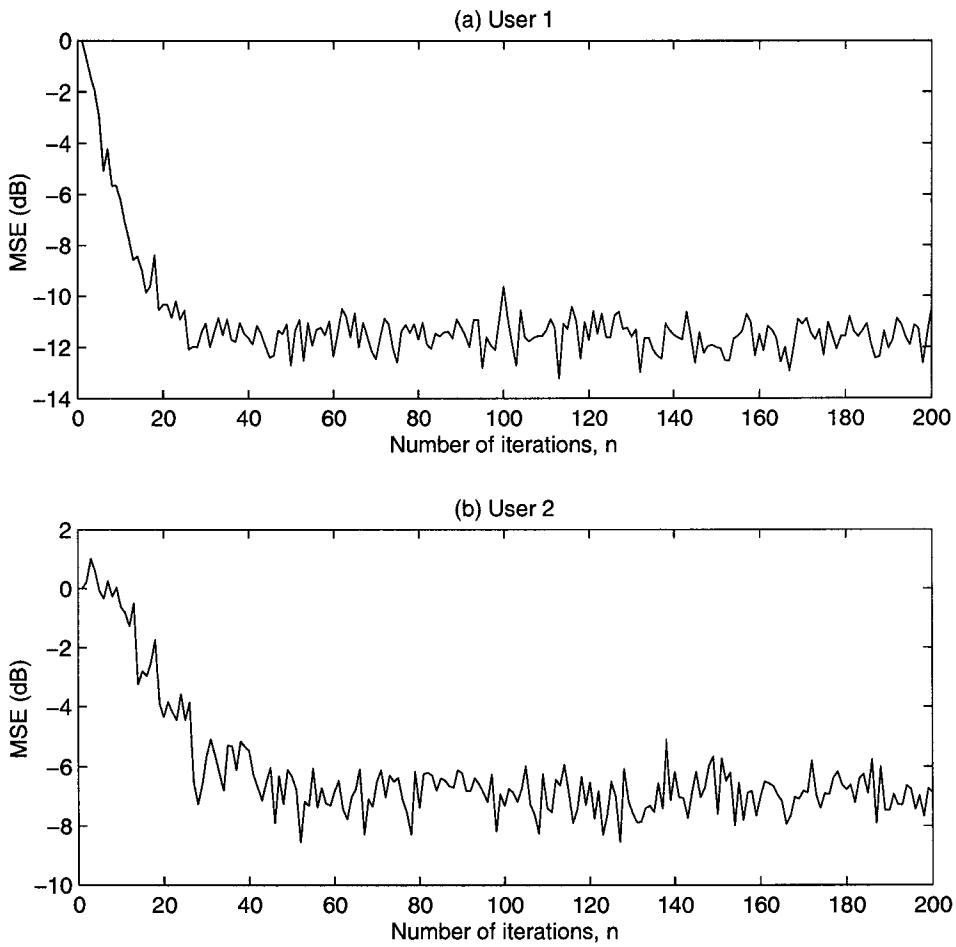

Figure 3.7. *MSE for a synchronous system (the third example), step size = 1/(input power).*

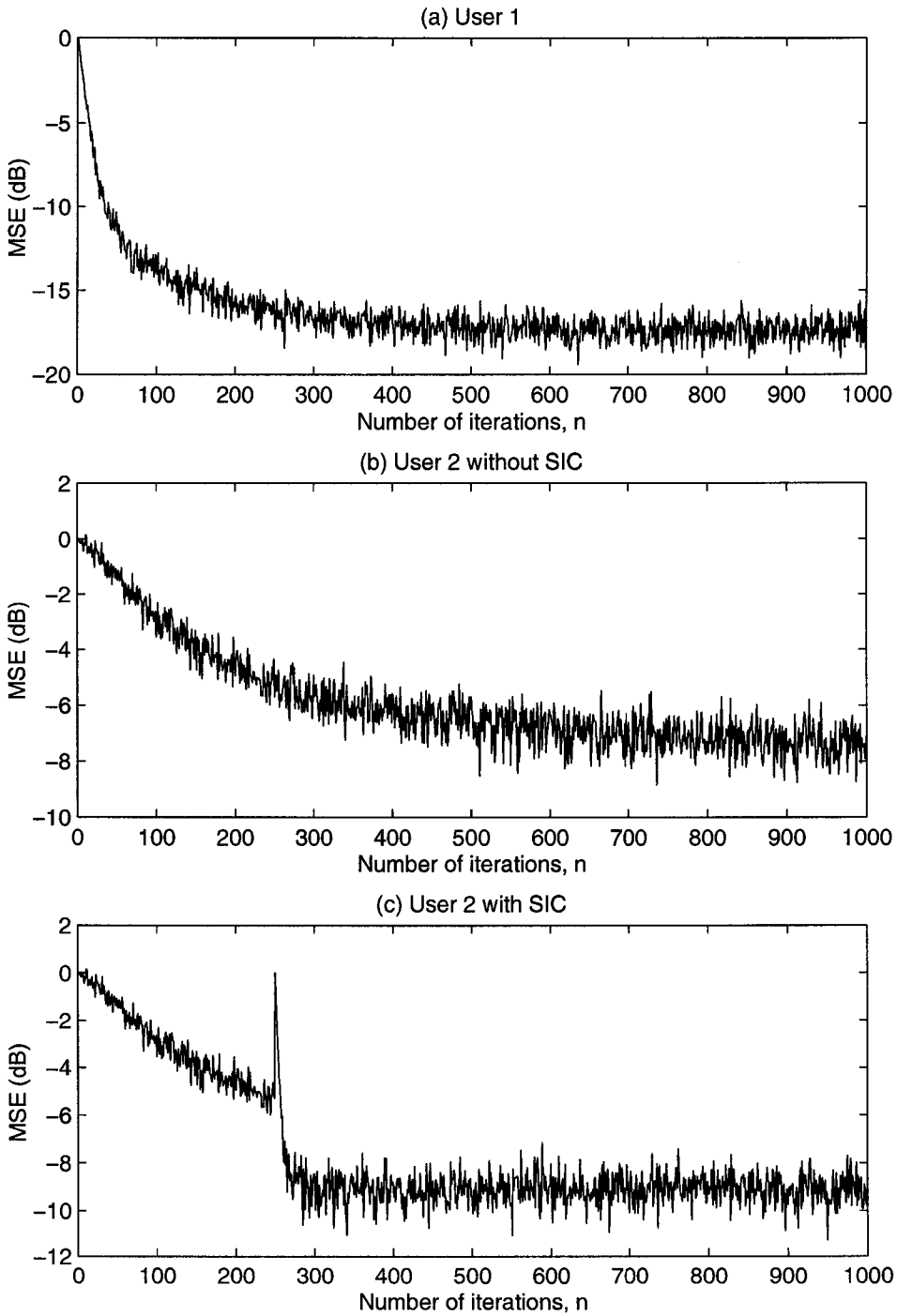

Figure 3.8. *MSE for an asynchronous system (the fourth example), step size = 0.25/(input power).*

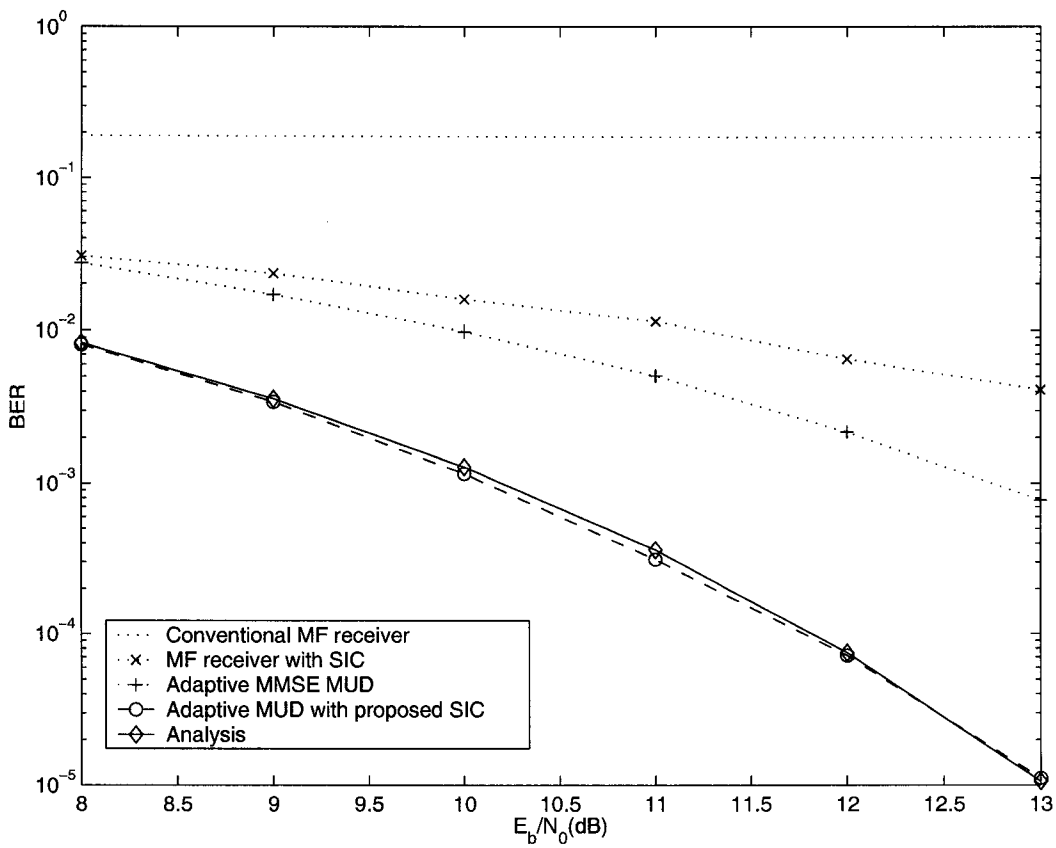

Figure 3.9. *BER of the detector for user 2 in an asynchronous system (the fourth example).*

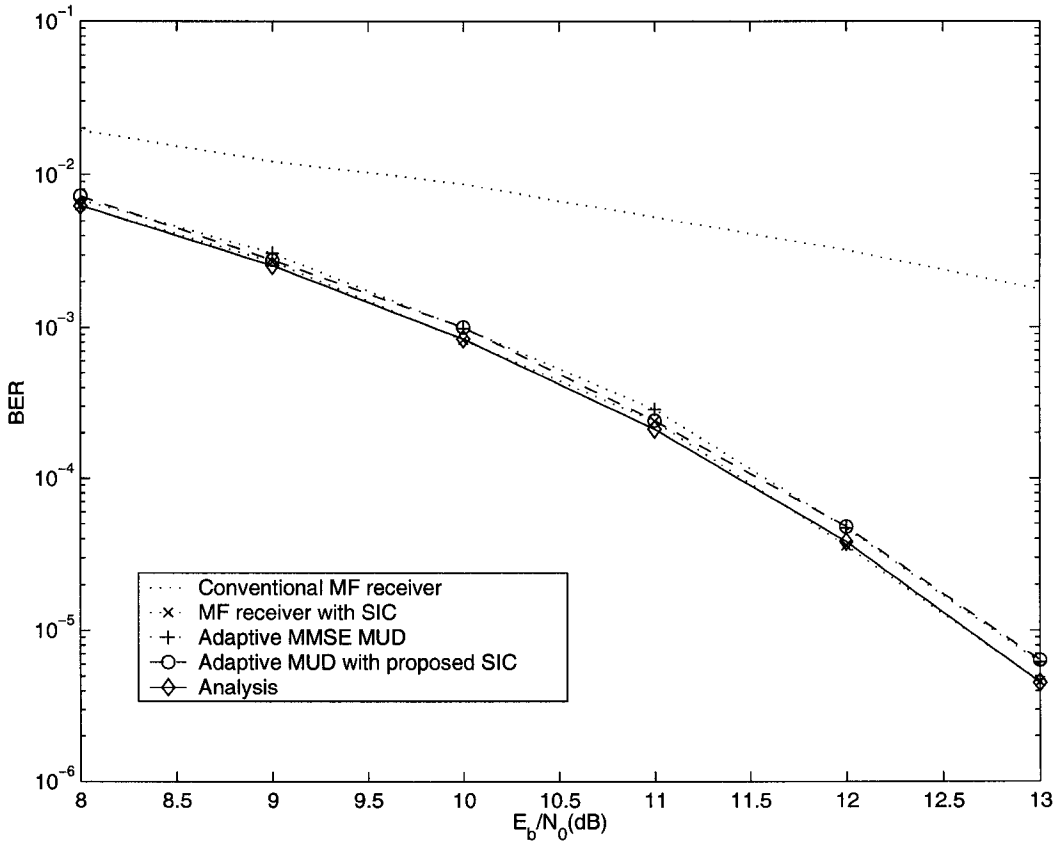

Figure 3.10. *BER of the detector for user 2 in a system with flat-fading channel (the fifth example).*

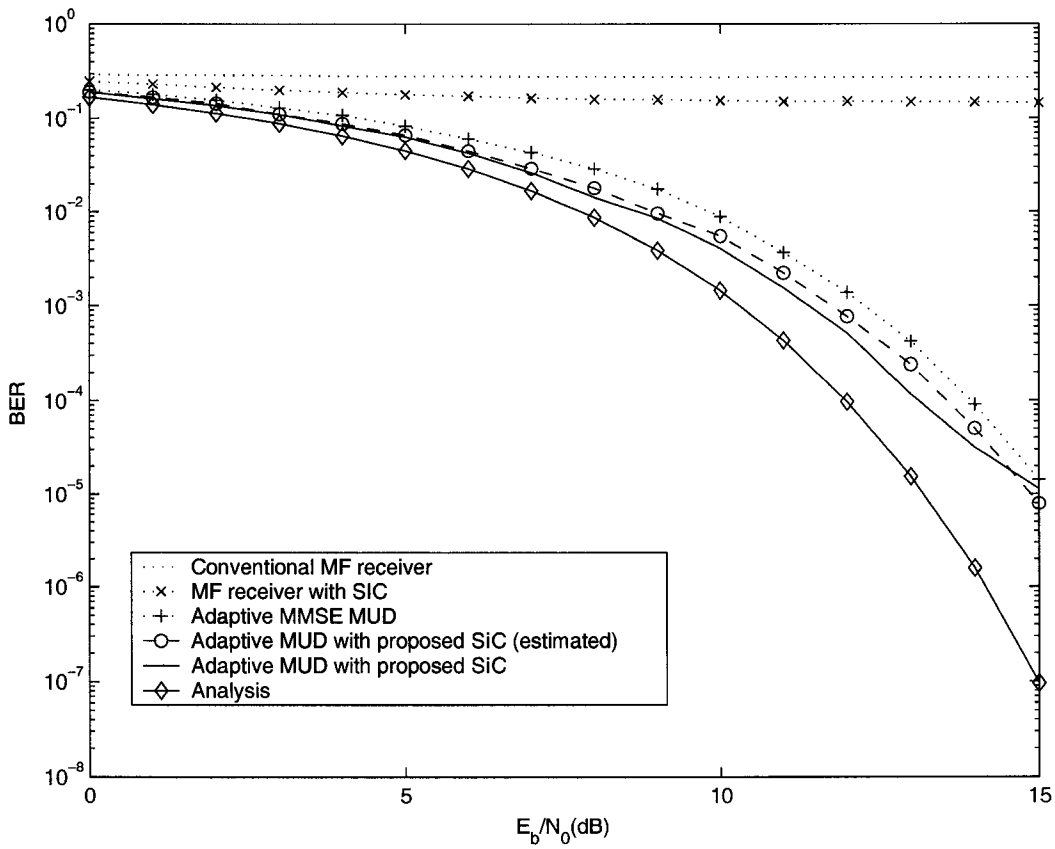

Figure 3.11. *BER of the detector for user 2 in a system with multipath channel (the sixth example).*

Table 3.1. *Comparison of transient terms of $J_k(i)$ in (3.15)*

		t_n and γ_n of all transient terms		dominant transient term(s)
Example 1	User 1	t_n	3.6060e-6 0.9978 0.9985 0.9990 0.9993 0.9995 0.9998 0.9998 0.9998 0.9998 0.9998 0.9998 0.9998 0.9998 0.9998	$0.9998 \times (3.6060\text{e-}6)^i$
		γ_n	0.9998 7.5896e-6 5.1814e-6 3.5288e-6 2.5001e-6 2.4483e-6 9.2030e-8 0.0000 0.0000 0.0000 0.0000 0.0000 0.0000 0.0000 0.0000	
	User 2	t_n	Same as User 1	$-0.9970 \times (3.6060\text{e-}6)^i + 1.7682 \times 0.9978^i$
		γ_n	-0.9970 1.7682 2.7438e-2 8.4424e-3 4.1265e-3 3.2869e-3 8.3536e-5 0.0000 0.0000 0.0000 0.0000 0.0000 0.0000 0.0000 0.0000	
Example 4	User 1	t_n	0.8850 0.9013 0.9420 0.9577 0.9754 0.9842 0.9877 0.9903 0.9961 0.9986 0.9986 0.9990 0.9990 0.9990 0.9990	$0.5330 \times 0.8850^i + 0.2179 \times 0.9013^i + (6.9234\text{e-}2) \times 0.9577^i$
		γ_n	0.5330 0.2179 4.3571e-2 6.9234e-2 4.5226e-2 2.3752e-2 4.9264e-3 3.7480e-2 4.5543e-3 3.8750e-4 1.0666e-4 2.1211e-6 0.0000 -0.0000 0.0000	
	User 2	t_n	0.8870 0.9212 0.9316 0.9575 0.9740 0.9867 0.9878 0.9906 0.9975 0.9986 0.9990 0.9990 0.9990 0.9990 0.9990	$0.5675 \times 0.9878^i + 0.1852 \times 0.9906^i + 0.1621 \times 0.9975^i$
		γ_n	-2.7705e-2 -1.3413e-2 -2.3893e-2 -4.0490e-3 3.0047e-3 -1.9378e-2 0.5675 0.1852 0.1621 8.5614e-5 7.8282e-6 1.7958e-5 0.0000 0.0000 -0.0000	

NOTE: For simplicity, the transient term with constant coefficient $\gamma_n > 0.05$ is selected as dominant transient term.

3.5 Conclusions

In this chapter, a GSIC-based fast converging adaptive MMSE multiuser detection method for DS-CDMA systems has been proposed and analyzed. In the proposed method, the convergence rates of the adaptive detectors for weak power users are increased by successively subtracting the interference of strong power user signals, whose corresponding adaptive detectors usually have higher convergence rates. As a result, the length of the training sequence required for the system is reduced. The order and the estimated signals used in the interference cancellation are determined from the convergence rates and the steady state parameters of the adaptive MMSE detectors, respectively. The analyses and the simulation results presented have shown that the proposed method provides a satisfactory performance in various near-far scenarios, even in the case that the alternative MF detector with successive cancellation fails. It has also been shown that the proposed analysis gives a good estimation of the true BER.

Because of the similarity of the adaptive MMSE multiuser detector and the blind adaptive multiuser detectors, the proposed detection scheme can be readily extended to the case of blind adaptive multiuser detectors.

Chapter 4

Semi-Blind Linear Parallel Interference Cancellation Multiuser Detectors

It is well known that the performance of DS-CDMA systems is limited by MAI. To overcome this problem, multiuser detection has been proposed to demodulate the received signal by considering the existence of other users, and it has been a very active research area over the past decade. Many multiuser detector schemes have been proposed [12], most of which fall into one of the following three categories: The signature codes of all users in the system are needed at the receiver, or only the signature code of the desired user is needed, or a training sequence is needed to the receiver. Among the multiuser detectors that have been proposed, the SIC and the PIC have received much attention for their easy implementations, and the PIC generally causes much less processing delay than the SIC. Both detectors need to know the signature codes of all users.

However, in the reverse link of CDMA systems, the received signal at BS comes from both intra-cell and inter-cell users, among which only the intra-cell users' signature codes are known to the BS receiver. In this chapter, we will consider multiuser detectors in this scenario which are called "semi-blind" [80]. Three semi-blind linear PIC multiuser detectors based on the signal subspace decomposition method are proposed. In the proposed detectors, the information of the inter-cell users needed in the PIC structures are estimated by utilizing the known intra-cell users' signature codes. Comparisons with other semi-blind detectors show that the proposed detectors are especially appropriate for practical

implementations and have satisfactory performances under practical conditions.

This chapter is organized as follows. In Section 4.1, we describe the reverse link of a DS-CDMA system. Section 4.2 gives a brief review on the existing linear PIC detectors. In Section 4.3, three new semi-blind linear PIC detectors based on signal subspace decomposition are proposed and their adaptation implementation is discussed. Some numerical results are presented in Section 4.4 and conclusions are made in Section 4.5.

4.1 System Description

Consider the reverse link of a DS-CDMA system in which the transmitted signals are antipodal. It is assumed that there are K intra-cell users in the system whose signature codes are known to the receiver and $\tilde{K}$ inter-cell users whose signature codes are unknown to the receiver. For the simplicity of discussion, it is assumed that all users in the system, including both intra-cell and inter-cell users, are synchronous. Thus the received signal at the BS can be expressed as

$$r(t) = \sum_{k=1}^{K} A_k b_k s_k(t) + \sum_{k=1}^{\tilde{K}} \tilde{A}_k \tilde{b}_k \tilde{s}_k(t) + n(t), \quad \text{for } 0 \leq t \leq T, \tag{4.1}$$

where $b_k \in \{+1, -1\}$, A_k and $s_k(t)$ are the information symbol, the signal amplitude and the signature waveform of the kth intra-cell user signal respectively, and $\tilde{b}_k$, $\tilde{A}_k$ and $\tilde{s}_k(t)$ are their counterparts associated with the kth inter-cell user signal. T is the symbol interval, $n(t)$ is AWGN with zero mean and variance σ^2. The signature waveform of the kth intra-cell user $s_k(t)$ is given by

$$s_k(t) = \sum_{i=0}^{N-1} a_k^i \psi(t - iT_c), \tag{4.2}$$

where N is the processing gain, $a_k^i \in \{+1, -1\}$ is the ith element of the kth intra-cell user's signature code, T_c is the chip interval, and $\psi(t)$ is the chip waveform which only takes nonzero value in the interval $[0,\ T_c]$. Denoting the ith element of the kth inter-cell user's signature code as $\tilde{a}_k^i$, the signature waveform of the kth inter-cell user $\tilde{s}_k(t)$ can be

expressed in a similar way as in (4.2). $s_k(t)$ and $\tilde{s}_k(t)$ are normalized so that $\|s_k(t)\|^2 = \|\tilde{s}_k(t)\|^2 = 1$, and $\mathbf{s}_k = [a_k^0\ a_k^1\ \cdots\ a_k^{N-1}]^T$ and $\tilde{\mathbf{s}}_k = [\tilde{a}_k^0\ \tilde{a}_k^1\ \cdots\ \tilde{a}_k^{N-1}]^T$ are the signature code vectors of the kth intra-cell user and the kth inter-cell user, respectively.

The demodulation begins by filtering the received signal with a chip-MF followed by a chip rate sampler. The ith sampling output is given by

$$r_i = \int_{iT_c}^{(i+1)T_c} r(t)\psi(t - iT_c)dt. \tag{4.3}$$

If we collect N sampling outputs to form the received vector $\mathbf{r} = [r_0\ r_1\ \cdots\ r_{N-1}]^T$, the signal model in (4.1) can be expressed in matrix form as

$$\begin{aligned}\mathbf{r} =& \sum_{k=1}^{K} A_k b_k \mathbf{s}_k + \sum_{k=1}^{\tilde{K}} \tilde{A}_k \tilde{b}_k \tilde{\mathbf{s}}_k + \mathbf{n} \\ =& \mathbf{S}\mathbf{A}\mathbf{b} + \tilde{\mathbf{S}}\tilde{\mathbf{A}}\tilde{\mathbf{b}} + \mathbf{n} = \bar{\mathbf{S}}\bar{\mathbf{A}}\bar{\mathbf{b}} + \mathbf{n},\end{aligned} \tag{4.4}$$

where $\mathbf{S} = [\mathbf{s}_1\ \mathbf{s}_2\ \cdots\ \mathbf{s}_K]$, $\tilde{\mathbf{S}} = [\tilde{\mathbf{s}}_1\ \tilde{\mathbf{s}}_2\ \cdots\ \tilde{\mathbf{s}}_{\tilde{K}}]$, $\mathbf{A} = \text{diag}\{A_1,\ A_2,\ \ldots,\ A_K\}$, $\tilde{\mathbf{A}} = \text{diag}\{\tilde{A}_1,\ \tilde{A}_2,\ \ldots,\ \tilde{A}_{\tilde{K}}\}$, $\mathbf{b} = [b_1\ b_2\ \cdots\ b_K]^T$, $\tilde{\mathbf{b}} = \left[\tilde{b}_1\ \tilde{b}_2\ \cdots\ \tilde{b}_{\tilde{K}}\right]^T$, $\bar{\mathbf{S}} = \left[\mathbf{S}\ \tilde{\mathbf{S}}\right]$, $\bar{\mathbf{A}} = \text{diag}\{\mathbf{A}, \tilde{\mathbf{A}}\}$, and $\bar{\mathbf{b}} = \left[\mathbf{b}^T\ \tilde{\mathbf{b}}^T\right]^T$. The noise vector $\mathbf{n}$ is Gaussian with zero mean and covariance matrix $\sigma^2\mathbf{I}_N$ with $\mathbf{I}_N$ denoting the $N \times N$ identity matrix. The covariance matrix of the received vector $\mathbf{r}$ is

$$\mathbf{C}_r = \mathrm{E}\left[\mathbf{r}\mathbf{r}^T\right] = \mathbf{S}\mathbf{A}^2\mathbf{S}^T + \tilde{\mathbf{S}}\tilde{\mathbf{A}}^2\tilde{\mathbf{S}}^T + \sigma^2\mathbf{I}_N. \tag{4.5}$$

Without the loss of generality, it is assumed that all signature codes of the intra-cell and inter-cell users are linearly independent, i.e., $N \geq (K + \tilde{K})$, so the matrix $\bar{\mathbf{S}}$ has full column rank. Note that it is easy to extend the detection schemes which will be proposed in this chapter to asynchronous system [34, 37].

4.2 Linear Parallel Interference Cancellation

There are several distinct PIC schemes in the literature [32, 34, 36, 88, 89, 90]. In this section, we make a brief review on the existing linear PIC detectors, in which soft-decisions

are used in estimating the interference signals. In the remainder of Section 4.2, we assume that the signature codes of all users are known to the receiver, i.e., $\tilde{K} = 0$.

4.2.1 Conventional Linear PIC

The output vector of the conventional linear PIC at the ith stage can be expressed as [32, 88]

$$\mathbf{x}_i = \mathbf{y}_0 + (\mathbf{I}_K - \mathbf{R})\mathbf{x}_{i-1}, \tag{4.6}$$

where $\mathbf{y}_0 = \mathbf{S}^T\mathbf{r}$, $\mathbf{R} = \mathbf{S}^T\mathbf{S}$, $\mathbf{x}_i = [x_{i,1}\ x_{i,2}\ \cdots\ x_{i,K}]^T$ with $x_{i,k}$ being the output for the kth user at stage i and $\mathbf{x}_0$ is initialized as $\mathbf{0}$. The conventional linear PIC can be considered as the Jacobi iteration for approximating the inversion of $\mathbf{R}$, and it will converge to the DD if the maximal eigenvalue of $\mathbf{R}$ is less than 2 [88].

4.2.2 Partial Linear PIC

The output vector of the partial linear PIC at the ith stage can be expressed as [34, 89]

$$\mathbf{x}_i = \mathbf{x}_{i-1} + \mu_i(\mathbf{y}_0 - \mathbf{R}\mathbf{x}_{i-1}), \tag{4.7}$$

where μ_i is the cancellation factor at the ith stage. The partial linear PIC can be considered as an iterative approach to find out the minimum point of the quadratic function

$$f(\mathbf{x}) = \frac{1}{2}\mathbf{x}^T\mathbf{R}\mathbf{x} - \mathbf{y}_0^T\mathbf{x} \tag{4.8}$$

using the steepest descent method (SDM) with step size μ_i[91]. It is obvious that the conventional linear PIC is a special case of the partial linear PIC when $\mu_i = 1$. The solution of the above minimization problem is the DD [89]. Replacing $\mathbf{R}$ in (4.6)-(4.8) by $\mathbf{R} + \sigma^2\mathbf{A}^{-2}$, the conventional linear PIC and the partial linear PIC can be extended to approach the MMSE detector [12]. The MMSE extension can be implemented with minor changes in the linear PIC structures which approach the DD. To make the following discussion convenient, we express $\mathbf{R}$ and $\mathbf{R} + \sigma^2\mathbf{A}^{-2}$ in a unified form $\mathbf{R} + \mathbf{\Gamma}\mathbf{A}^{-2}$, where

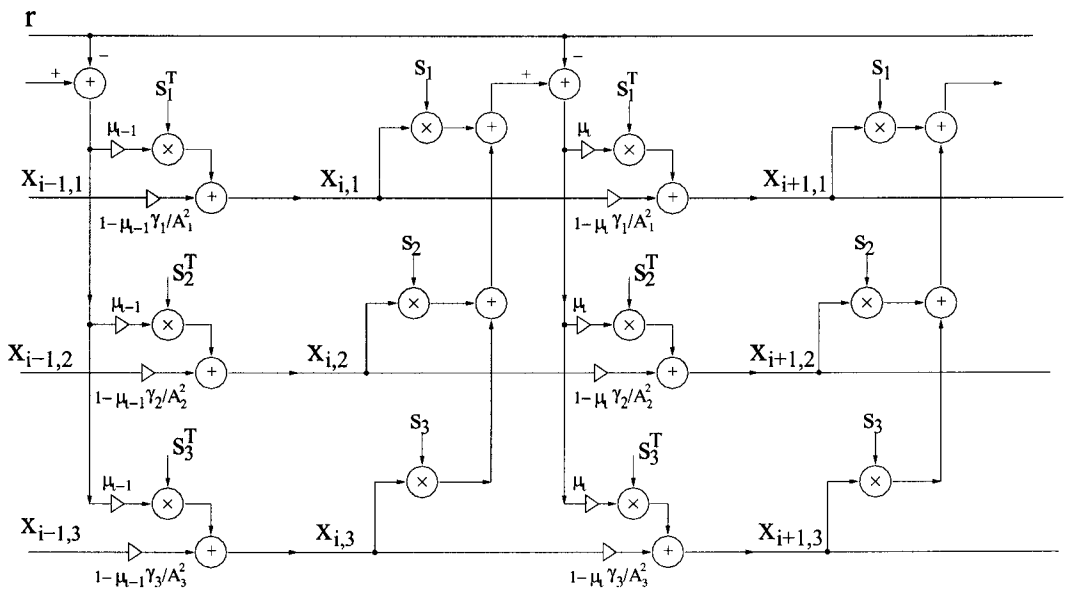

Figure 4.1. *The partial linear PIC structure based on noise component for a three-user system.*

$\Gamma = \text{diag}\{\gamma_1, \gamma_2, \ldots, \gamma_K\}$ with γ_k being the noise component of the kth user. The ith stage of the partial linear PIC structure based on the users' noise components is given in Fig. 4.1. When the noise components of all the users are zeroes, the PIC structures implement the DD, and when they are all equal to σ^2, the MMSE detector is implemented.

However, the Jacobi iteration is not guaranteed to converge, this explains the unstable behavior of the conventional linear PIC in some system scenario. And the partial linear PIC based on the SDM sometimes has slow convergence rate [36].

4.2.3 Conjugate Gradient Method-Based Linear PIC

To overcome the shortcomings of slow convergence of the SDM-based partial linear PIC, the conjugate gradient method (CGM) was proposed to approach the minimum point of the quadratic function $f(\mathbf{x})$ in (4.8), resulting in the CGM-based linear PIC [36, 90]. Because $\mathbf{R}$ and $\mathbf{R} + \sigma^2\mathbf{A}^{-2}$ are positive definite, by using the CGM iterations, the solution can be obtained by at most K stages in this problem [91].

From the above description, it can be seen that by using different iterative methods, different linear PIC schemes try to approach the linear multiuser detector

$$\mathbf{y} = (\mathbf{R}_0 + \mathbf{\Gamma}\mathbf{A}_0^{-2})^{-1}\mathbf{S}_0^T\mathbf{r} \tag{4.9}$$

where $\mathbf{R}_0 = \mathbf{S}_0^T\mathbf{S}_0$, $\mathbf{S}_0 = [\mathbf{s}_{0,1}\ \mathbf{s}_{0,2}\ \cdots\ \mathbf{s}_{0,K}]$, $\mathbf{A}_0 = \text{diag}\{A_{0,1},\ A_{0,2},\ \ldots,\ A_{0,K}\}$, $\mathbf{s}_{0,k}$ and $A_{0,k}$ are the signature codes and signal amplitudes used in the PIC structure.

4.3 Semi-Blind Linear PIC Using Subspace Method

It can be seen from Section 4.2 that the signature codes and signal amplitudes of both the intra-cell and the inter-cell users are required in the linear PIC structures to approach the DD and the MMSE detectors. For semi-blind PIC detectors, however, only the intra-cell users' signature codes are known to the receiver. In what follows, we consider estimating the required information about the inter-cell users by using the signal subspace decomposition method.

It is noted from (4.5) that the impact of the intra-cell users on the received vector covariance matrix $\mathbf{C}_r$ can be removed as [92]

$$\mathbf{C}_I = \mathbf{C}_r - \sum_{k=1}^{K} A_k^2\mathbf{s}_k\mathbf{s}_k^T \tag{4.10}$$

$$= \tilde{\mathbf{S}}\tilde{\mathbf{A}}^2\tilde{\mathbf{S}}^T + \sigma^2\mathbf{I}_N. \tag{4.11}$$

The eigenvalue decomposition (ED) of $\mathbf{C}_I$ is given as

$$\mathbf{C}_I = [\mathbf{U}_I\ \mathbf{U}_n]\begin{bmatrix}\mathbf{\Lambda}_I & \\ & \sigma^2\mathbf{I}_{N-\tilde{K}}\end{bmatrix}\begin{bmatrix}\mathbf{U}_I^T \\ \mathbf{U}_n^T\end{bmatrix}, \tag{4.12}$$

where $\mathbf{\Lambda}_I = \text{diag}\{\lambda_1,\ \lambda_2,\ \ldots,\ \lambda_{\tilde{K}}\}$ contains the $\tilde{K}$ largest eigenvalues of $\mathbf{C}_I$, $\mathbf{U}_I = [\mathbf{u}_1\ \mathbf{u}_2\ \cdots\ \mathbf{u}_{\tilde{K}}]$ contains the corresponding orthonormal eigenvectors and $\mathbf{U}_n = [\mathbf{u}_{\tilde{K}+1}\ \cdots\ \mathbf{u}_N]$ contains the $(N - \tilde{K})$ orthonormal eigenvectors corresponding to the eigenvalues σ^2. It is easy to see that $\mathbf{U}_I$ spans the inter-cell user signal subspace and $\mathbf{U}_n$ spans the noise

subspace. The eigenpairs $(\lambda_k - \sigma^2, \mathbf{u}_k)$ for $k = 1, \ldots, \tilde{K}$ are termed as eigenvalues and eigenvectors of inter-cell user signal subspace.

We have noticed the fact which is stated as Lemma 1 in the following.

Lemma 1: The inter-cell user signal subspace projection matrix $\mathbf{U}_I\mathbf{U}_I^T$ can be expressed as

$$\mathbf{U}_I\mathbf{U}_I^T = \tilde{\mathbf{S}}\tilde{\mathbf{S}}^\dagger \tag{4.13}$$

Proof: From (4.11) and (4.12),

$$\tilde{\mathbf{S}}\tilde{\mathbf{A}}^2\tilde{\mathbf{S}}^T = [\mathbf{U}_I\ \mathbf{U}_n]\begin{bmatrix} \mathbf{\Lambda} & \\ & \mathbf{0} \end{bmatrix}\begin{bmatrix} \mathbf{U}_I^T \\ \mathbf{U}_n^T \end{bmatrix} = \mathbf{U}_I\mathbf{\Lambda}\mathbf{U}_I^T, \tag{4.14}$$

where $\mathbf{\Lambda} = \mathbf{\Lambda}_I - \sigma^2\mathbf{I}_{\tilde{K}}$. Denoting $\mathbf{T} = \tilde{\mathbf{S}}\tilde{\mathbf{A}}^2\tilde{\mathbf{S}}^T$, we have

$$\mathbf{U}_I = \mathbf{T}\mathbf{U}_I\mathbf{\Lambda}^{-1} \tag{4.15}$$

$$\mathbf{U}_I\mathbf{U}_I^T = \mathbf{T}\mathbf{U}_I\mathbf{\Lambda}^{-2}\mathbf{U}_I^T\mathbf{T} = \mathbf{T}\mathbf{T}^\dagger\mathbf{T}^\dagger\mathbf{T}. \tag{4.16}$$

Note that $\mathbf{T}^\dagger = (\tilde{\mathbf{S}}^T)^\dagger\tilde{\mathbf{A}}^{-2}\tilde{\mathbf{S}}^\dagger$ and $\tilde{\mathbf{S}}^\dagger = (\tilde{\mathbf{S}}^T\tilde{\mathbf{S}})^{-1}\tilde{\mathbf{S}}^T$ [93]. After some manipulations, (4.16) can be given as

$$\mathbf{U}_I\mathbf{U}_I^T = \tilde{\mathbf{S}}(\tilde{\mathbf{S}}^T\tilde{\mathbf{S}})^{-1}\tilde{\mathbf{S}}^T = \tilde{\mathbf{S}}\tilde{\mathbf{S}}^\dagger. \qquad \square$$

From Lemma 1, it is shown that the eigenvectors of the inter-cell user signal subspace can give some information about the inter-cell users' signature codes. Therefore, we propose to substitute the unknown signature codes of the inter-cell users with $\{\mathbf{u}_1, \mathbf{u}_2, \ldots, \mathbf{u}_{\tilde{K}}\}$ in the linear PIC structure. Furthermore, we also propose to substitute the signal amplitudes of the inter-cell users with $\{\sqrt{\lambda_1 - \sigma^2}, \sqrt{\lambda_2 - \sigma^2}, \ldots, \sqrt{\lambda_{\tilde{K}} - \sigma^2}\}$. The known signature codes and signal amplitudes of the intra-cell users are kept unchanged in the PIC structure, which is assumed throughout the following discussion. As shown in Fig. 4.2, where the partial linear PIC structure is taken as an example, the three proposed subspace-based semi-blind linear PIC detectors can be given in the following three definitions, respectively.

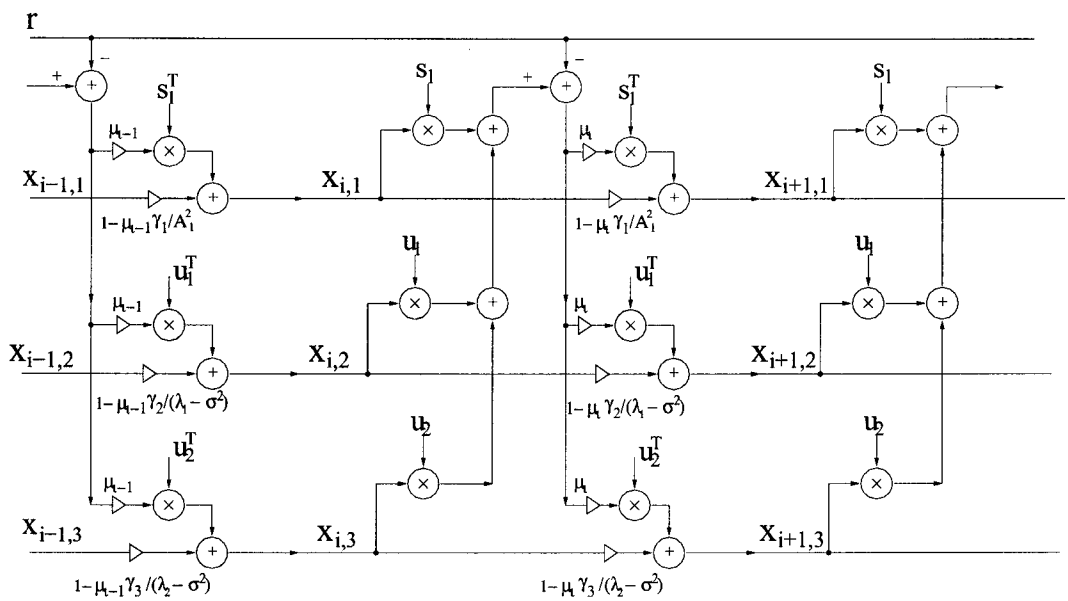

Figure 4.2. *The proposed subspace-based semi-blind linear PIC detector for a system with one intra-cell user and two inter-cell users.*

Definition 4.1: Subspace-Based Semi-Blind Linear PIC-I

The subspace-based semi-blind linear PIC-I is obtained by using $\{\mathbf{u}_1, \mathbf{u}_2, \ldots, \mathbf{u}_{\tilde{K}}\}$ as the unknown inter-cell user signature codes and setting all the noise components to zeroes.

Based on (4.9) and Definition 4.1, when the proposed semi-blind linear PIC-I converges, the output for the kth intra-cell user is expressed as

$$y_{1,k} = \bar{\mathbf{e}}_k^T \mathbf{R}_c^{-1} \mathbf{C}^T \mathbf{r}, \quad \text{for } k = 1, \ldots, K, \tag{4.17}$$

where $\mathbf{C} = [\mathbf{S}\ \mathbf{U}_I]$, $\mathbf{R}_c = \mathbf{C}^T\mathbf{C}$ and $\bar{\mathbf{e}}_k$ is the kth unit vector in $\mathcal{R}^{K+\tilde{K}}$ with the kth element being 1 and all the other elements being 0.

As shown in Appendix 4.A, the converged subspace-based semi-blind linear PIC-I yields the same BER performance as the non-blind linear DD.

Definition 4.2: Subspace-Based Semi-Blind Linear PIC-II

The subspace-based semi-blind linear PIC-II is obtained by using $\{\mathbf{u}_1, \mathbf{u}_2, \ldots, \mathbf{u}_{\tilde{K}}\}$ as the unknown inter-cell user signature codes, and setting the noise components of inter-cell users to zeroes and those of intra-cell users to σ^2.

Based on (4.9) and Definition 4.2, when the proposed semi-blind linear PIC-II converges, the output for the kth intra-cell user is expressed as

$$y_{2,k} = \bar{\mathbf{e}}_k^T \left(\mathbf{R}_c + \text{diag}\{\sigma^2 \mathbf{A}^{-2}, \mathbf{0}\}\right)^{-1} \mathbf{C}^T \mathbf{r}, \quad \text{for } k = 1, \ \ldots, \ K. \tag{4.18}$$

As shown in Appendix 4.B, the Gaussian approximated BER of the converged subspace-based semi-blind linear PIC-II is lower-bounded by the Gaussian approximated BER of the non-blind linear MMSE detector and upper-bounded by the BER of the non-blind linear DD. Based on the result in [68], the Gaussian approximation generally gives a very good estimation to the true BER performance. Therefore, it is expected that the BER performance of the proposed subspace-based semi-blind linear PIC-II is generally better than that of the non-blind DD but worse than that of the non-blind MMSE detector.

Definition 4.3: Subspace-Based Semi-Blind Linear PIC-III

The subspace-based semi-blind linear PIC-III is obtained by using $\{\mathbf{u}_1, \ \mathbf{u}_2, \ \ldots, \ \mathbf{u}_{\tilde{K}}\}$ and $\{\sqrt{\lambda_1 - \sigma^2}, \ \sqrt{\lambda_2 - \sigma^2}, \ \ldots, \ \sqrt{\lambda_{\tilde{K}} - \sigma^2}\}$ as the unknown inter-cell user signature codes and signal amplitudes respectively, and setting all the noise components of intra-cell and inter-cell users to σ^2.

Based on (4.9) and Definition 4.3, when the proposed semi-blind linear PIC-III converges, the output for the kth intra-cell user is expressed as

$$y_{3,k} = \bar{\mathbf{e}}_k^T \left(\mathbf{R}_c + \text{diag}\{\sigma^2 \mathbf{A}^{-2}, \sigma^2 (\mathbf{\Lambda}_I - \sigma^2 \mathbf{I}_{\tilde{K}})^{-1}\}\right)^{-1} \mathbf{C}^T \mathbf{r}, \quad \text{for } k = 1, \ \ldots, \ K. \tag{4.19}$$

From the above discussion, it can be seen that the amplitudes of the intra-cell user signal A_k ($k = 1, \ \ldots, \ K$) and the noise variance σ^2 are needed in the proposed schemes. In practical implementations, A_k can be estimated by averaging the outputs of the symbol-MFs, whose estimated value is denoted as $\hat{A}_k$. And $\mathbf{C}_I$ can be estimated as

$$\hat{\mathbf{C}}_I = \frac{1}{M} \sum_{i=1}^{M} \mathbf{r}(i)\mathbf{r}(i)^T - \sum_{k=1}^{K} \hat{A}_k^2 \mathbf{s}_k \mathbf{s}_k^T \tag{4.20}$$

where M is the window size of the sample signal. By averaging the $(N - \tilde{K})$ smallest eigenvalues of $\hat{\mathbf{C}}_I$, an estimate of σ^2 can be obtained. Although the number of inter-cell

users, i.e. $\tilde{K}$ can be determined based on the estimated eigenvalues [26], it is assumed known throughout this chapter for simplicity.

4.3.1 Adaptation Implementation

Like the traditional PIC, the proposed subspace-based semi-blind linear PIC detectors can be implemented using simple processing elements. Therefore, the proposed detectors are especially appropriate for practical implementations compared with the existing semi-blind multiuser detectors [80]. However, the closed-form solutions of the proposed subspace-based semi-blind multiuser detectors, as well as those in [80] involve high computational complexity and long processing latency. To overcome these problems, adaptive subspace tracking techniques can be used to solve this subspace-based semi-blind detection problem iteratively.

A number of adaptive algorithms have been proposed in the literature for subspace tracking [94, 95, 96]. In this chapter, the deflation-based projection approximation subspace tracking (PASTd) algorithm developed in [96] is used. In each iteration, the intra-cell user signals are estimated and subtracted from the received signal first, using the knowledge of their signature codes. The residual is an estimate of the sum of the received inter-cell signals and noise, which is used as the input to the PASTd algorithm. The forgetting factor in the PASTd algorithm is set to one to get the eigenvalues of the inter-cell signal subspace [97]. Finally, the resulting eigenvectors and eigenvalues from the PASTd algorithm are used to update the eigenpairs of the inter-cell user signal subspace used in the PIC structure. Table 4.1 summarizes the adaptation algorithm for the proposed subspace-based semi-blind linear PIC detectors. The quantity $a_k(t)$ in Table 4.1 is the estimated signal amplitude of the kth intra-cell user.

In order to evaluate the computational complexity, the required number of operations of the proposed subspace-based semi-blind PIC detectors in each adaptation iteration is summarized in Table 4.2, where one operation is defined as one multiplication or division plus an optional addition. The PIC structure in [88] with $K + \tilde{K}$ stages are used in this evalua-

Table 4.1. *Adaptation Algorithm for the Proposed Semi-Blind Linear PIC Detectors*

Initialization $a_k(0)$ (k=1, ..., K),

$\lambda_k(0)$ and $\mathbf{u}_k(0)$ $(k = 1, \ldots, \tilde{K})$,

FOR $t = 1, 2, \ldots$

$\mathbf{r}_I(t) = \mathbf{r}(t)$

FOR $k = 1 : K$

$z_k(t) = \mathbf{r}^T(t)\mathbf{s}_k$

$a_k(t) = \frac{t}{t+1}a_k(t-1) + \frac{1}{t+1}|z_k(t)|$

$\mathbf{r}_I(t) = \mathbf{r}_I(t) - a_k(t) \cdot \text{sign}[z_k(t)] \cdot \mathbf{s}_k$

END

$\mathbf{x}_1(t) = \mathbf{r}_I(t)$

FOR $k = 1 : \tilde{K}$

$y_k(t) = \mathbf{u}_k^T(t-1)\mathbf{x}_k(t)$

$\lambda_k(t) = \frac{t}{t+1}\lambda_k(t-1) + \frac{1}{t+1}|y_k(t)|^2$

$\mathbf{u}_k(t) = \mathbf{u}_k(t-1) + [\mathbf{x}_k(t) - y_k(t)\mathbf{u}_k(t-1)]y_k(t)/\lambda_k(t)/(t+1)$

$\mathbf{x}_{k+1}(t) = \mathbf{x}_k(t) - y_k(t)\mathbf{u}_k(t)$

END

Update the values of λ_k and $\mathbf{u}_k$ in the PIC structure.

END

tion. For comparison purposes, we also give the required number of operations per iteration of the form-I and form-II semi-blind hybrid detectors in [80]. It can be seen from Table 4.2 that the detectors proposed in this section have comparable computational complexity with the form-II hybrid detector, which is much less than that of the form-I hybrid detector. It is also noted that in the proposed detectors, both the pre-processing and detection process can be implemented using simple processing elements in a parallel structure, while the form-I and form-II hybrid detectors can not. Therefore, the adaptation implementations are easier and incur much less processing latency to the proposed subspace-based semi-blind detectors than to those in [80]. This is a favorable property of the proposed detectors especially from the practical point of view.

Table 4.2. *Required Number of Operations in Each Adaptation Iteration*

Semi-Blind Detector	Pre-Processing	PASTd Algorithm	Detection Process
Proposed Subspace-Based Detectors	$NK + 3K$	$4N\tilde{K} + 4\tilde{K}$	$2N(K+\tilde{K})^2 + 2(K+\tilde{K})^2$
Form-I Hybrid Detector in [80]	$2N^3$ [80, (44)]	$4N\tilde{K} + 4\tilde{K}$	$N^3 + 2N^2K + N(K+\tilde{K})$ $+\tilde{K}$[80, (49)]
Form-II Hybrid Detector in [80]	Not Needed	$4N(K+\tilde{K})$ $+4(K+\tilde{K})$	$2NK(K+\tilde{K})$ $+N(K^2+K)+K^3$ $+(K+\tilde{K})(K^2+K+1)$ [80, (52)]

K: number of intra-cell users, $\tilde{K}$: number of inter-cell users, N: processing gain

4.4 Simulation Results

Computer simulations were carried out to evaluate the performance of the proposed semi-blind linear PIC detectors in terms of BER. In the following simulations, a synchronous DS-CDMA system with fifteen users was considered, among which ten were intra-cell users and the other five were inter-cell users. The user of interest was one of the intra-cell users. The signature codes were of length 30, which were obtained by repeating each chip of the length 15 Gold codes twice. After obtaining the subspace-based semi-blind linear PIC detectors based on the sample data block of length 200, i.e. $M = 200$, the detectors were applied to independent data to find out the BER.

In the first example, the received signal power of all the users was identical. We first compare the performance of the proposed subspace-based semi-blind detectors using perfect coefficients, where $\mathbf{C}_I$ was obtained using (4.11) with perfect knowledge of the signal amplitudes and signature codes of the inter-cell users and noise power. The BERs of the user of interest versus signal-to-noise ratio (SNR) for the three proposed detectors are plotted in Fig. 4.3a. For comparison purposes, we also plot the BERs of the form-I semi-blind multiuser detectors developed in [80]. It can be observed that in perfect conditions the proposed subspace-based semi-blind linear PIC-I has the same BER performance as the

semi-blind DD in [80], which is the worst among those of all the detectors listed in Fig. 4.3a. As anticipated, the proposed semi-blind linear PIC-II has a better BER performance than the non-blind DD but a worse one than the non-blind MMSE detector. The BER performance of the proposed subspace-based semi-blind linear PIC-III and the semi-blind MMSE detector in [80] is consistently close to each other and the proposed semi-blind linear PIC-III has the best BER performance in Fig. 4.3a.

Next, we compare the performance of the proposed subspace-based semi-blind detectors with estimated coefficients, where $\hat{\mathbf{C}}_I$ was obtained using (4.20). Fig. 4.3b plots the BERs of the three estimated subspace-based semi-blind detectors proposed in this chapter with perfect knowledge of A_k ($k = 1, \ldots, K$) and σ^2 and Fig. 4.3c plots the BERs with estimated A_k ($k = 1, \ldots, K$) and σ^2 using the method mentioned in Sec. IV. The BERs of the estimated semi-blind multiuser detectors in [80] are also included in Figs. 4.3b and 4.3c. From these figures, it can be seen that in this simulation scenario, the proposed subspace-based semi-blind linear PIC multiuser detectors are robust to estimation errors of intra-cell user signal amplitudes and noise power and perform well under practical conditions. Including the adaptation algorithm, the proposed semi-blind detectors show great improvement in performance, which is almost indistinguishable from those using perfect coefficients. This can be easily seen from Fig. 4.3d.

The system parameters of the second and the third examples were kept the same as the first one except that we examined near-far scenarios in these examples. The received signal power of the inter-cell users was 10 dB stronger than those of the intra-cell users in the second example, while it was 10 dB weaker than those of the intra-cell users in the third example. The performances are given in Figs. 4.4 and 4.5, respectively. In the third example, the weakness of the inter-cell user signals relative to the intra-cell user signals leads to some errors in the adaptive inter-cell user signal subspace estimation. This is evident by the bumpy BER curve of the proposed semi-blind linear PIC-I in Fig. 4.5d. However, the inter-cell user signal subspace estimation errors are overcome in the proposed semi-blind linear PIC-II and III, which can be shown from Fig. 4.5d.

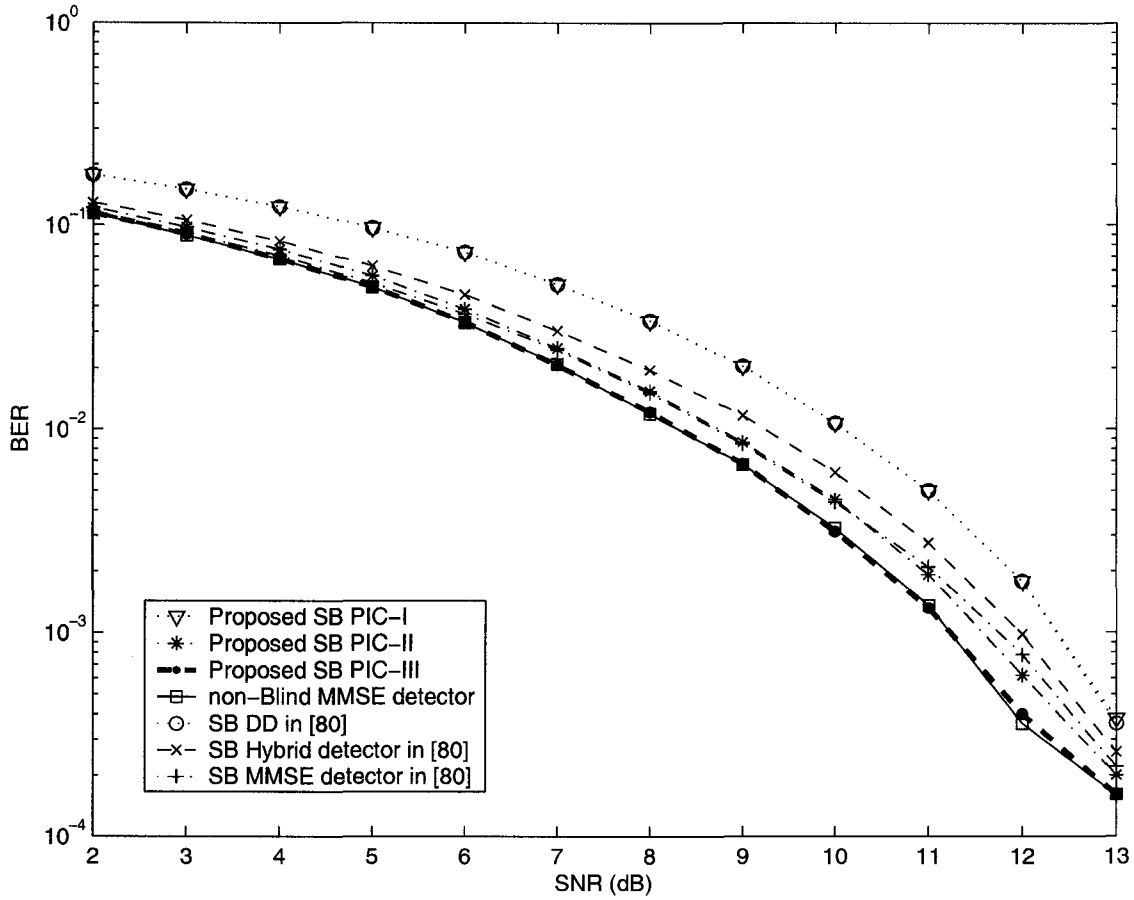

Figure 4.3a . *BER of the semi-blind multiuser detectors: Example 1. (Detectors with perfect coefficients.)*

From the above three examples, it can be concluded that generally speaking, the proposed subspace-based semi-blind linear PIC-III detector performs very well in different system scenarios compared with other semi-blind detectors. Therefore, it is a good choice in this semi-blind system scenario.

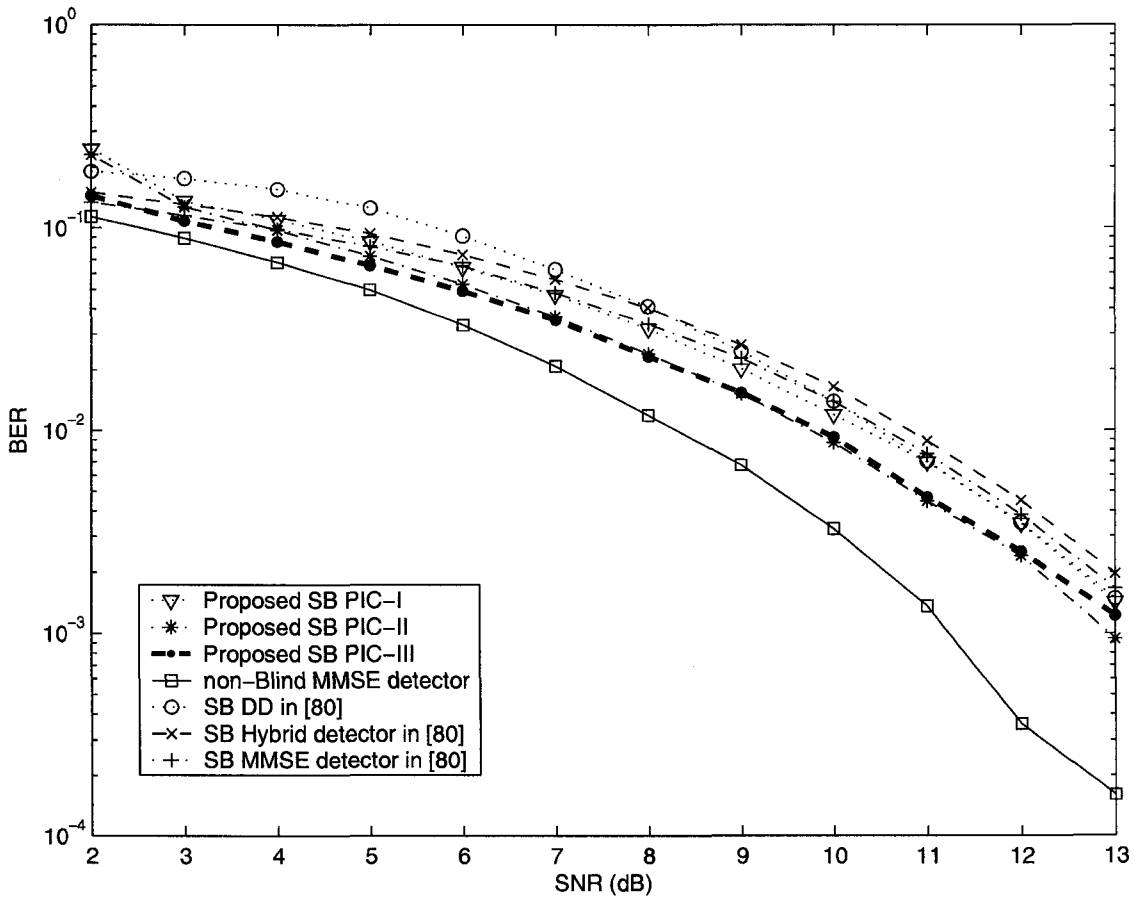

Figure 4.3b. *BER of the semi-blind multiuser detectors: Example 1. (Estimated detectors with perfect A_k and σ^2.)*

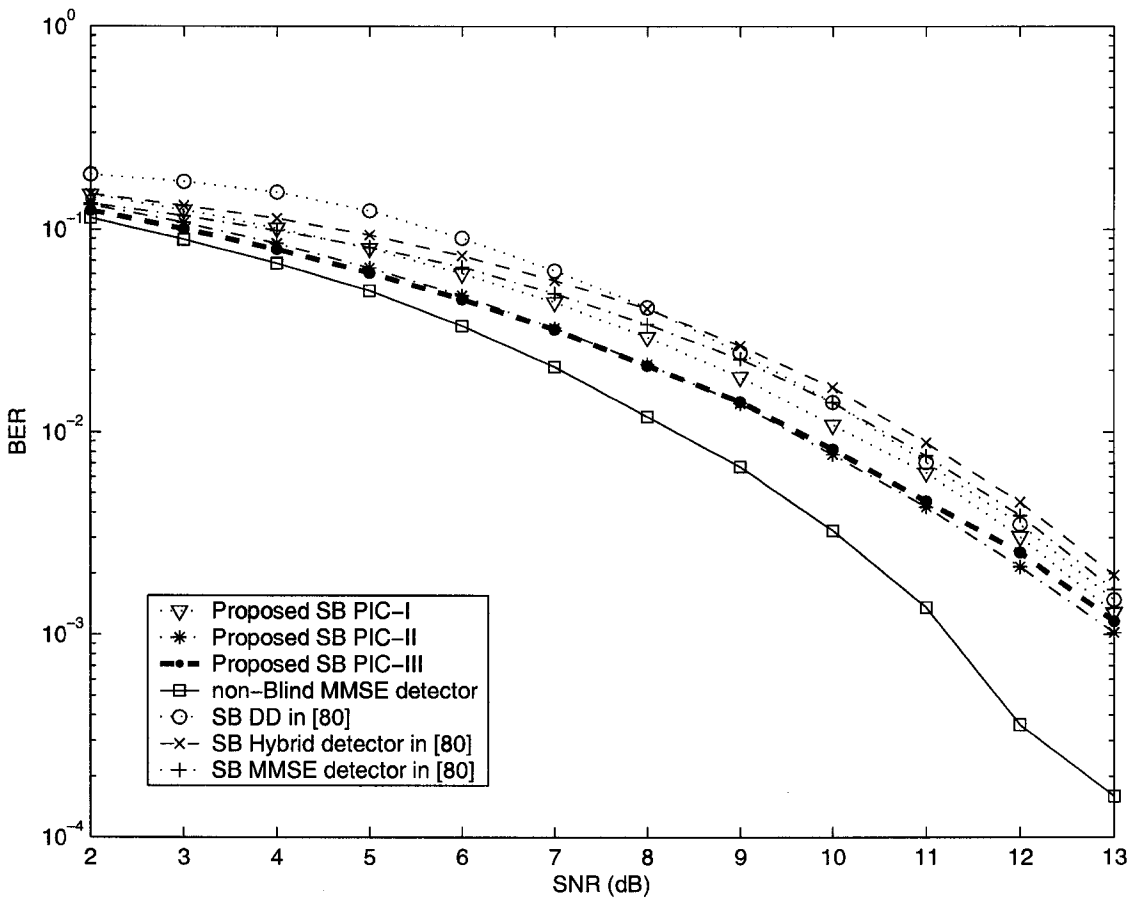

Figure 4.3c . *BER of the semi-blind multiuser detectors: Example 1. (Estimated detectors with estimated A_k and σ^2.)*

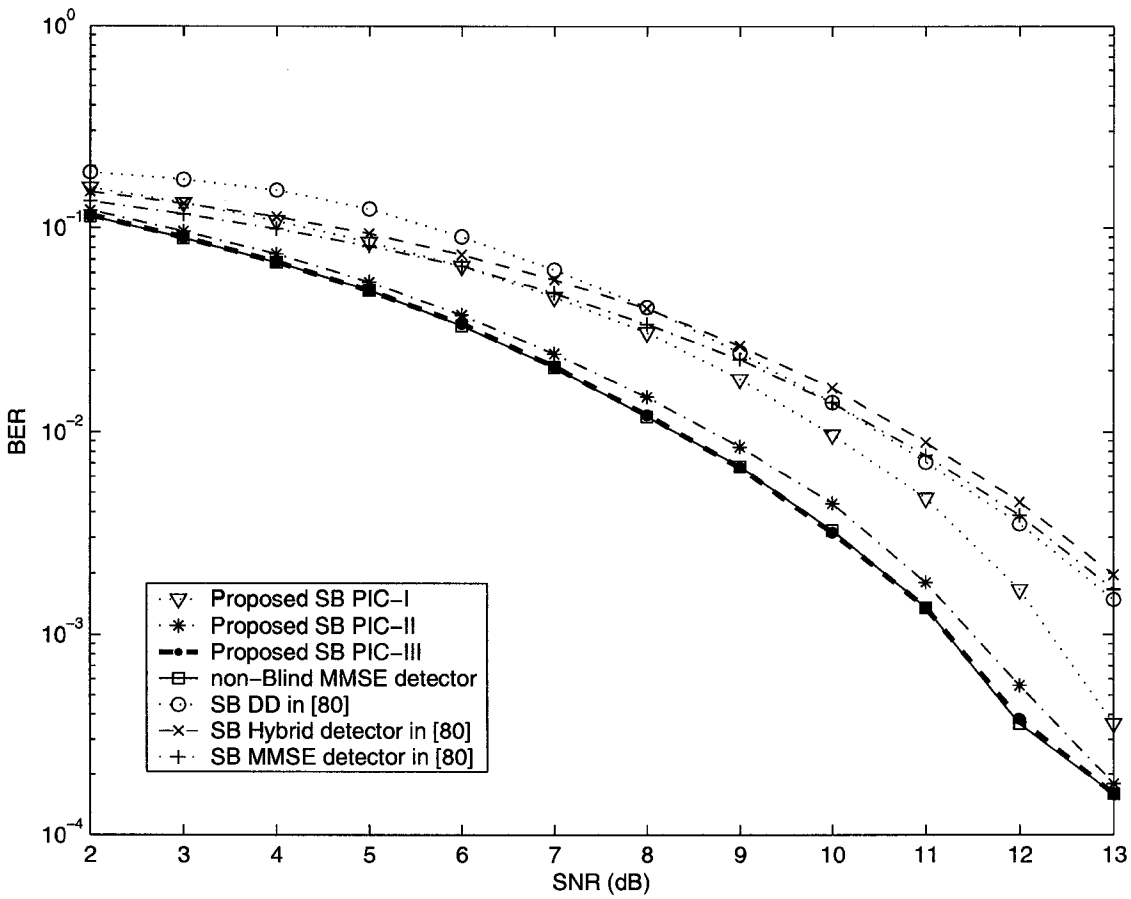

Figure 4.3d. *BER of the semi-blind multiuser detectors: Example 1. (Estimated detectors with recursive subspace tracking technique used in the proposed methods.)*

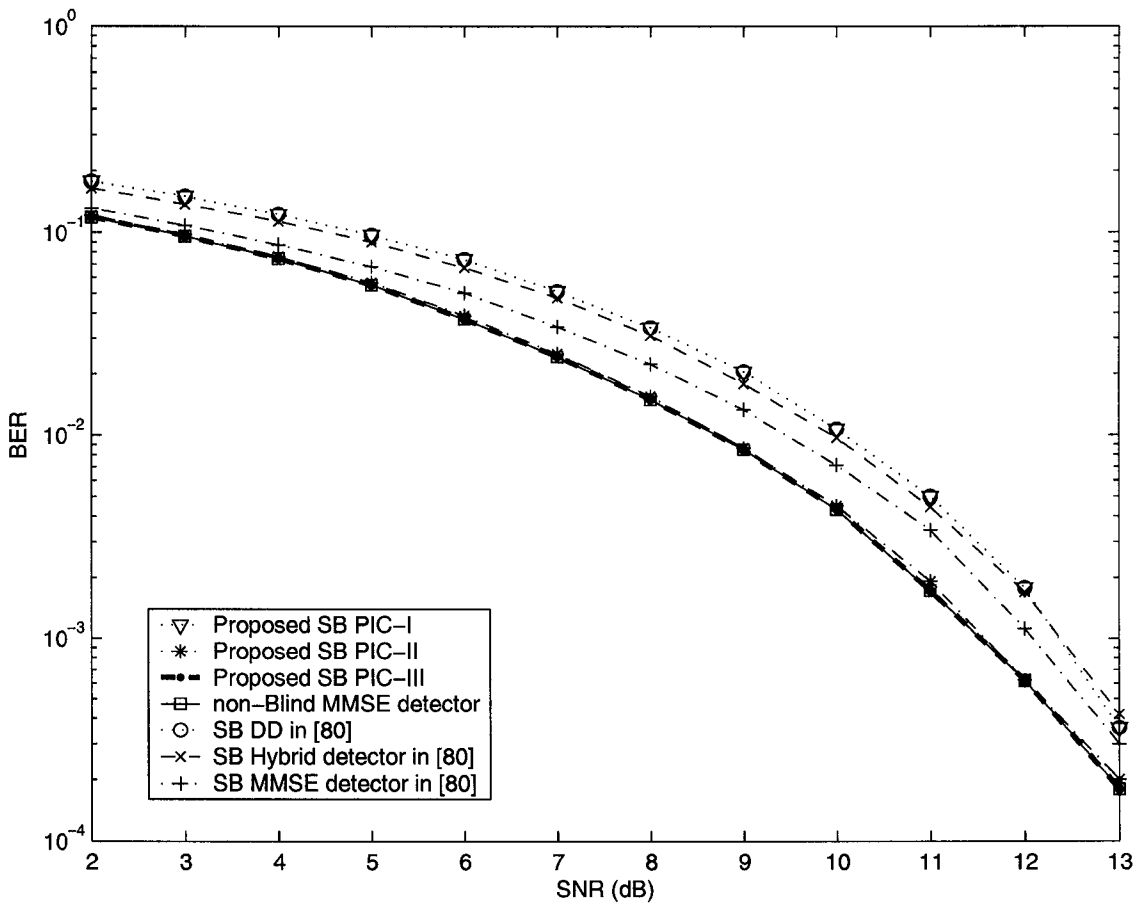

Figure 4.4a . *BER of the semi-blind multiuser detectors: Example 2. (Detectors with perfect coefficients.)*

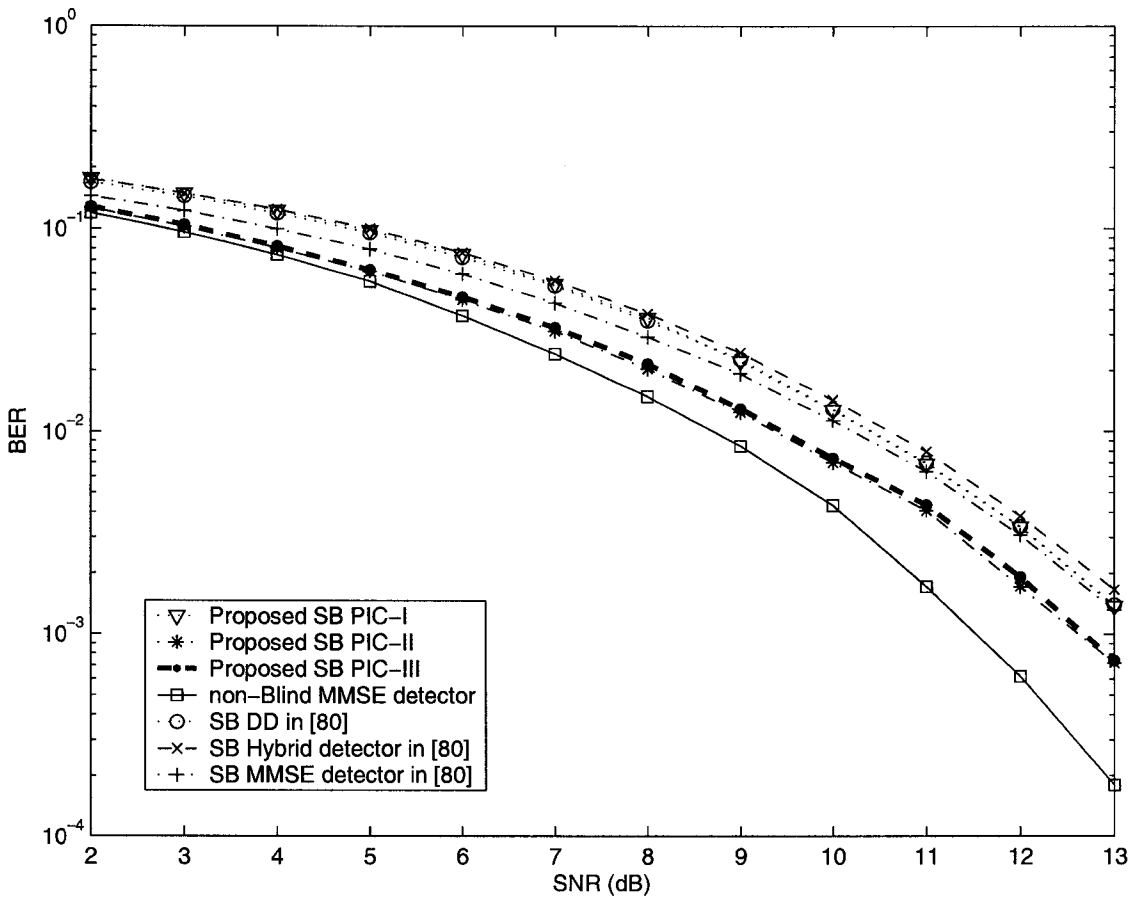

Figure 4.4b. *BER of the semi-blind multiuser detectors: Example 2. (Estimated detectors with perfect A_k and σ^2.)*

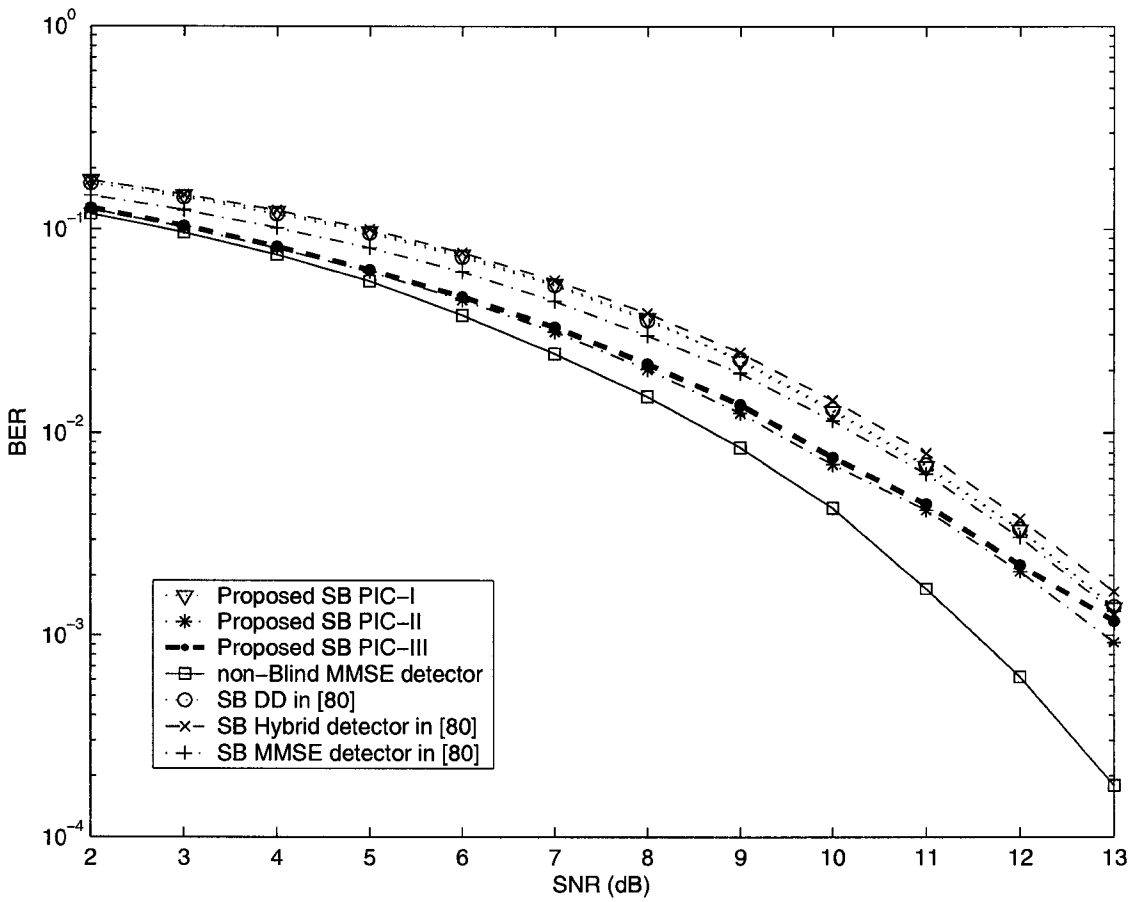

Figure 4.4c . *BER of the semi-blind multiuser detectors: Example 2. (Estimated detectors with estimated A_k and σ^2.)*

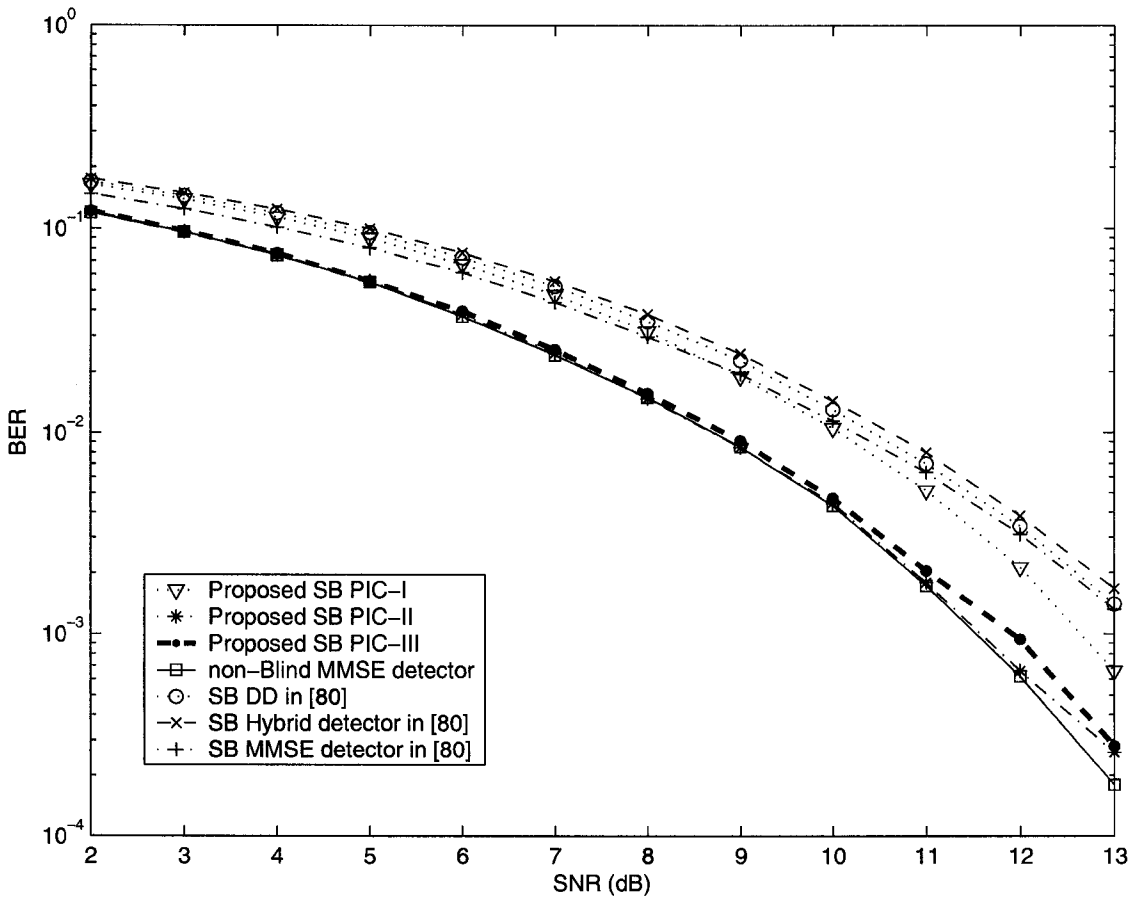

Figure 4.4d. *BER of the semi-blind multiuser detectors: Example 2. (Estimated detectors with recursive subspace tracking technique used in the proposed methods.)*

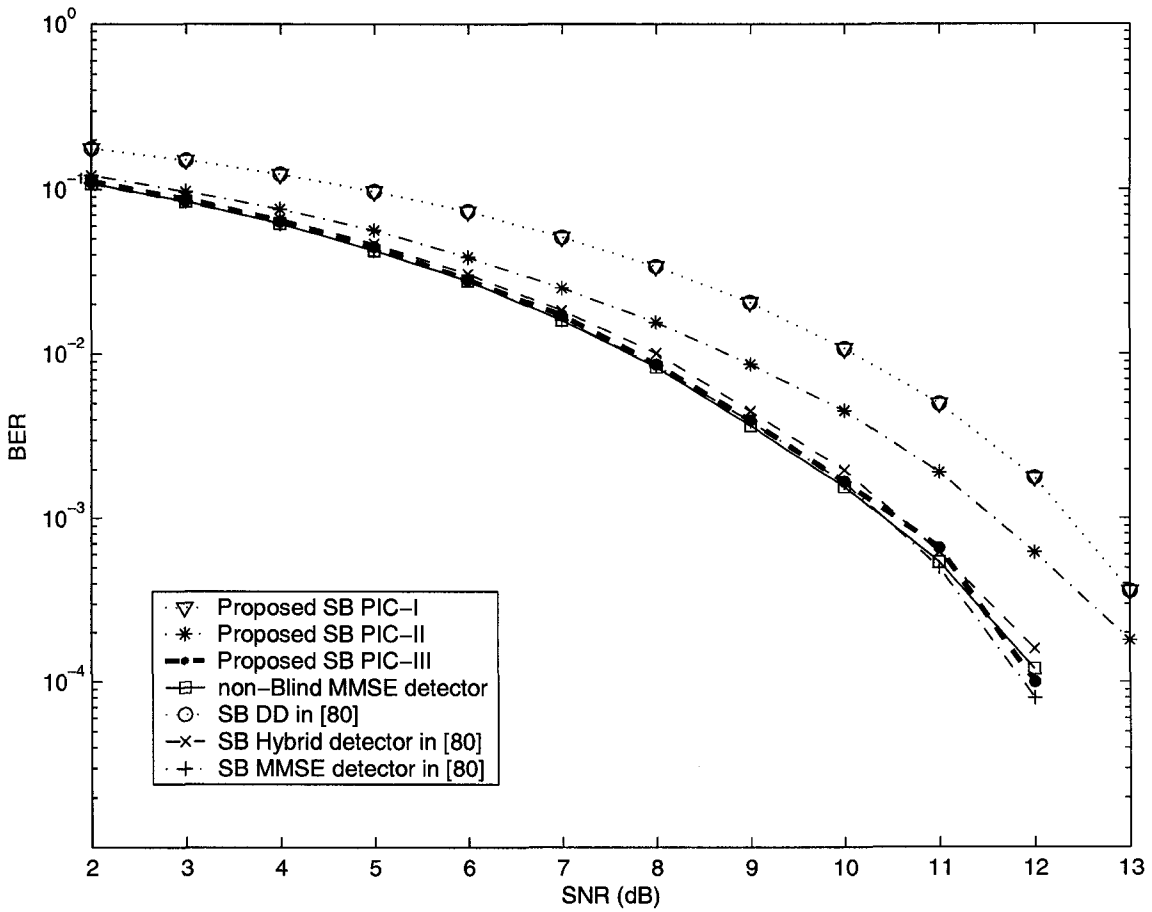

Figure 4.5a . *BER of the semi-blind multiuser detectors: Example 3. (Detectors with perfect coefficients.)*

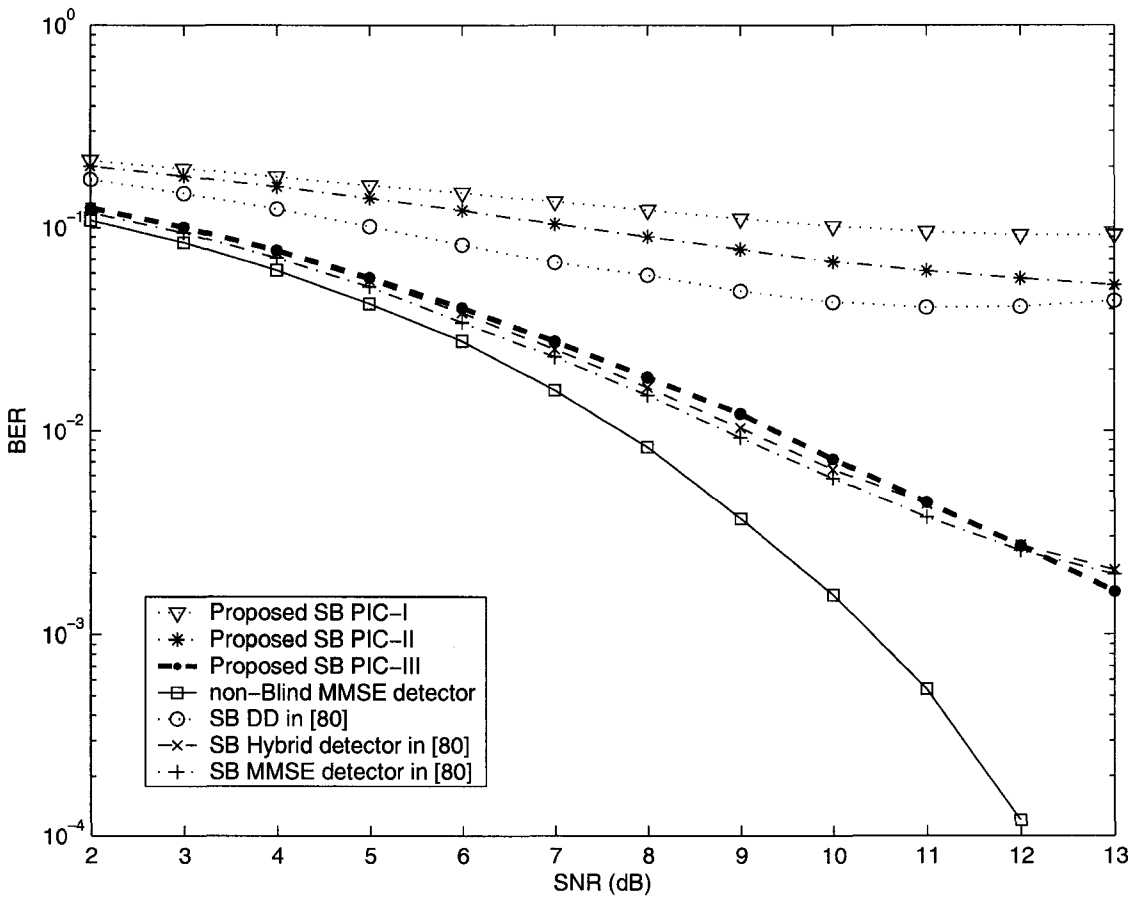

Figure 4.5b. *BER of the semi-blind multiuser detectors: Example 3. (Estimated detectors with perfect A_k and σ^2.)*

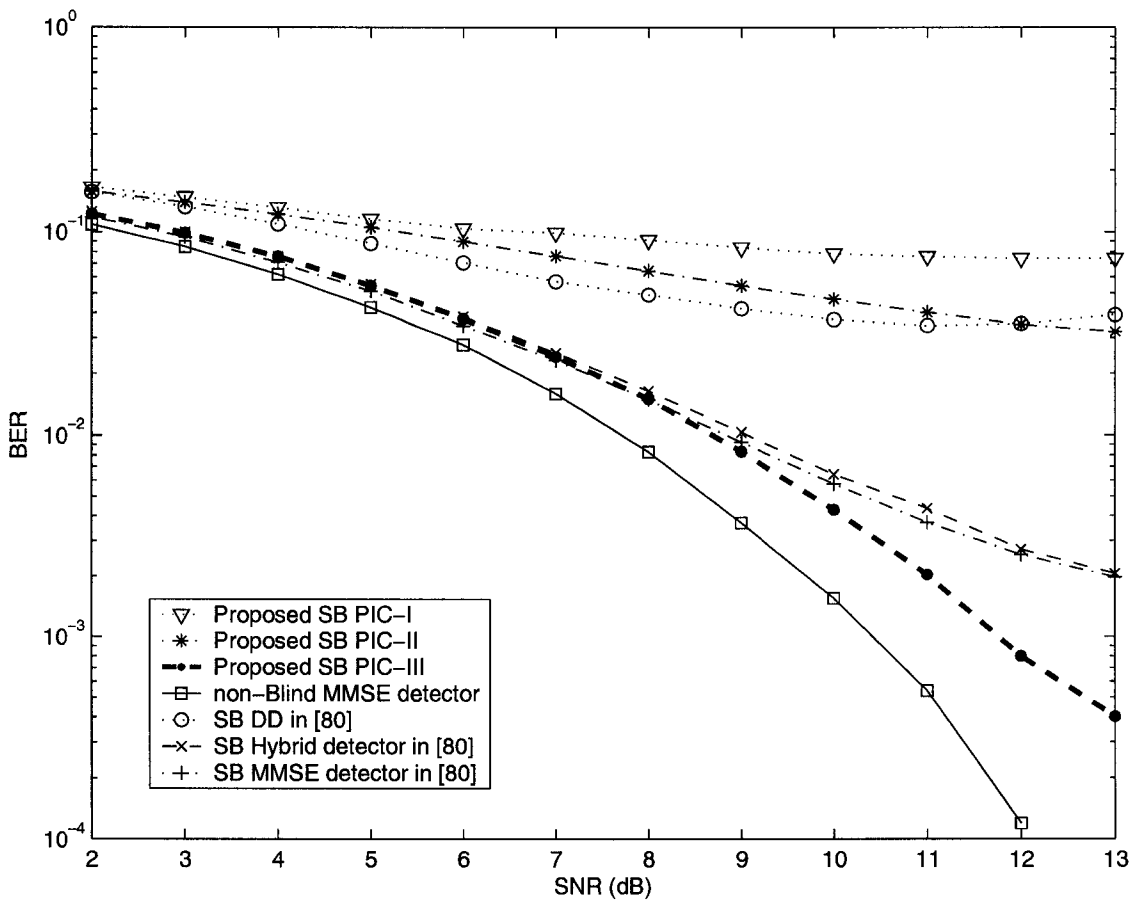

Figure 4.5c . *BER of the semi-blind multiuser detectors: Example 3. (Estimated detectors with estimated A_k and σ^2.)*

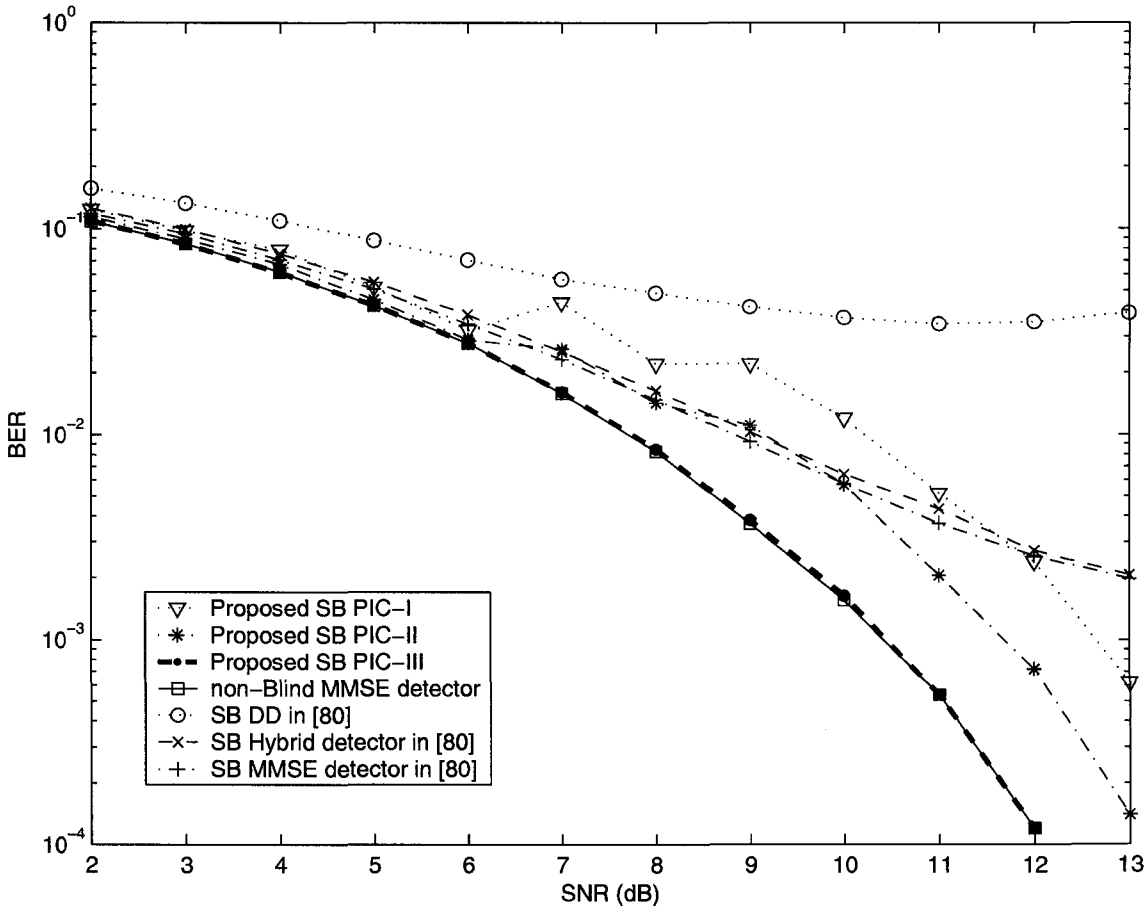

Figure 4.5d. *BER of the semi-blind multiuser detectors: Example 3. (Estimated detectors with recursive subspace tracking technique used in the proposed methods.)*

4.5 Conclusions

In this chapter, the multiuser detection problem for CDMA reverse link is considered. In the reverse link, although the interference comes from both intra-cell and inter-cell users, the BS only knows the signature codes of intra-cell users but does not know those of inter-cell users. Under this "semi-blind" system scenario, three semi-blind linear PIC multiuser detectors based on signal subspace decomposition are proposed. In the proposed detectors, the eigenvectors and eigenvalues of the inter-cell user signal subspace, which is obtained by making use of the known intra-cell users' signature codes, were used in PIC structures to help the demodulation of intra-cell user signals. It has been shown by numerical results that the proposed detectors, which are especially suitable for practical implementations, have a satisfactory performance in various near-far scenarios. Generally speaking, the proposed subspace-based semi-blind linear PIC-III is the best choice.

Appendix 4.A

$y_{1,k}$ in (4.17) can be given as

$$y_{1,k} = \bar{\mathbf{e}}_k^T \begin{bmatrix} \mathbf{S}^T\mathbf{S} & \mathbf{S}^T\mathbf{U}_I \\ \mathbf{U}_I^T\mathbf{S} & \mathbf{I}_{\tilde{K}} \end{bmatrix}^{-1} \begin{bmatrix} \mathbf{S}^T\mathbf{S} & \mathbf{S}^T\tilde{\mathbf{S}} \\ \mathbf{U}_I^T\mathbf{S} & \mathbf{U}_I^T\tilde{\mathbf{S}} \end{bmatrix} \begin{bmatrix} \mathbf{A} & \mathbf{0} \\ \mathbf{0} & \tilde{\mathbf{A}} \end{bmatrix} \begin{bmatrix} \mathbf{b} \\ \tilde{\mathbf{b}} \end{bmatrix} + \bar{\mathbf{e}}_k^T \mathbf{n}' \quad (4.21)$$

$$= \bar{\mathbf{e}}_k^T \begin{bmatrix} \mathbf{Y}_{11} & \mathbf{Y}_{12} \\ \mathbf{Y}_{21} & \mathbf{Y}_{22} \end{bmatrix} \begin{bmatrix} \mathbf{A}\mathbf{b} \\ \tilde{\mathbf{A}}\tilde{\mathbf{b}} \end{bmatrix} + \bar{\mathbf{e}}_k^T \mathbf{n}', \quad (4.22)$$

where $\mathrm{E}[\mathbf{n}'\mathbf{n}'^T] = \sigma^2\mathbf{R}_c^{-1}$ and (4.21) follows from the fact that $\mathbf{U}_I^T\mathbf{U}_I = \mathbf{I}_{\tilde{K}}$. The matrix inverse in (4.21) is given as

$$\begin{bmatrix} \mathbf{S}^T\mathbf{S} & \mathbf{S}^T\mathbf{U}_I \\ \mathbf{U}_I^T\mathbf{S} & \mathbf{I}_{\tilde{K}} \end{bmatrix}^{-1} = \begin{bmatrix} \mathbf{B}_{11} & \mathbf{B}_{12} \\ \mathbf{B}_{21} & \mathbf{B}_{22} \end{bmatrix} \quad (4.23)$$

where

$$\begin{aligned}
\mathbf{B}_{11} =& \left(\mathbf{S}^T\mathbf{S} - \mathbf{S}^T\mathbf{U}_I\mathbf{U}_I^T\mathbf{S}\right)^{-1} \\
\mathbf{B}_{22} =& \left(\mathbf{I}_{\tilde{K}} - \mathbf{U}_I^T\mathbf{S}(\mathbf{S}^T\mathbf{S})^{-1}\mathbf{S}^T\mathbf{U}_I\right)^{-1} \\
\mathbf{B}_{12} =& -\mathbf{B}_{11}\mathbf{S}^T\mathbf{U}_I \\
\mathbf{B}_{21} =& -\mathbf{B}_{22}\mathbf{U}_I^T\mathbf{S}(\mathbf{S}^T\mathbf{S})^{-1}.
\end{aligned}$$

Thus, $\mathbf{Y}_{11}$ and $\mathbf{Y}_{12}$ in (4.22) can be given as

$$\mathbf{Y}_{11} = \mathbf{B}_{11}\left(\mathbf{S}^T\mathbf{S} - \mathbf{S}^T\mathbf{U}_I\mathbf{U}_I^T\mathbf{S}\right) = \mathbf{I}_K \tag{4.24}$$

$$\mathbf{Y}_{12} = \mathbf{B}_{11}\left(\mathbf{S}^T\tilde{\mathbf{S}} - \mathbf{S}^T\mathbf{U}_I\mathbf{U}_I^T\tilde{\mathbf{S}}\right) \tag{4.25}$$

By Lemma 1, we have

$$\mathbf{S}^T\tilde{\mathbf{S}} - \mathbf{S}^T\mathbf{U}_I\mathbf{U}_I^T\tilde{\mathbf{S}} = \mathbf{S}^T\tilde{\mathbf{S}} - \mathbf{S}^T\tilde{\mathbf{S}}\tilde{\mathbf{S}}^\dagger\tilde{\mathbf{S}} = \mathbf{0}.$$

Hence

$$\mathbf{Y}_{12} = \mathbf{0}. \tag{4.26}$$

Therefore, from (4.22), (4.24) and (4.26), we have

$$y_{1,k} = A_k b_k + n_k', \qquad \text{for } k = 1, \ldots, K \tag{4.27}$$

where

$$\begin{aligned}
\mathrm{E}[n_k'^2] =& \sigma^2\left[(\mathbf{C}^T\mathbf{C})^{-1}\right]_{k,k} = \sigma^2\left[\mathbf{B}_{11}\right]_{k,k} \\
=& \sigma^2\left[\left(\mathbf{S}^T\mathbf{S} - \mathbf{S}^T\tilde{\mathbf{S}}\tilde{\mathbf{S}}^\dagger\mathbf{S}\right)^{-1}\right]_{k,k}.
\end{aligned} \tag{4.28}$$

(4.28) is obtained by using Lemma 1. On the other hand, the decision statistic of the kth intra-cell user for the non-blind linear DD is given by

$$\bar{y}_{d,k} = \bar{\mathbf{e}}_k^T(\bar{\mathbf{S}}^T\bar{\mathbf{S}})^{-1}\bar{\mathbf{S}}^T\mathbf{r} = A_k b_k + \bar{n}_k, \qquad \text{for } k = 1, \ldots, K \tag{4.29}$$

where

$$\begin{aligned}\mathrm{E}[\bar{n}_k^2] =& \sigma^2 \left[(\bar{\mathbf{S}}^T\bar{\mathbf{S}})^{-1}\right]_{k,k} = \sigma^2 \left\{ \begin{bmatrix} \mathbf{S}^T\mathbf{S} & \mathbf{S}^T\tilde{\mathbf{S}} \\ \tilde{\mathbf{S}}^T\mathbf{S} & \tilde{\mathbf{S}}^T\tilde{\mathbf{S}} \end{bmatrix}^{-1} \right\}_{k,k} \\ =& \sigma^2 \left[\left(\mathbf{S}^T\mathbf{S} - \mathbf{S}^T\tilde{\mathbf{S}}(\tilde{\mathbf{S}}^T\tilde{\mathbf{S}})^{-1}\tilde{\mathbf{S}}^T\mathbf{S} \right)^{-1} \right]_{k,k}. \end{aligned} \tag{4.30}$$

Since the matrix $\bar{\mathbf{S}}$ is assumed to have full column rank, $\left(\bar{\mathbf{S}}^T\bar{\mathbf{S}}\right)$ is nonsingular. From (4.30) it is obvious that $\left(\mathbf{S}^T\mathbf{S} - \mathbf{S}^T\tilde{\mathbf{S}}(\tilde{\mathbf{S}}^T\tilde{\mathbf{S}})^{-1}\tilde{\mathbf{S}}^T\mathbf{S}\right)$ is also nonsingular.

From (4.28) and (4.30), $\mathrm{E}[n_k'^2] = \mathrm{E}[\bar{n}_k^2]$. And from (4.27) and (4.29), it can be concluded that the converged subspace-based semi-blind linear PIC-I yields the same BER as the non-blind linear DD.

Appendix 4.B

By using the similar analysis process as in Appendix 4.A and approximating the MAI at the detector output with a Gaussian *r.v.* of identical variance, the BER of the kth intra-cell user of the converged semi-blind PIC-II can be given as [68]

$$p_2^k = p\left(A_k, (\mathbf{L}_I)_{k,k}\right) \qquad \text{for } k = 1, \ldots, K \tag{4.31}$$

where

$$p(x, y) = \mathcal{Q}\left(\frac{x}{\sigma}\sqrt{\frac{1}{y} - \frac{\sigma^2}{x^2}} \right)$$

with $\mathcal{Q}(x) = \frac{1}{\sqrt{2\pi}} \int_x^\infty e^{-t^2/2} dt$, and $\mathbf{L}_I = (\mathbf{R}_I + \sigma^2\mathbf{A}^{-2})^{-1}$ with $\mathbf{R}_I = \mathbf{S}^T\mathbf{S} - \mathbf{S}^T\mathbf{U}_I\mathbf{U}_I^T\mathbf{S}$. By Lemma 1, we have

$$\mathbf{L}_I = \left(\mathbf{S}^T\mathbf{S} + \sigma^2\mathbf{A}^{-2} - \mathbf{S}^T\tilde{\mathbf{S}}\tilde{\mathbf{S}}^\dagger\mathbf{S}\right)^{-1} \tag{4.32}$$

On the other hand, the Gaussian approximated BER of the kth intra-cell user of the non-blind linear MMSE detector is given as

$$\bar{p}_m^k = p\left(A_k, \bar{\mathbf{L}}_{k,k}\right) \qquad \text{for } k = 1, \ldots, K \tag{4.33}$$

where $\bar{\mathbf{L}} = (\bar{\mathbf{S}}\bar{\mathbf{S}}^T + \sigma^2\bar{\mathbf{A}}^{-2})^{-1}$. Note that

$$\bar{\mathbf{L}}_{k,k} = \left[\left(\mathbf{S}^T\mathbf{S} + \sigma^2\mathbf{A}^{-2} - \mathbf{S}^T\tilde{\mathbf{S}}(\tilde{\mathbf{S}}^T\tilde{\mathbf{S}} + \sigma^2\tilde{\mathbf{A}}^{-2})^{-1}\tilde{\mathbf{S}}^T\mathbf{S}\right)^{-1}\right]_{k,k} \quad \text{for } k = 1, \ldots, K \tag{4.34}$$

From (4.32) and (4.34), by using the matrix inversion lemma and after some manipulations we have

$$(\mathbf{L}_I)_{k,k} - \bar{\mathbf{L}}_{k,k} = \mathbf{e}_k^T\mathbf{F}\mathbf{M}_1^{-1}(\mathbf{M}_1^{-1} + \sigma^{-2}\tilde{\mathbf{A}}^2)^{-1}\mathbf{M}_1^{-T}\mathbf{F}^T\mathbf{e}_k \quad \text{for } k = 1, \ldots, K \tag{4.35}$$

where

$$\begin{aligned}\mathbf{F} =& (\mathbf{S}^T\mathbf{S} + \sigma^2\mathbf{A}^{-2})^{-1}\mathbf{S}^T\tilde{\mathbf{S}},\\ \mathbf{M}_1 =& \tilde{\mathbf{S}}^T\tilde{\mathbf{S}} - \tilde{\mathbf{S}}^T\mathbf{S}\mathbf{F},\end{aligned}$$

and $\mathbf{e}_k$ is the kth unit vector in $\mathcal{R}^K$. Note that

$$\mathbf{M}_1^{-1} + \sigma^{-2}\tilde{\mathbf{A}}^2 = \tilde{\mathbf{S}}^\dagger(\mathbf{I}_N + \mathbf{S}\sigma^{-2}\mathbf{A}^2\mathbf{S}^T)(\tilde{\mathbf{S}}^\dagger)^T + \sigma^{-2}\tilde{\mathbf{A}}^2 \succ \mathbf{0} \tag{4.36}$$

The notation $\mathbf{M}_1^{-1} + \sigma^{-2}\tilde{\mathbf{A}}^2 \succ \mathbf{0}$ denotes that the matrix $\mathbf{M}_1^{-1} + \sigma^{-2}\tilde{\mathbf{A}}^2$ is positive definite. Therefore $(\mathbf{L}_I)_{k,k} - \bar{\mathbf{L}}_{k,k} \geq 0$, and $p_2^k \geq \bar{p}_m^k$ $(k = 1, \ldots, K)$.

From (4.29) and (4.30) in Appendix 4.A, the BER of the kth intra-cell user of the non-blind linear DD is given as

$$\bar{p}_d^k = \mathcal{Q}\left(\frac{A_k}{\sigma}\sqrt{\frac{1}{(\mathbf{R}_I^{-1})_{k,k}}}\right) \quad \text{for } k = 1, \ldots, K \tag{4.37}$$

By using the matrix inversion lemma and after some manipulations we have

$$(\mathbf{R}_I^{-1})_{k,k} - (\mathbf{L}_I)_{k,k} - \frac{\sigma^2}{A_k^2}(\mathbf{L}_I)_{k,k}(\mathbf{R}_I^{-1})_{k,k} = \mathbf{e}_k^T\mathbf{R}_I^{-1}\mathbf{M}_2\mathbf{R}_I^{-1}\mathbf{e}_k \tag{4.38}$$

where

$$\begin{aligned}\mathbf{M}_2 =& (\mathbf{R}_I^{-1} + \sigma^{-2}\mathbf{A}^2)^{-1} - \frac{\sigma^2}{A_k^2}\mathbf{e}_k\mathbf{e}_k^T(\mathbf{R}_I^{-1} + \sigma^2\mathbf{A}^{-2})^{-1}\mathbf{R}_I\\ =& \mathbf{D}(\mathbf{R}_I^{-1} + \sigma^2\mathbf{A}^{-2})^{-1}\mathbf{R}_I\end{aligned} \tag{4.39}$$

with $\mathbf{D} = \sigma^2\mathbf{A}^{-2} - \frac{\sigma^2}{A_k^2}\mathbf{e}_k\mathbf{e}_k^T \succeq \mathbf{0}$. The notation $\mathbf{D} \succeq \mathbf{0}$ denotes that the matrix $\mathbf{D}$ is positive semidefinite. As shown in Appendix 4.A, $\mathbf{R}_I$ is nonsingular and

$$\mathbf{R}_I = \mathbf{S}^T\mathbf{S} - \mathbf{S}^T\mathbf{U}_I\mathbf{U}_I^T\mathbf{S} = \mathbf{S}^T\mathbf{U}_n\mathbf{U}_n^T\mathbf{S} = \mathbf{R}_I^T, \tag{4.40}$$

therefore we have $\mathbf{R}_I \succ \mathbf{0}$ and $(\mathbf{R}_I^{-1} + \sigma^{-2}\mathbf{A}^2)^{-1} \succ \mathbf{0}$. According to the result in [98], $\mathbf{M}_2 \succeq \mathbf{0}$. From (4.38), we have

$$(\mathbf{R}_I^{-1})_{k,k} - (\mathbf{L}_I)_{k,k} - \frac{\sigma^2}{A_k^2}(\mathbf{L}_I)_{k,k}(\mathbf{R}_I^{-1})_{k,k} \geq 0 \tag{4.41}$$

From (4.31), it can be seen that $1 - \frac{\sigma^2}{A_k^2}(\mathbf{L}_I)_{k,k} > 0$, therefore we have $\frac{(\mathbf{L}_I)_{k,k}}{1-\frac{\sigma^2}{A_k^2}(\mathbf{L}_I)_{k,k}} \leq (\mathbf{R}_I^{-1})_{k,k}$ and $p_2^k \leq \bar{p}_d^k$ $(k = 1, \ldots, K)$.

From the above discussion, we have

$$\bar{p}_m^k \leq p_2^k \leq \bar{p}_d^k \qquad \text{for } k = 1, \ldots, K \tag{4.42}$$

Chapter 5

Conclusions and Future Work

5.1 Conclusions

We have investigated the DS-CDMA systems with multiuser detectors used at the receiver and developed two kinds of multiuser detectors for the DS-CDMA systems.

After briefly introducing the research area of this dissertation in Chapter 1, in Chapter 2, we have investigated both the reverse link and the forward link of DS-CDMA systems, where heterogeneous traffic is supported and DD for multi-rate systems is used at the receiver. It has been shown that the system performance is sensitive to power control errors and the existence of outer-cell interferers, which are related to the realistic system scenarios. Because of the limited BS transmission power and the QoS requirements of each user in the system, the forward link power allocation problem can be formulated as a constrained optimization problem based on the measurements of random characteristics of received signals. It has been shown that by imposing another appropriate constraint, the problem is converted to a CP problem for both single-cell and multiple-cell systems, which can be solved easily. Two power allocation algorithms have been proposed to first identify the feasible region of this CP problem and then allocate the BS transmission power efficiently. The comparison of these two algorithms through numerical examples shows that the performance of the UTXPA algorithm is close to that of the optimal algorithm with considerably reduced computational complexity.

In Chapter 3, we focused on adaptive MMSE multiuser detection. It has been shown

that (a) in communication channels with near-far problem, the convergence rates of adaptive MMSE detectors for strong power users are usually much higher than those for weak power users by using the adaptive algorithms invoving low computational complexity like the LMS algorithm; and (b) by using RLS algorithm, the differences in the convergence rates can be alleviated, but at the cost of significantly increased computational complexity. We have developed a fast converging adaptive MMSE detector with low computational complexity based on the GSIC technique. By successively subtracting the interference of the strong power user signals from the received signal, the convergence rates of adaptive detectors for weak power users are significantly increased. A parameter estimation scheme has also been developed, which utilizes the steady state parameters of the corresponding adaptive detectors. Numerical examples have shown that the proposed method provides satisfactory convergence rates and BER performance in various near-far scenarios. Since the proposed scheme can reduce the effect of MAI significantly, a significant BER performance improvement may be obtained by using the proposed scheme.

Although the proposed adaptive MMSE detector needs a training sequence, the idea and the results presented in Chapter 3 can be easily extended to the case of blind adaptive multiuser detectors, where only information about the interested users' signature codes are needed and no training sequence is required. Although it is natural to use the proposed fast converging adaptive detection schemes in the reverse link, they can be used in the forward link as well.

In Chapter 4, we focused on the multiuser detection scheme design for the reverse link of CDMA systems with multiple cells. In this application scenario, the received signal comes from intra-cell users as well as inter-cell users. But the BS only knows the information about intra-cell users. We proposed to deal with this "semi-blind" multiuser detection problem based on the ideas of signal subspace decomposition and linear PIC. The detection process was made up of two steps: First we obtain the inter-cell user signal subspace by making use of the known information about intra-cell users, and then the eigenvectors and eigenvalues of this subspace, which are obtained through ED, are used in place of the un-

known inter-cell users' signature codes and signal amplitudes in the traditional linear PIC structure. Three semi-blind linear PIC detectors were proposed based on this idea. By making use of the PASTd algorithm, an efficient adaptation implementation method has also been developed. It has been shown by analysis and computer simulations that in most system scenarios (a) the proposed semi-blind linear PIC-I yields the same BER performance as the non-blind linear DD where signature codes of both intra-cell and inter-cell users are known; (b) the BER performance of the proposed semi-blind linear PIC-II is better than that of the non-blind DD but worse than that of the non-blind MMSE detector; and (c) the BER performance of the proposed semi-blind linear PIC-III is almost indistinguishable from that of the non-blind MMSE detector. Generally speaking, the proposed semi-blind linear PIC-III is a good choice in the semi-blind system scenario.

5.2 Future Work

As a continuation of the work in this dissertation, possible future research topics are listed as follows:

1. We can continue the research on semi-blind multiuser detectors. In Chapter 4, the performance of the proposed semi-blind linear PIC detectors was analyzed based on the true detectors, which are obtained assuming that the inter-cell user signal subspace and the background noise power are perfectly known. In a realistic scenario, however, the proposed detectors can only be estimated from the received signal. The estimated detectors coincide with the true detectors only when the length of the sample signal, denoted as M in Chapter 4, approximates infinity. Therefore, it is desirable to find out the performance of the estimated proposed semi-blind detectors. In addition, the semi-blind detectors developed in Chapter 4 are for DS-CDMA systems using short-codes, where the users' signature codes repeat in every bit. In conventional CDMA systems, e.g. IS-95, long-codes are employed where the code length is much longer than the processing gain and the users' signature codes change in each

symbol period. Extending the semi-blind linear PIC detectors developed in Chapter 4 to long-code CDMA systems is not trivial extension and deserves further studies.

2. In the discussion of Chapter 2, multiuser detectors designed for single-cell systems were used directly in multiple-cell systems, and inter-cell interference was approximated as Gaussian noise. It is shown that the interference from inter-cell users causes considerable system capacity degradation. Considering the existence of inter-cell interferers, semi-blind multiuser detection schemes have been developed in Chapter 4, whose BER performance is very close to that of the non-blind linear detectors. We can combine the studies in Chapter 2 and Chapter 4. We can study the performance of the multiple-cell CDMA system reverse link where heterogeneous traffic is supported, power control is imperfect, and semi-blind multiuser detectors are used at the receiver. System capacity is expected to be much higher in this scenario than what we have obtained in Chapter 2.
3. In Chapter 3, the different convergence behavior of adaptive MMSE multiuser detectors for users with different power in a definite near-far scenario was explained through transient MSE analysis based on general adaptive filtering theory. It is shown that although the values of transient coefficients are the same or similar for users with different powers, their associated constant coefficients are quite different, resulting in different dominant transient terms. This was investigated using simulation examples. It would be interesting to explain why the constant coefficients are different for users with different power using a matrix analysis method.

Bibliography

[1] T. S. Rappaport, *Wireless Communications: Principles & Practice*, Upper Saddle River, NJ: Prentice Hall, 1996.

[2] M. Zeng, A. Annamalai and V. K. Bhargava, "Recent advances in cellular wireless communications", *IEEE Commun. Magazine*, pp. 128-138, Sept. 1999.

[3] http://www.3g-generation.com/.

[4] A. J. Viterbi, *CDMA: Principles of Spread Spectrum Communication*, Addison-Wesley, 1995.

[5] M. K. Simon, J. K. Omura, R. A. Scholtz and B. K. Levitt, *Spread Spectrum Communications Handbook*, McGraw-Hill, 1994.

[6] E. H. Dinam and B. Jabbari, "Spreading codes for direct sequence CDMA and wideband CDMA cellular networks", *IEEE Commun. Magazine*, pp. 48-54, Sept. 1998.

[7] K. S. Gilhousen, I. M. Jacobs, R. Padovani, A. J. Viterbi, A. Weaver and C. E. Wheatley, "On the capacity of a cellular CDMA system," *IEEE Trans. Veh. Technol.*, vol. 40, no. 2, pp. 303-311, May 1991.

[8] Telecommunications Industry Association, "Mobile station-base station compatibility standard for dual-mode wideband spread spectrum cellular system," Tech. Rep. TIA/EIA/IS-95, Electronic Industries Association, July 1993.

[9] J. G. Proakis, *Digital Communications*, New York: McGraw-Hill, 1995.

[10] H. V. Poor, *Tutorial Notes - Multiuser Detection: Advanced Signal Processing for Wireless Systems*, IEEE VTC'2002 Fall, Sept. 2002.

[11] S. Moshavi, "Multi-user detection for DS-CDMA communications", *IEEE Commun. Magazine*, pp. 124-136, Oct. 1996.

[12] S. Verdú, *Multiuser Detection*, Cambridge: Cambridge University Press, 1998.

[13] S. Verdú, "Minimum probability of error for asynchronous Gaussian multiple-access channels," *IEEE Trans. Inform. Theory*, vol. 32, pp. 85-96, Jan. 1986.

[14] K. S. Schneider, "Optimum detection of code division multiplexed signals", *IEEE Trans. Aerospace Elec. Sys.*, vol. AES-15, pp. 181-185, Jan. 1979.

[15] R. Kohno, M. Hatori and H. Imai, "Cancellation techniques of co-channel interference

in asynchronous spread spectrum multiple access systems", *Elect. and Commun. in Japan*, vol. 66-A, no. 5, pp. 20-29, 1983.

[16] R. Lupas and S. Verdú, "Linear multiuser detectors for synchronous code-division multiple-access channels", *IEEE Trans. Inform. Theory*, vol. 35, no. 1, pp. 123-136, 1989.

[17] R. Lupas and S. Verdú, "Near-far resistance of multiuser detectors in asynchronous channels", *IEEE Trans. Commun.*, vol. 38, no. 4, pp. 496-508, 1990.

[18] Z. Xie, R. T. Short and C. K. Rushforth, "A family of suboptimum detectors for coherent multi-user communications", *IEEE J. Select. Areas Commun.*, vol. 8, no. 4, pp. 683-690, May 1990.

[19] D. S. Chen and S. Roy, "An adaptive multiuser receiver for CDMA systems", *IEEE J. Select. Areas Commun.*, vol. 12, no. 5, pp. 808-816, June 1994.

[20] P. B. Rapajic and B. S. Vucetic, "Adaptive receiver structures for asynchronous CDMA systems", *IEEE J. Select. Areas Commun.*, vol. 12, no. 4, pp. 685-697, May 1994.

[21] P. B. Rapajic and B. S. Vucetic, "Application of fast adaptive algorithms in asynchronous CDMA systems", *Int. Symp. on Inform. Theory and Its Applications*, pp. 97-102, Nov. 1994.

[22] U. Madhow and M. L. Honig, "MMSE interference suppression for direct-sequence spread-spectrum CDMA", *IEEE Trans. Commun.*, vol. 42, no. 12, pp. 3178-3188, 1994.

[23] S. L. Miller, "An adaptive direct-sequence code-division multiple-access receiver for multiuser interference rejection", *IEEE Trans. Commun.*, vol. 43, no. 2/3/4, pp. 1746-1755, Feb./Mar./Apr. 1995.

[24] M. L. Honig, U. Madhow and S. Verdú, "Blind adaptive multiuser detection", *IEEE Trans. Inform. Theory*, vol. 41, no. 4, pp. 944-960, 1995.

[25] J. Míguez and L. Castedo, "A linearly constrained constant modulus approach to blind adaptive multiuser interference suppression", *IEEE Commun. Letter*, vol. 2, no. 8, pp. 217-219, 1998.

[26] X. Wang and H. V. Poor, "Blind multiuser detection: A subspace approach", *IEEE Trans. Inform. Theory*, vol. 44, no. 2, pp. 677-690, Mar. 1998.

[27] A. J. Viterbi, "Very low rate convolutional codes for maximum theoretical performance of spread-spectrum multiple-access channels", *IEEE J. Select. Areas Commun.*, vol. 8, pp. 641-649, May 1990.

[28] R. Kohno, H. Imai, M. Hatori and S. Pasupathy, "Combination of an adaptive array

and a canceller of interference for direct sequence spread spectrum multiple access system", *IEEE J. Select. Areas Commun.*, vol. 8, pp. 675-682, May 1990.

[29] R. Kohno, "Pseudo-noise sequences and interference cancellation techniques for spread spectrum systems - spread spectrum theory and techniques in Japan", *IEICE Trans. Commun.*, vol. E74, pp. 1083-1092, May 1991.

[30] P. R. Patel and J. M. Holtzman, "Analysis of a DS/CDMA successive interference cancellation scheme using correlations", *Proc. GLOBECOM'93*, pp. 76-80, Nov. 1993.

[31] P. R. Patel and J. M. Holtzman, "Analysis of a simple successive interference cancellation scheme in a DS/CDMA system", *IEEE J. Select. Areas Commun.*, vol. 12, no. 5, pp. 796-807, June 1994.

[32] M. K. Varanasi and B. Aazhang, "Multistage detection in asynchronous code-division multiple-access communications", *IEEE Trans. Commun.*, vol. 38, pp. 509-519, Apr. 1990.

[33] M. K. Varanasi and B. Aazhang, "Near optimal detectors in synchronous code-division multiple-access systems", *IEEE Trans. Commun.*, vol. 39, pp. 725-736, May 1991.

[34] D. Divsalar, M. K. Simon and D. Raphaeli, "Improved parallel interference cancellation for CDMA", *IEEE Trans. Commun.*, vol. 46, pp. 258-268, Feb. 1998.

[35] G. Xue, J. Weng, T. Le-Ngoc and S. Tahar, "Adaptive multistage parallel interference cancellation for CDMA", *IEEE J. Select. Areas Commun.*, vol. 17, no. 10, pp. 1815-1827, Oct. 1999.

[36] H. Elders-Boll, H. D. Schotten and A. Busboom, "Efficient implementation of linear multiuser detectors for asynchronous CDMA systems by linear interference cancellation", *European Trans. Telecommun.*, vol. 9, pp. 427-438, Sept.-Oct. 1998.

[37] A. Yener, R. D. Yates and S. Ulukus, "CDMA multiuser detection: a nonlinear programming approach", *IEEE Trans. Commun.*, vol. 50, no. 6, pp. 1016-1024, June 2002.

[38] A. Duel-Hallen, "Decorrelating decision-feedback multi-user detector for synchronous code-division multiple access channel", *IEEE Trans. Commun.*, vol. 41, pp. 285-290, Feb. 1993.

[39] A. Duel-Hallen, "A family of multi-user decision-feedback detectors for asynchronous code-division multiple access channels", *IEEE Trans. Commun.*, vol. 43, pp. 421-434, Feb./Mar./Apr. 1995.

[40] M. Kavehrad and J. Salz, "Cross-polarization cancellation and equalization in digital

transmission over dually polorized multipath fading channels", *AT & T Technical Journal*, vol. 64, pp. 2211-2245, Dec. 1985.

[41] M. Varanasi and T. Guess, "Optimum decision feedback multiuser equalization with successive decoding achieves the total capacity of the Gaussian multiple access channel", *Proc. Asilomar Conf. Signal, Systems and Computing*, pp. 1405-1409, Monterrey, CA, Nov. 1997.

[42] C.-L. I and K. K. Sabnani, "Variable spreading gain CDMA with adaptive control for integrated traffic in wireless networks", *Proc. IEEE VTC'95*, pp. 794-798, July 1995.

[43] S.-J. Oh and K. M. Wasserman, "Dynamic spreading gain control in multiservice CDMA networks", *IEEE J. Select. Areas Commun.*, vol. 17, no. 5, pp. 918-927, 1999.

[44] T.-H. Wu and E. Geraniotis, "CDMA with multiple chip rates for multi-media communications", *Proc. Information Science and Systems*, Princeton, NJ, pp. 992-997, 1994.

[45] C.-L. I, G. P. Pollini, L. Ozarow and R. D. Gitlin, "Performance of multi-code CDMA wireless personal communications networks", *Proc. IEEE VTC'95*, pp. 907-911, July 1995.

[46] C.-L. I and R. D. Gitlin, "Multi-code CDMA wireless personal communications networks", *Proc. ICC'95*, pp. 1060-1064, 1995.

[47] U. Mitra, "Observations on jointly optimal detection for multi-rate DS/CDMA systems", *Proc. of the 4th IEEE Communication Theory Mini-Conf., GLOBECOM'96*, pp. 116-120, Nov. 1996.

[48] M. Saquib, R. Yates and N. Mandayam, "Decorrelating detectors for a dual rate synchronous DS/CDMA channel", *Wireless Personal Commun.*, Kluwer Academic Publishers, vol. 9, no. 3, pp. 197-216, May 1999.

[49] J. Chen and U. Mitra, "Analysis of decorrelator-based receivers for multirate DS/CDMA communications", *IEEE Trans. Veh. Technol.*, vol. 48, no. 6, pp. 1966-1983, Nov. 1999.

[50] H. Ge, "Multiuser detection for integrated multi-rate CDMA", *Proc. of the First International Conference on Information, Communications and Signal Processing (ICICS'97)*, pp. 858-862, Sept. 1997.

[51] H. Ge and J. Ma, "Multi-rate LMMSE detectors for asynchronous multi-rate CDMA systems", *Proc. ICC'98*, pp. 714-718, 1998.

[52] S. Buzzi, M. Lops and A. M. Tulino, "MMSE multiuser detection for asynchronous dual-rate direct sequence CDMA communications", *Proc. Personal, Indoor and Mobile Radio Communications'98*, pp. 223-227, 1998.

[53] N. Seidl, I. Howitt and J. Richie, "Blind adaptive linear multiuser detection for multi-rate CDMA systems", *Proc. IEEE VTC'2000-Fall*, pp. 1296-1303, Sept. 2000.

[54] J. Zander, "Performance of optimum transmitter power control in cellular radio systems", *IEEE Trans. Veh. Technol.*, vol. 41, no. 1, pp. 57-62, Feb. 1992.

[55] T.-H. Lee, J.-C. Lin and Y. T. Su, "Downlink power control algorithms for cellular radio systems", *IEEE Trans. Veh. Technol.*, vol. 44, no. 1, pp. 89-94, Feb. 1995.

[56] M. Anderson, Z. Rosberg and J. Zander, "Gradual removals in cellular PCS with constrained power control and noise", *ACM/Baltzer Journal of Wireless Networks*, vol. 2, pp. 27-43, 1996.

[57] Q. Wu, "Performance of optimum transmitter power control in CDMA cellular mobile systems", *IEEE Trans. Veh. Technol.*, vol. 48, no. 2, pp. 571-575, Mar. 1999.

[58] P. S. Kumar and J. Holtzman, "Power control for a spread spectrum system with multiuser receivers", *Proc. IEEE Int. Symp. Personal, Indoor and Mobile Radio Communications*, vol. 3, pp. 955-959, Sept. 1995.

[59] M. Varanasi, "Power control for multiuser detection", *Proc. 30th Annual Conf. Inform. Sciences and Systems*, pp. 866-873, Princeton, NJ, Mar. 1996.

[60] M. Saquib, R. D. Yates and A. Ganti, "Power control for an asynchronous multirate decorrelator", *IEEE Trans. Commun.*, vol. 48, no. 5, pp. 804-812, May 2000.

[61] M. J. Juntti, "System concept comparisons for multirate CDMA with multiuser detection", *Proc. IEEE VTC'98*, pp. 36-40, May 1998.

[62] M. J. Juntti, "Performance of multiuser detection in multirate CDMA systems", *Wireless Personal Commun.*, Kluwer Academic Publishers, vol. 11, no. 3, pp. 293-311, Dec. 1999.

[63] M.-H. Chung and K.-C. Chen, "Power allocation for multi-rate multiuser detection in wideband CDMA systems", *Proc. IEEE VTC'99-Fall*, pp. 608-612, Sept. 1999.

[64] M. J. Juntti and B. Aazhang, "Finite memory-length linear multiuser detection for asynchronous CDMA communications", *IEEE Trans. Commun.*, vol. 45, no. 5, pp. 611-622, May 1997.

[65] M.-S. Alouini and A. J. Goldsmith, "Area spectral efficiency of cellular mobile radio systems", *IEEE Trans. Veh. Technol.*, vol. 48, no. 4, pp. 1047-1066, July 1999.

[66] A. J. Viterbi, A. M. Viterbi and E. Zehavi, "Performance of power-controlled wideband terrestrial digital communication", *IEEE Trans. Commun.*, vol. 41, no. 4, pp. 559-569, Apr. 1993.

[67] R. Prasad, M. G. Jansen and A. Kegel, "Capacity analysis of a cellular direct sequence

code division multiple access system with imperfect power control", *IEICE Trans. Commun.*, vol. E76-B, no. 8, pp. 894-904, Aug. 1993.

[68] H. V. Poor and S. Verdú, "Probability of error in MMSE multiuser detection", *IEEE Trans. Inform. Theory*, vol. 43, no. 3, pp. 858-871, 1997.

[69] G. L. Stüber, *Principle of Mobile Communication*, Kluwer Academic Publishers, 1996.

[70] L. F. Fenton, "The sum of log-normal probability distributions in scatter transmission systems", *IRE Trans. Commun. Syst.*, vol. C5-8, pp. 57-67, Mar. 1960.

[71] S. C. Schwartz and Y. S. Yeh, "On the distribution function and moments of power sums with log-normal components", *Bell Syst. Tech. J.*, vol. 61, no. 7, pp. 1441-1462, Sept. 1982.

[72] A. Antoniou and W.-S. Lu, *Lecture Notes: Engineering Design by Optimization*, 2002.

[73] Y. Ye, *Interior-Point Algorithm: Theory and Analysis*, New York: Wiley, 1997.

[74] J. Zou and V. K. Bhargava, "Design issues in a CDMA cellular system with heterogeneous traffic types", *IEEE Trans. Veh. Technol.*, vol. 47, no. 3, pp. 871-884, Nov. 1998.

[75] J. Zou, V. K. Bhargava, and Q. Wang, "Reverse link interference modeling and outage analysis for DS/CDMA cellular systems", *Wireless Personal Commun.*, Kluwer Academic Publishers, vol. 2, no. 3, pp. 189-215, 1995.

[76] I. S. Gradshteyn and I. M. Ryzhik, *Table of Integrals, Series, and Products*, sixth edition, New York: Academic Press, 2000.

[77] G. Woodward and B. S. Vucetic, "Adaptive detection for DS-CDMA", *Proc. of IEEE*, vol. 86, no. 7, pp. 1413-1434, July 1998.

[78] M. Honig and M. K. Tsatsanis, "Adaptive techniques for multiuser CDMA receivers", *IEEE Signal Processing Magazine*, vol. 17, no. 3, pp. 49-61, May 2000.

[79] F. Wijk, G. M. J. Janssen and R. Prasad, "Groupwise successive interference cancellation in a DS/CDMA system", *Proc. 1995 Int. Symp. Personal, Indoor and Mobile Radio Communications (PIMRC'95)*, pp. 742-746, 1995.

[80] X. Wang and A. Høst-Madsen, "Group-blind multiuser detection for uplink CDMA", *IEEE J. Select. Areas Commun.*, vol. 17, no. 11, pp. 1971-1984, Nov. 1999.

[81] S. Haykin, *Adaptive Filter Theory*, Upper Saddle River, NJ: Prentice Hall, 1996.

[82] P. S. R. Diniz, *Adaptive Filtering: Algorithms and Practical Implementation*, Kluwer Academic Publishers, 1997.

[83] G.-O. Glentis, K. Berberidis and S. Theodoridis, "Efficient least squares adaptive algorithms for FIR transversal filtering", *IEEE Signal Processing Magazine*, vol. 16, no. 4, pp. 13-41, 1999.

[84] M. K. Tsatsanis and Z. Xu, "Performance analysis of minimum variance CDMA receivers", *IEEE Trans. Signal Processing*, vol. 46, no. 11, pp. 3014-3022, 1998.

[85] T. J. Lim, Y. Gong and B. Farhang-Boroujeny, "Convergence analysis of chip- and fractionally spaced LMS adaptive multiuser CDMA detectors", *IEEE Trans. Signal Processing*, vol. 48, no. 8, pp. 2219-2228, Aug. 2000.

[86] S. L. Miller, "Training analysis of adaptive interference suppression for Direct-Sequence Code-Division Multiple-Access systems", *IEEE Trans. Commun.*, vol. 44, no. 4, pp. 488-495, Apr. 1996.

[87] S. L. Miller, U. Madhow and L. B. Milstein, "Performance analysis of MMSE receivers for DS-CDMA in frequency-selective fading channels", *IEEE Trans. Commun.*, vol. 48, no. 11, pp. 1919-1929, 2000.

[88] D. Guo, L. K. Rasmussen, S. Sun and T. J. Lim, "A matrix-algebraic approach to linear parallel interference cancellation in CDMA", *IEEE Trans. Commun.*, vol. 48, no. 1, pp. 152-161, Jan. 2000.

[89] Y.-H. Li, M. Chen and S.-X. Cheng, "Determination of cancellation factors for soft-decision partial PIC detector in DS/CDMA systems", *Electronics Letter*, vol. 36, no. 3, pp. 239-241, Feb. 2000.

[90] M. J. Juntti, B. Aazhang and J. O. Lilleberg, "Iterative implementation of linear multiuser detection for dynamic asynchronous CDMA systems", *IEEE Trans. Commun.*, vol. 46, no. 4, pp. 503-508, Apr. 1998.

[91] G. Golub and C. Van Loan, *Matrix Computations*, second edition, Baltimore, MD: Johns Hopkins University Press, 1989.

[92] D. Samardzija, N. Mandayam and I. Seskar, "Blind successive interference cancellation for DS-CDMA systems", *IEEE Trans. Commun.*, vol. 50, no. 2, pp. 276-290, Feb. 2002.

[93] F. A. Graybill, *Matrices with Applications in Statistics*, Belmont, California: Wadsworth Publishing Company, 1983.

[94] J. Karhunen, "Adaptive algorithms for estimating eigenvectors of correlation type matrices", *Proc. IEEE ICASSP*, pp. 14.6.1-14.6.4, Mar. 1984.

[95] J. Yang and M. Kaveh, "Adaptive eigensubspace algorithms for direction or frequency estimation and tracking", *IEEE Trans. Acoust. Speech. Signal Processing*, vol. 36, no. 2, pp. 241-251, Feb. 1988.

[96] B. Yang, "Projection approximation subspace tracking", *IEEE Trans. Signal Processing*, vol. 43, no. 1, pp. 95-107, Jan. 1995.

[97] B. Yang, "Asymptotic convergence analysis of the projection approximation subspace tracking algorithms", *Signal Processing*, vol. 50, pp. 123-136, 1996.

[98] Y. Song, "Estimations for the eigenvalues of the product of matrices", *Journal of Nanjing Normal University*, vol. 16, no. 2, pp. 10-13, 1994. (in Chinese) (English version is available on http://202.119.104.32/teachers/syz/papers.htm)